



Call: H2020-SC5-2014-two-stage

Topic: SC5-01-2014

PRIMAVERA

Grant Agreement 641727



**PRocess-based climate sIMulation: AdVances in high resolution modelling and
European climate Risk Assessment**

Deliverable D2.2

***Quantification of the benefits of increased model
resolution in the Stream 1 simulations***

Deliverable Title	Quantification of the benefits of increased model resolution in the Stream 1 simulations	
Brief Description	Quantification of the benefits of increased resolution in the atmosphere only versus in the coupled system, as well as their robustness across the WP6 Stream 1 simulations, for processes which impact European weather and climate such as atmospheric blocking, ocean-sea-ice-atmosphere interactions in the Arctic region and for tropical cyclones and their extra-tropical transition	
WP number	2	
Lead Beneficiary	ECMWF	
Contributors	<i>Franco Molteni (ECMWF)</i> <i>Christopher Roberts (ECMWF)</i> <i>Retish Senan (ECMWF)</i> <i>David Docquier (UCLouvain)</i> <i>François Massonnet (UCLouvain)</i> <i>Thierry Fichefet (UCLouvain)</i> <i>Alessio Bellucci (CMCC)</i> <i>Panos Athanasiadis (CMCC)</i> <i>Daniele Peano (CMCC)</i> <i>Enrico Scoccimarro (CMCC)</i> <i>Kristian Strommen (UOXF)</i> <i>Federico Fabiano (CNR)</i> <i>Susanna Corti (CNR)</i> <i>Irene Mavilia (CNR)</i> <i>Malcolm Roberts (Met Office)</i> <i>Sarah Ineson (Met Office)</i> <i>Galia Guentchev (Met Office)</i> <i>Jeremy Grist (NERC)</i>	
Creation Date	24/10/18	
Version Number	2.2	
Version Date	06/11/18	
Deliverable Due Date	31/10/18	
Actual Delivery Date	06/11/18	
Nature of the Deliverable	R	R - Report
		P - Prototype
		D - Demonstrator
		O - Other
Dissemination Level/ Audience	PU	PU - Public
		PP - Restricted to other programme participants, including the Commission services
		RE - Restricted to a group specified by the consortium, including the Commission services
		CO - Confidential, only for members of the consortium, including the Commission services

Version	Date	Modified by	Comments
1	30/10/18	F Molteni, C Roberts (ECMWF)	Original contributions included, S3.1 and 4 added
2	02/11/18	F Molteni, C Roberts (ECMWF), WP2 partners	Executive summary and sections 3.5, 3.6, 5 added; corrections from partners included
3	06/11/18	F Molteni, C Roberts (ECMWF)	Final corrections to text and figures

Table of Contents

1. Executive Summary	5
2. Project Objectives	7
3. Detailed Report	8
3.1 <i>Stream 1 simulations available for D2.2 analyses and nominal model resolution</i>	8
3.2 <i>Impact of atmospheric resolution in AMIP-type multi-model experiments</i>	12
3.3 <i>Impact of resolution in coupled multi-model experiments</i>	47
3.4 <i>Case studies based on different configurations of a single model</i>	65
3.5 <i>Peer-reviewed articles arising from the project</i>	76
3.6 <i>Other references</i>	77
4. Lessons Learnt	81
4.1 <i>Impact of atmospheric resolution in AMIP-type and coupled simulations</i>	81
4.2 <i>Ocean resolution in the coupled systems</i>	82
5. Links Built.....	83

1. Executive Summary

This deliverable summarizes the key outcomes from investigations within WP2 that have utilized climate model data delivered by WP6. The Stream 1 simulations provided by WP6 are designed to facilitate a systematic evaluation of the impact of ocean and atmosphere resolution and conform to the protocols of the High Resolution Model Intercomparison Project (HighResMip) and phase 6 of the Coupled Model Intercomparison Project (CMIP6). Information about the models and experiments used for stream 1 are given in Sect. 3.1.

Unfortunately, unforeseen delays and issues with data delivery (mainly because of the late availability of CMIP6 forcings) means that comprehensive multi-model analysis of the coupled ocean-atmosphere systems have been correspondingly delayed. For this reason, we report here on multi-model analyses of the available atmosphere-only and coupled model data (sections 3.2 and 3.3) and on studies that have considered either a single PRIMAVERA model in detail or prototype simulations from the so-called “pre-PRIMAVERA” data set (section 3.4).

Results on the sensitivity to atmospheric resolution in WP6 Stream 1 simulation are broadly in line with earlier findings on this topic, either from published literature or from earlier deliverables of the PRIMAVERA project. In general, long-term biases in atmospheric variables and statistics are only weakly affected by an increase in atmospheric resolution, which contrasts with the larger response to increases in ocean resolution. The spatial pattern of large scale-modes of variability (EOFs, teleconnection patterns, circulation regimes) in individual models often shows significant differences between the lower- and the higher-resolution versions, but improvements with resolution are not consistent across models. Among the different circulation regimes affecting the European and North Atlantic region, blocking is the one showing the clearer benefits of increased resolution; this is manifested in the frequency of long-lived episodes or in the spatial correlation of 2-dimensional patterns of blocking frequency between models and observations.

A question raised by a number of contributors is whether results obtained from a single 65-year simulation for each model are robust enough to provide a statistically significant assessment of low-frequency variability. It was noted that ensembles of at least 3 members and possibly up to 10 members would be needed for a robust assessment of trends, teleconnections and regime properties.

Aspects that showed a consistent benefit of atmospheric resolution increase are those related to extreme events and intense storms, as well as some aspects of the hydrological cycle. Over Europe and the northern extratropics, a positive impact was noted in trends of summer temperature extremes, statistics of extreme precipitation over Europe, and in biases of storm intensity. For tropical cyclones, the relationship between pressure minima and maximum lifetime and the representation of specific humidity within cyclones is improved. Positively affected aspects of the hydrological cycle include trends in boreal spring snow cover and the overall proportion of land/orographic precipitation.

Results on the impact of increased resolution in ocean models show a strong degree of consistency. The transition from 100 km to 50-10 km ocean resolutions has a substantial impact on the mean climate and variability of the coupled system. There is some evidence that the impact on the mean state of changes in ocean resolution are larger than the

corresponding changes in atmospheric resolution. This is likely due the transition of ocean models from the eddy-parameterized (~ 100 km) to eddy-permitting/-resolving (< 50 km) regime, which results in a step-change in the ability of the resolved ocean dynamics to simulate sharp gradients and non-linear processes such as mesoscale eddies. Increased ocean resolution in the PRIMAVERA models is associated with improvements to the poleward transport of heat in the North Atlantic, which leads to improvements to related regional climate biases (e.g. Arctic sea-ice volume, North Atlantic SST biases).

The move to eddy-permitting ocean resolutions is also associated with a step-change in the representation of ocean-atmosphere coupling in areas of high eddy activity such as the Gulf Stream. Work is ongoing to evaluate the associated atmospheric impacts and their timescale dependence. This work is important to quantify the relevance of results obtained within PRIMAVERA for coupled forecasts on sub-seasonal to seasonal timescales.

Finally, we note that several models within the PRIMAVERA ensemble share an ocean model configuration (NEMO) and therefore results should be considered within the context of the existing literature. The NEMO model typically shows an increase in the strength of the Atlantic Meridional Overturning Circulation (AMOC) and associated heat transports at higher ocean resolutions. However, previous studies suggest that this result cannot be generalized to all coupled modelling systems, as the transition from eddy-parameterized to eddy-resolving ocean resolutions has also been linked to a weakening AMOC.

2. Project Objectives

With this deliverable, the project has contributed to the achievement of the following objectives (DOA, Part B Section 1.1) WP numbers are in brackets:

No.	Objective	Yes	No
A	To develop a new generation of global high-resolution climate models. (3, 4, 6)		
B	To develop new strategies and tools for evaluating global high-resolution climate models at a process level, and for quantifying the uncertainties in the predictions of regional climate. (1, 2, 5, 9, 10)	Yes	
C	To provide new high-resolution protocols and flagship simulations for the World Climate Research Programme (WCRP)'s Coupled Model Intercomparison Project (CMIP6) project, to inform the Intergovernmental Panel on Climate Change (IPCC) assessments and in support of emerging Climate Services. (4, 6, 9)		No
D	To explore the scientific and technological frontiers of capability in global climate modelling to provide guidance for the development of future generations of prediction systems, global climate and Earth System models (informing post-CMIP6 and beyond). (3, 4)		No
E	To advance understanding of past and future, natural and anthropogenic, drivers of variability and changes in European climate, including high impact events, by exploiting new capabilities in high-resolution global climate modelling. (1, 2, 5)	Yes	
F	To produce new, more robust and trustworthy projections of European climate for the next few decades based on improved global models and advances in process understanding. (2, 3, 5, 6, 10)	Yes	
G	To engage with targeted end-user groups in key European economic sectors to strengthen their competitiveness, growth, resilience and ability by exploiting new scientific progress. (10, 11)		No
H	To establish cooperation between science and policy actions at European and international level, to support the development of effective climate change policies, optimize public decision making and increase capability to manage climate risks. (5, 8, 10)		No

3. Detailed Report

3.1 Stream 1 simulations available for D2.2 analyses and nominal model resolutions

3.1.1 PRIMAVERA experiments

This deliverable summarizes the key outcomes from investigations within WP2 that have utilized climate model data delivered by WP6. The model simulations provided by WP6 are designed to facilitate a systematic evaluation of the impact of ocean and atmosphere resolution (see Table 3.1.1 – nominal resolutions) and conform to the protocols of the High Resolution Model Intercomparison Project (HighResMip) and phase 6 of the Coupled Model Intercomparison Project (CMIP6). This report refers to the following specific simulations:

- (1) HighresSST-present: atmosphere-only integrations forced with observed SSTs, observed sea-ice concentrations, and external radiative forcings over the period 1950-2014.
- (2) spinup-1950: a 30-50 year coupled integration with constant 1950s forcings in which the ocean is integrated until near-surface ocean and sea-ice biases have reached an approximate steady state.
- (3) control-1950: a 100-year continuation of spinup-1950 that is designed to enable identification of long-term trends associated with model drift that are unrelated to changes in external radiative forcings.
- (4) hist-1950: coupled experiments initialized from the end of spinup-1950 and integrated with time-varying external forcings over the period 1950-2014.

3.1.2 Delays in data availability

Unfortunately, unforeseen delays and issues with data provided by WP6 (mainly because of the late availability of CMIP6 forcings) means that WP2 analyses, and particularly multi-model analysis of the coupled ocean-atmosphere systems, have been correspondingly delayed. For this reason, we report here on multi-model analyses of the available atmosphere-only and coupled model data (sections 3.2 and 3.3) and on studies that have considered either a single PRIMAVERA model in detail or prototype simulations from the so-called “pre-PRIMAVERA” data set (section 3.4). The model data availability on 1 Oct. 2018 is shown in Fig. 3.1.1.

3.1.3 Atmospheric resolutions

Centres participating in PRIMAVERA have provided models covering a wide range of atmospheric resolutions. While referring to such resolutions, different centres adopt different nomenclatures (see table 3.1.1), and therefore the official model name is not necessarily a good indicator of the actual resolution. A further difficulty is that, depending on the specific dynamical cores and adopted numerics, the definition of horizontal resolution may be based on different criteria. In grid-point models with a constant grid spacing in both latitude and longitude, the grid size (in km) is dependent on latitude. Spectral models with spectral truncation at total wavenumber N may use gaussian grids with (at least) $2N+1$, $3N+1$, or $4N+1$ points along the Equator to compute advective terms and physical parametrization tendencies (these are usually referred to as linear, quadratic and cubic grids respectively),

so that the ratio between resolutions in two different spectral models may not correspond to the ratio of spectral truncation. For example, within the PRIMAVERA models, the higher-resolution version of ECMWF-IFS has a finer grid mesh, but a lower spectral truncation, than the higher-resolution version of EC-Earth3P.

In this report, two approaches have been used to deal with resolution comparisons. One approach is to compare the performance of versions of the same model with higher and lower resolution, and then show for which / how many models the higher-resolution performs better. In the second approach, data from different models are pooled together to create two multi-model ensembles, one including lower-resolution versions and the other the higher-resolution version. While potentially alleviating the problem of limited statistical significance often encountered in diagnostics of single-member simulations, it is important to recognize that such multi-model ensembles include models whose resolutions may vary (within each ensemble) as much as different versions of the same model.

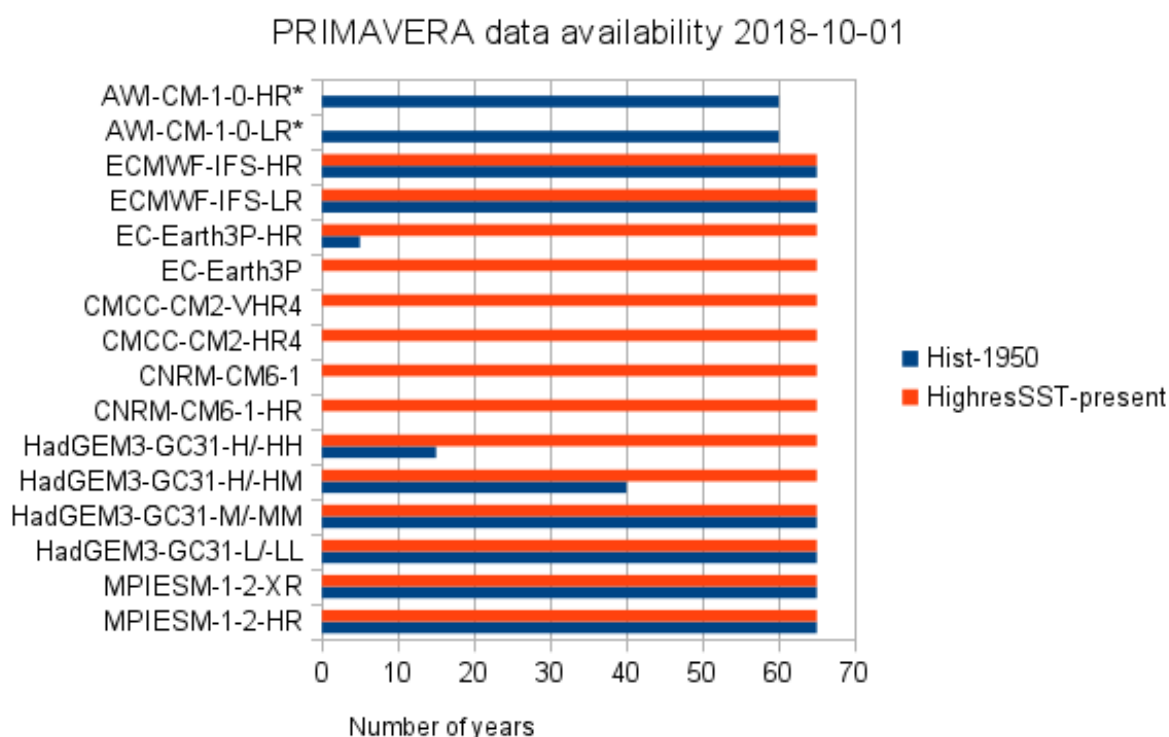


Figure 3.1.1. PRIMAVERA data available through the JASMIN data management tool as of October 1st 2018. *Note: bars for the AWI-CM-1-0 model are representative of the availability of ocean and sea-ice data as atmospheric data is not yet available.

3.1.4 Ocean resolutions

The PRIMAVERA ensemble includes ocean models with a range of horizontal resolutions, from ~100 km to ~10 km. These models can be broadly categorized by their ability to adequately resolve the first baroclinic Rossby radius of deformation (L_R ; Hallberg, 2013).

“Eddy-parameterized” ocean models have a grid-spacing of ~ 100 km such that L_R is unresolved and the effects of eddies on the large-scale circulation must be parameterized. “Eddy-permitting” ocean models have resolutions of 25-50 km such that L_R is resolved in the low latitudes and the circulation permits the development of non-linear mesoscale eddies and sharp gradients associated with ocean fronts. “Eddy resolving” or “eddy active” ocean models have a grid-spacing of ~ 10 km such that L_R is resolved over most of the mid- and high-latitude oceans, though much finer resolution is required to resolve L_R over the shallow continental shelves (Hallberg, 2013; Hewitt et al. 2016). The PRIMAVERA ensemble includes ocean models from each of these different regimes. This situation in the ocean can be contrasted with that in the atmosphere, where even the lowest resolution atmospheric models (~ 250 km) can resolve L_R in the mid-latitude atmosphere (~ 1000 km).

3.1.4 Nominal resolutions of atmosphere and ocean components

Table 3.1.1 below lists the official names and nominal resolutions of the models contributing to the Stream 1 of PRIMAVERA WP6. The so-called HighResSST (AMIP-type) simulations have been performed with the atmosphere/land-only component of the coupled models, with boundary conditions for sea-surface temperature (SST) and sea-ice concentration (SIC) provided by the HadISST2 dataset (Kennedy et al. 2017). In the table, we have separated the lower-resolution from the higher-resolution versions of the models (and, for some participants, a middle/mixed-resolution version), to emphasize the variety of actual resolutions in each category. Data are taken from the document:

https://rawgit.com/WCRP-CMIP/CMIP6_CVs/master/src/CMIP6_source_id.html

where additional information is provided on the model configuration and grid structure.

Originating/leading institution (Participant no.)	Model name	Nominal resolution atmosphere (no. of latitude lines)	Nominal resolution: ocean
<i>Lower-resolution versions</i>			
MetOffice (1)	HadGEM3-GC3.1-LL	250 km (144 lat. l.)	100 km (1 deg)
EC-Earth consortium (3, 4, 8, 12)	EC-Earth3P	100 km (256 lat. l.)	100 km (1 deg)
CNRM/CERFACS (5)	CNRM-CM6-1	250 km (128 lat. l.)	100 km (1 deg)
Max Planck Gesellschaft (6)	MPI-ESM1-2-HR	100 km (192 lat. l.)	40 km (0.4 deg)
CMCC (9)	CMCC-CM2-HR4	100 km (192 lat. l.)	25 km (0.25 deg)
Alfred Wegener Institut (10)	AWI-CM-1-1-LR	250 km (96 lat. l.)	50 km (~0.5 deg)
ECMWF (13)	ECMWF-IFS-LR	50 km (400 lat. l.)	100 km (1 deg)
<i>Middle/mixed-resol. versions</i>			
MetOffice (1)	HadGEM3-GC3.1-MM	100 km (324 lat. l.)	25km (0.25 deg)
ECMWF (13)	ECMWF-IFS-MR	50 km (400 lat. l.)	25 km (0.25 deg)
<i>Higher-resolution versions</i>			
MetOffice (1)	HadGEM3-GC3.1-HH	50 km (768 lat. l.)	10 km (1/12 deg)
EC-Earth consortium (3, 4, 8, 12)	EC-Earth3P-HR	50 km (512 lat. l.)	25km (0.25 deg)
CNRM/CERFACS (5)	CNRM-CM6-1-HR	100 km (360 lat. l.)	25 km (0.25 deg)
Max Planck Gesellschaft (6)	MPI-ESM1-2-XR	50 km (384 lat. l.)	40 km (0.4 deg)
CMCC (9)	CMCC-CM2-VHR4	25 km (768 lat. l.)	25 km (0.25 deg)
Alfred Wegener Institut (10)	AWI-CM-1-1-HR	100 km (192 lat. l.)	25 km (~0.25 deg)
ECMWF (13)	ECMWF-IFS-HR	25 km (800 lat. l.)	25 km (0.25 deg)

Table 3.1.1 Nominal resolution of models used in WP6 Stream 1 simulations.

3.2 Impact of atmospheric resolution in AMIP-type multi-model experiments

3.2.1 Effective resolution of Stream 1 models (KNMI)

The stream 1 simulations are performed with the standard- and high-resolution version of each model. This enables to investigate for each model the impact of increased resolution. However, the resolutions of the models differ substantially among the standard as well as the high resolutions. For a multi-model analyses, which is key for PRIMAVERA, a parameter is needed that describes the resolution of each model. This poses two problems. First the model formulation differs widely, grid point versus spectral models, specific choice of gaussian grid for spectral models, etc. Second even after the computation of a nominal grid distance for each model this is not the resolution that is representative of the impact of resolution on the dynamics of the model. The first problem can be solved relatively easy, because spectral models use Gaussian grid for the computation of the non-linear terms and the model physics, a nominal grid box distance L_{box} can be computed for each model. It is based on a weighted mean grid box distance similar as used in the algorithm for computing nominal resolution according to the CMIP6 convention. The KNMI contribution has been focused on computing an effective resolution based on the energy spectrum of each atmosphere model and to compare that with the nominal resolution.

The effective resolution is determined by the shape of the kinetic energy spectrum. Observations as well as theoretical arguments reveal that the spectrum follows a k^{-3} power law for the synoptic scales and a $k^{-5/3}$ power law for the meso-scales, where k is the wavelength. It is well known that models do not realistically simulate the Earth's atmosphere at scales that are close to the grid resolution scale. Parameterizations, numerical diffusion, aliasing and anti-aliasing filters lead to dissipation of kinetic energy and consequently to a breakdown of the atmospheric power laws, not unlike the microscales in the atmosphere where viscosity becomes important. The kinetic energy spectrum can be used to indicate the breakdown of the atmospheric power laws and therefore be used to determine the cut-off scale beyond which the kinetic energy is unrealistically small. This scale is referred to as the effective resolution. Smaller scales are incorrectly simulated and should be disregarded from interpretational climate studies.

We have analysed the effective resolution of the six atmospheric PRIMAVERA models. They generally simulate the atmospheric kinetic energy content realistically down to scales of roughly three times the nominal grid box distance (Fig. 3.2.1.1). Furthermore, the low- and high-resolution versions exhibit inter-model systematic differences for wavenumbers in the resolved range of scales. This analysis of effective resolution provides a framework for inter model comparison over a wide range research area's in PRIMAVERA. The manuscript (Klaver et al. 2018) will be submitted to GRL this month.

Key results:

- There appears to be constant scaling between nominal and effective resolution over a wide range of models although differences exist among the PRIMAVERA models.

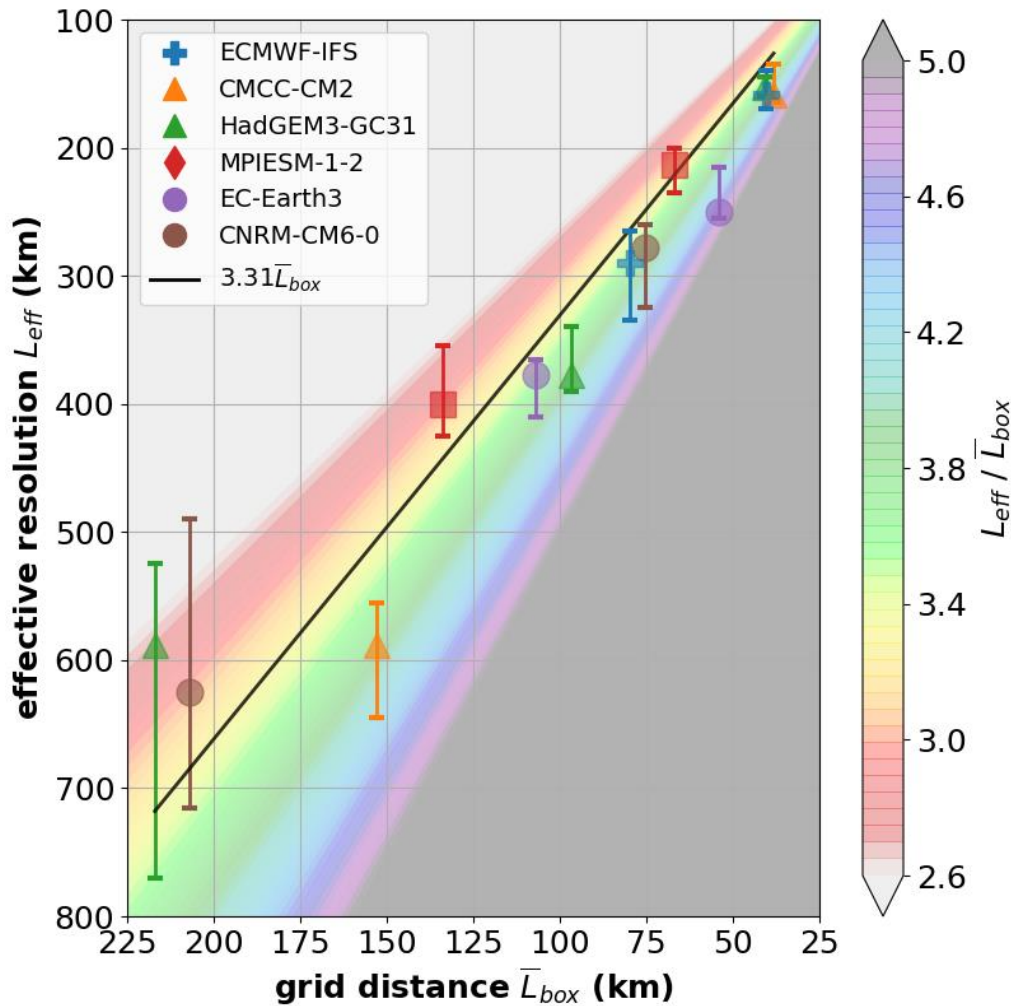


Figure 3.2.1.1. Scatter plot of the effective resolution L_{eff} versus a weighted mean grid distance L_{box} of the models' native grids. Colour shading depicts the scaling between effective resolution and grid box distance (i.e. $y=x$).

3.2.2 Summer temperature trends and variability over Europe (CERFACS)

a) Recent summer temperature trends over Europe

Large surface temperature trends have been observed over Western Europe in summer since the 1950s, much larger than for the global average (Bhend and Whetton, 2013). The climate models tend to underestimate these trends (van Oldenborgh et al., 2009; Bhend and Whetton, 2013). The causes of the frequent inconsistency between simulated and observed summer temperature trends are not clear. Based on the PRIMAVERA multi-model AMIP simulations from all the models, two questions are addressed here: (i) Is it possible that part of this inconsistency is due to the low resolution of climate models? i.e. does resolution impact summer temperature trends over Western Europe? (ii) May differences between simulated and observed sea surface temperature (SST) trends explain the inconsistency regarding summer temperature trends over Western Europe?

Here, 2-metre summer temperature trends are computed on the 1951-2014 period to minimize the potential impact of internal variability thanks to a long period. Observations

from Berkeley Earth (Rohde et al., 2013) show a large positive trend over Western Europe, close to 2 K over the south of Western Europe (Figure 3.2.2.1a. Note that results are very similar for other observation datasets, not shown). The observed trends are much weaker in Eastern Europe, especially in the northern part. The CMIP5 coupled climate models generally largely underestimate the temperature trends over Western Europe, but the trends are overestimated over Eastern Europe (Figure 3.2.2.1b). The bias pattern is actually very similar in PRIMAVERA models demonstrating that the SST evolution is not responsible for the bias in summer temperature trends noted previously in coupled climate models. The inclusion or not of CNRM-CM6 does not impact this conclusion as its results are very similar to the ones from other PRIMAVERA models despite its forcing issue in the Arctic. Note that the bias pattern seen in the different ensembles is largely due to observed large scale circulation trends that tend to amplify the observed warming over Western Europe and reduce it over Eastern Europe and are generally not captured by the models (not shown). The differences in the trends averaged over Western Europe between individual PRIMAVERA simulations and the observations are shown in Figure 3.2.2.2. The differences are negative in most simulations. However, some PRIMAVERA models are not inconsistent with the observations because the warming trend of at least one of their members is close to the observations. An interpretation of this result could be that these models simulate realistically the recent warming forced by the ocean and external forcings, and that the observed amplification of the warming signal over Western Europe as well as the weaker warming over Eastern Europe are the result of internal atmospheric variability.

In Figure 3.2.2.1, the bias in summer temperature trend over Western Europe is somewhat smaller in higher resolution models, but as the resolutions vastly differ between PRIMAVERA models, this result is difficult to interpret. We now examine the impact of resolution on temperature trends over Western Europe for each model separately. We assess whether for a given model the difference potentially due to resolution is compatible or not with internal climate variability, i.e. whether the differences between simulations of the same model at two resolutions are greater than the difference between members at the same resolution. We therefore compare the pairwise differences of temperature trends averaged over Western Europe between the simulations at different resolutions for each model and the pairwise differences of the trends between members from the same model (all possible combinations are considered, Figure 3.2.2.2).

Only CNRM-CM6 provides a large enough ensemble of 10 members (for both resolutions) to estimate robustly the impact of internal variability in this context (we don't expect an important impact of the forcing issue in this model for this analysis, but we will verify it as soon as possible. This is why it is included here). HadGEM3 also provides 3 members for each of the 3 resolutions. The pairwise differences for members of this model are consistent with the CNRM-CM6 distribution. For CNRM-CM6 it seems that there is an impact of resolution on the spread, but it will be the object of a future study.

For HadGEM3, the warming trends are generally larger for higher resolution simulations suggesting an impact of resolution in this model but the individual differences still generally remain compatible with the simple impact of internal variability. The difference associated with resolution for CNRM-CM6 is close to 0 in average. For the other models, for which only one member is available the differences potentially due to resolution remain compatible with the impact of internal variability estimated with CNRM-CM6 or HadGEM3, even if the difference is quite large for MPIESM.

Key results:

Given the large impact of internal variability on temperature trends even in the forced atmospheric framework followed here, it is not possible to conclude robustly to a general impact of resolution of temperature trends over Western Europe, based on the current PRIMAVERA AMIP ensemble. Larger ensembles would be necessary to reach stronger conclusions. Our analyses also show that the generally colder trends in coupled GCMs over Western Europe described by previous studies cannot be primarily attributed to unrealistic sea surface temperature evolution as they are also seen in the forced PRIMAVERA simulations studied here. A paper describing these results is in preparation.

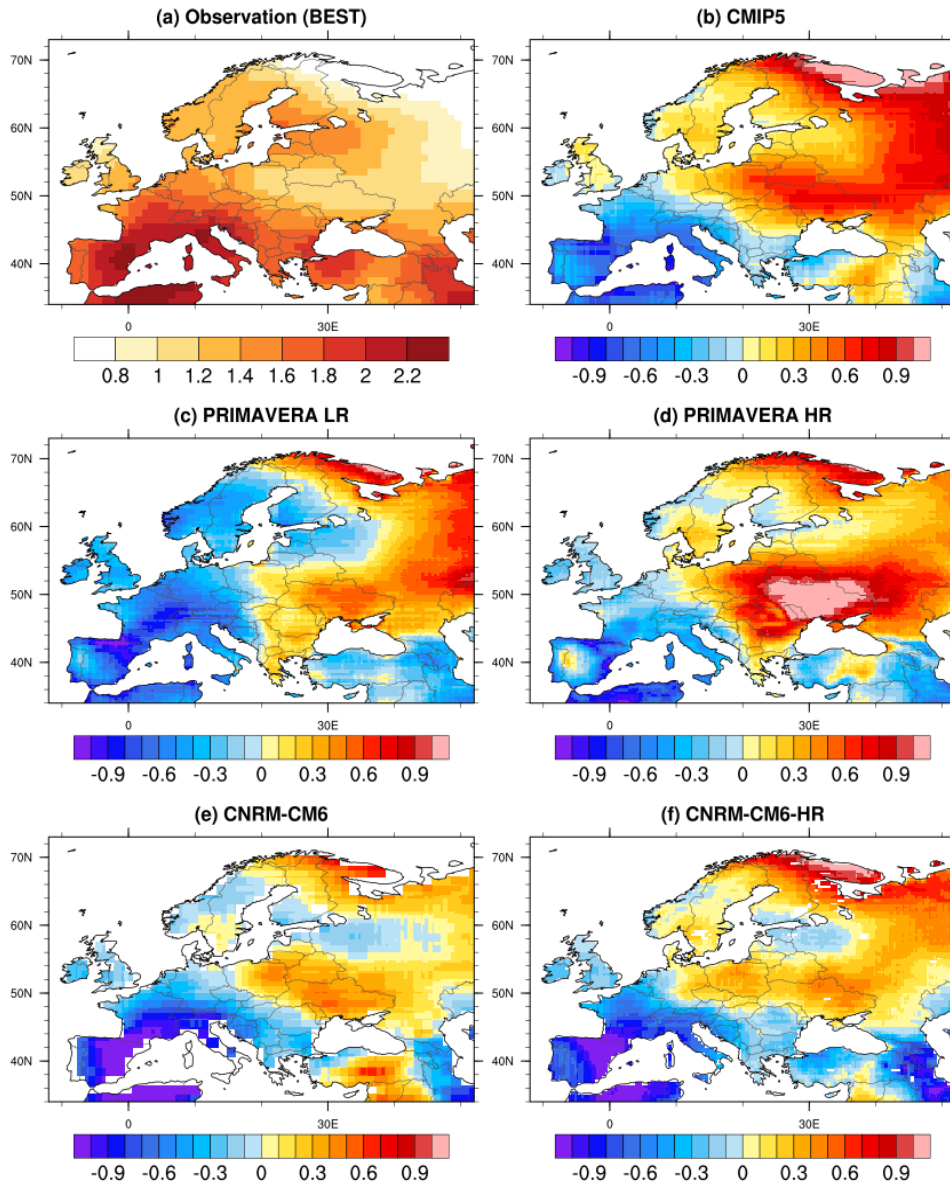


Figure 3.2.2.1: Trend in summer (JJA) 2-m temperature over Europe from 1951 to 2014 (K) in (a) Berkeley Earth Surface Temperature observations (Rohde et al., 2013). (b) Multi-model mean bias for an ensemble of 34 CMIP5 models. (c) Multi-model mean bias for PRIMAVERA AMIP LR simulations, without CNRM-CM6. (d) Multi-model mean bias for PRIMAVERA AMIP HR simulations, without CNRM-CM6-HR (e) Ensemble mean bias for CNRM-CM6 AMIP simulations. (f) Ensemble mean bias for CNRM-CM6-HR AMIP simulations. For (c) and (d), only one member is used for HadGEM3. The LM version is used for (c) and the HM version is used for (d).

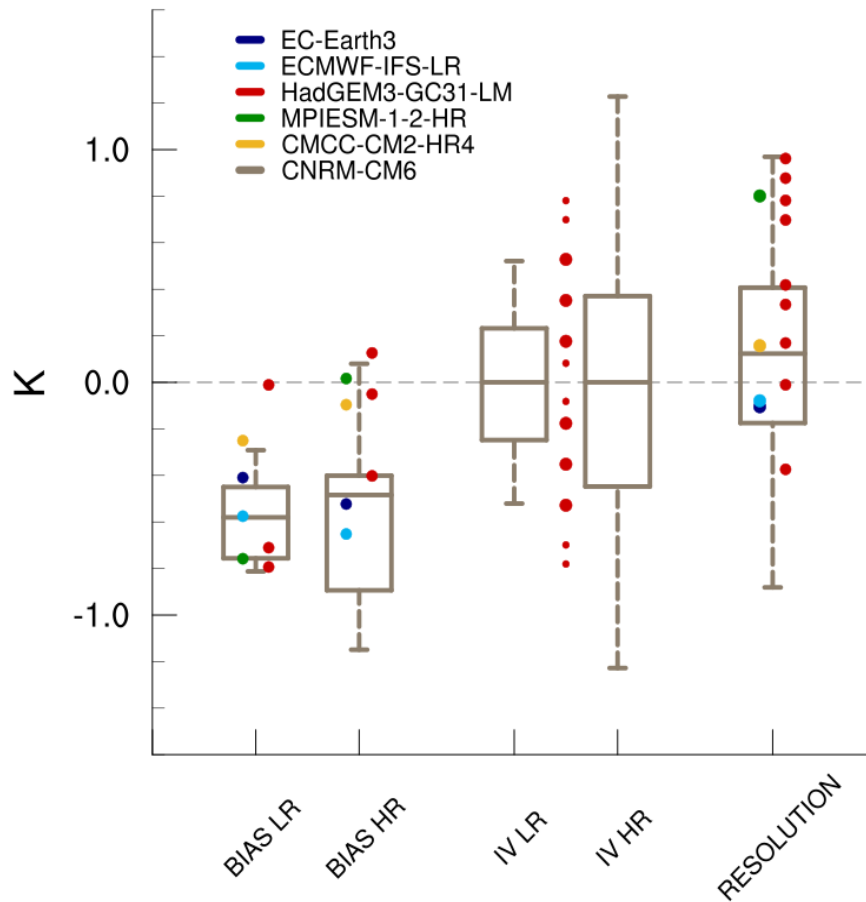


Figure 3.2.2.2: Pairwise differences between the JJA surface temperature trends averaged over Western Europe (35N, 72N, -10E, 15E, land points only): (BIAS LR) Between the observations and the PRIMAVERA LR simulations. (BIAS HR) Between the observations and the PRIMAVERA HR simulations; (IV LR) Between the 10 members of CNRM-CM6, (IV HR) Between the 10 members of CNRM-CM6-HR. The red points between IV LR and IV HR correspond to the pairwise differences between (big points) HadGEM3-GC31-HM members and (small points) HadGEM3-GC31-LM members. (RESOLUTION) Between the LR and HR simulations PRIMAVERA AMIP simulations for each model. For HadGEM3, the LM and HM versions are used. In all cases, the pairwise differences are computed for all the combinations of members. For CNRM-CM6 and CNRM-CM6-HR, as we have 10 members for each resolution, box-and-whiskers plot showing the distribution are used. The whiskers show the min and max, and the boxes show the first, second and third quartiles.

b) Changes in the number of summer warm days over Europe

Days of temperature extremes are known to impact significantly on, among other things, human health and mortality, ecological systems, infrastructure and agriculture. It is therefore not surprising that in the presence of the current and rapid climate change considerable research activity is being directed at documenting how these temperature extremes have changed in recent decades and how they might be expected to change in the future, as well as at identifying the fundamental atmospheric mechanisms associated with such changes. Here, we focus on the first question and use the PRIMAVERA stream 1 AMIP-type simulations to document and investigate changes in extreme heat indexes in summer (JJA)

over Europe. These simulations are constrained by all external forcings and observed sea surface temperature and sea-ice concentrations. The simulated period is 1950-2014 for all models that have all been run at low and high spatial resolution (LR and HR respectively). Figure 3.2.2.3 shows the changes in the number of summer days (the unit here is in number of days per 65 years) with temperature greater than 25°C (thereafter warm days) over the 1950-2014 period. The observations show a large increase over Western Europe and the Mediterranean region, a moderate one in Central Europe and no change in Northern Europe and Scandinavia. The PRIMAVERA models agree very well with observations for Northern Europe and Scandinavia. They do not agree among themselves with regard to the regions with the largest changes (indeed this is to be expected as we only have one realization per model version). However, most of the PRIMAVERA models seem to indicate a larger increase in the number of warm days with their high-resolution version, bringing them closer to the observed trend (in particular for Western and Central Europe).

In order to go one step further in term of attribution, the same analysis has also been applied to the CESM1 large ensemble (30 members used). First, Figure 3.2.2.4 illustrates that internal variability can have a very substantial influence on 65-year trends (in the number of warm days). This strengthens the need for a probabilistic assessment when one is trying to compare model results with observations. Based on the CESM model, we can derive an estimate of the forced response to external forcing by taking the ensemble mean of all CESM simulated trends (Figure 3.2.2.2, 1st row, middle panel). Regions with the largest forced response are Central Europe and the margins of the Mediterranean Sea. The spatial pattern of the forced response suggests that most of the observed Mediterranean region signal is a forced response. We can then derive an estimate of the internal variability contribution to the observed trend (simply by taking the difference between the observed and forced trends). This suggests that internal variability has led to an additional increase in warm days over Western Europe and a decrease over Central Europe (Figure 3.2.2.4, 1st row, right panel). This is possibly in agreement with recent work on the possible influence of Atlantic Multi-decadal variability (AMV) on summer extremes. Analyses are on-going to complete these preliminary attribution statements.

Key results:

Regarding warm summer extreme events in Europe, most of the PRIMAVERA-AMIP models seem to indicate a larger increase in the number of warm days with their high-resolution version, bringing them closer to the observed trend (in particular for Western and Central Europe). However, the results of 65-yr trend for CESM1 (10 members) indicate that trends are largely affected by the presence of the internal variability and more than one realization per model should be used in this assessment.

PRIMAVERA Models: SU(JJA) 1950-2014 Trend in days/65yrs

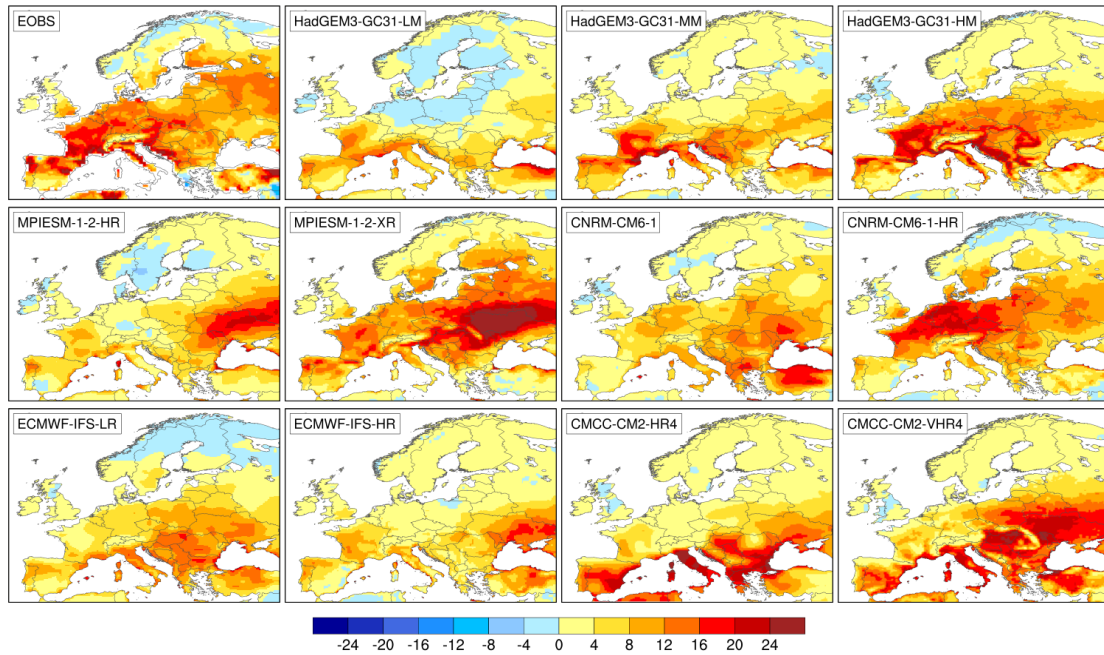


Figure 3.2.2.3: Linear trends in the number of summer days with daily maximum temperature greater than 25°C for the observations (EOBS) and all LR and HR AMIP simulations with the PRIMAVERA models

CESM LENS: SU(JJA) 1950-2014 Trend in days/65yrs

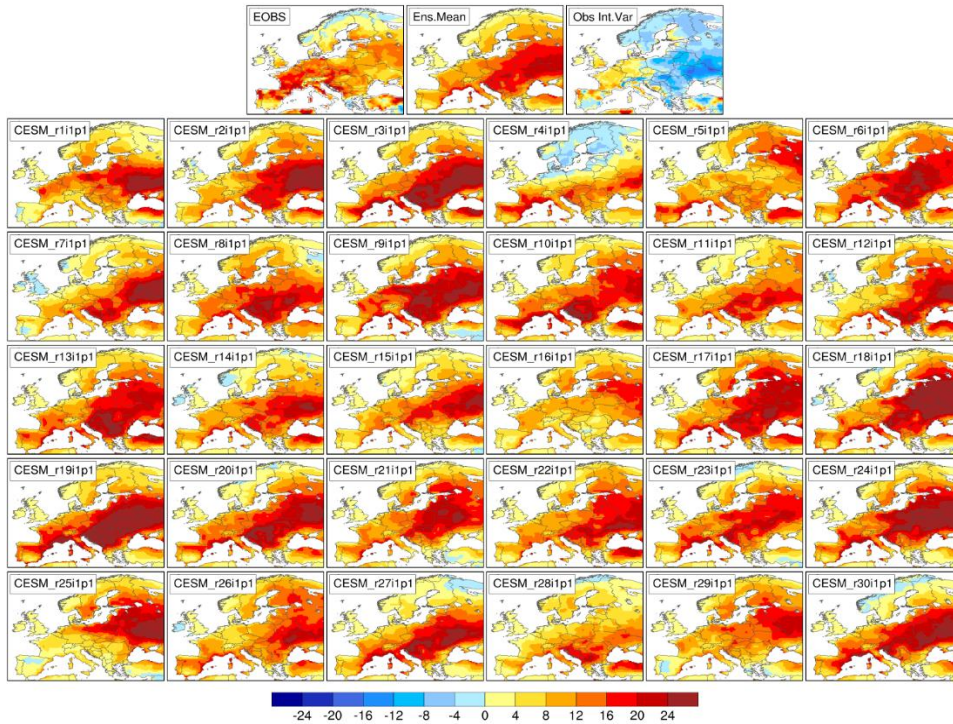


Figure 3.2.2.4: same as figure 3.2.2.1 but for the CESM large ensemble. The first row shows the observations (EOBS dataset), the forced response (the ensemble mean of the 30 individual trends) and the difference between the two.

DEVIATIONS FROM PLANS:

A problem has been identified in the current CNRM-CM6-LR and CNRM-CM6-HR AMIP simulations. The problem is the following: the atmospheric component of CNRM-CM6 only sees ocean SST values and not the ice values as calculated by the 1-D sea-ice model included in our surface scheme. The outcome is that instead of having strongly negative surface air temperature over sea-ice in winter, the values are close to the freezing point ($\sim -2^{\circ}\text{C}$). Another obvious consequence is that the interannual variability of surface air temperature is very weak over sea-ice. Depending on the analysis done by the different partners, this problem may strongly (or not so much) impact the results. The problem has been fixed and these experiments are being run again. We expect to be able to finish the LR within a month and the HR before the end of the year. We will then upload them to Jasmin and replace the old ones.

3.2.3 Extreme precipitation events over Europe (UOXF)

Several studies have shown that spatial resolution can influence the representation of precipitation, particularly extreme precipitation events, in general circulation models, including over Europe (e.g. Scher et al 2017, van Haren et al. 2015). We performed a simple analysis of how the distribution of daily precipitation over Europe changed with resolution in the stream 1 atmosphere-only simulations.

The methodology followed that of Watson et al. (2017). A latitude-longitude box containing Europe was defined as 35-72N, 10W-40E. Model data and re-analysis was first coarsened to a common 2.5x2.5 degree grid, and then subsetted to this region. The primary observational dataset used was daily GPCP data, available from 1996 onwards: model data prior to 1996 was therefore not included. TRMM was used as an alternative dataset to indicate variability between different observational products. Once the data is restricted to the European box over the specified time period, the histogram across all grid-points in the box was computed.

Figure 3.2.3.1 shows the combined histograms for all low and high resolution stream 1 simulations, as well as those of GPCP and TRMM. Remarkably, the change in distribution was virtually identical across each individual stream 1 dataset, matching that shown in figure 3.2.3.1. For all stream 1 models, the low-resolution model shows too little weight in the tail of the distribution, representing too few extreme precipitation events relative to both GPCP and TRMM. In all cases, the increased resolution results in the distribution matching that of GPCP very closely, suggesting that these high-resolution models are now representing the broad-scale distribution of precipitation across Europe very well.

As more nuanced analysis of local changes globally was carried out by Alex Baker et al. from Reading as part of their contribution to this deliverable, no more detailed analysis was carried out of the regional changes within Europe itself. However, to estimate if this increase in precipitation extremes also manifested itself in changes to wind extremes, we computed the same diagnostic for daily maximum surface windspeeds over Europe. This is shown in figure 3.2.3.2, again computed across all stream 1 simulations, for which the changes were broadly similar across the individual models. The changes suggest that there is an increase in extreme weather over Europe more broadly with high resolution, both in terms of precipitation and winds.

Key findings: Increased horizontal resolution leads to an improved representation of extreme precipitation events over Europe.

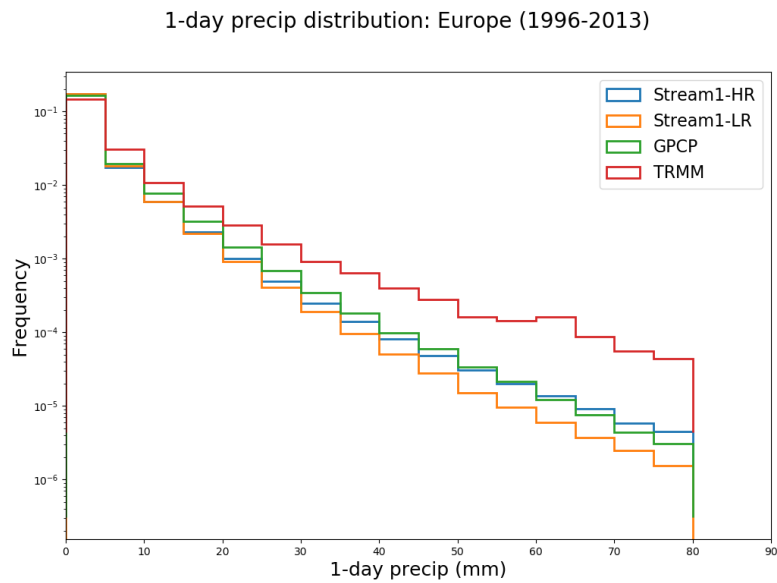


Figure 3.2.3.1: Histograms of daily precipitation over Europe, plotted on a log scale. All low-resolution simulations (orange), all high-resolution simulations (blue), GPCP (green) and TRMM (red).

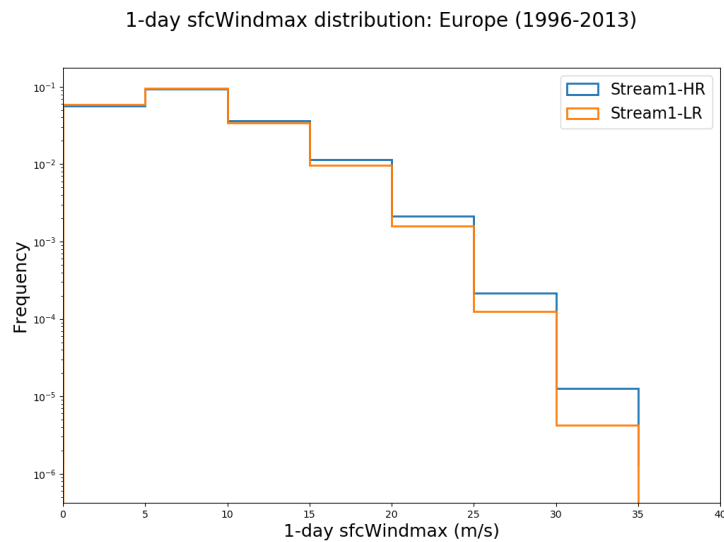


Figure 3.2.3.2: Histograms of daily maximum surface windspeed over Europe, plotted on a log scale. Low-resolution simulations (orange), high-resolution simulations (blue).

3.2.4 Precipitation bias and low frequency variability of tropical summer precipitation (ECMWF)

The annual mean bias in precipitation and its summer-time low frequency variability in the Tropics in Stream 1 AMIP simulations is assessed.

All models exhibit a general wet bias with excessive precipitation over most of the tropics that is largely insensitive to model resolution changes (Fig 3.2.4.1). However, there are marked differences in the spatial patterns of the wet bias across the models. The ECMWF-IFS and EC-Earth3 models have a general wet bias over the west Pacific which is insensitive to the model resolution. CMCC-CM2 shows a prominent narrow band of excessive precipitation over the equatorial Pacific which does not improve with resolution. However, the large wet bias in North Indian Ocean is reduced in their higher resolution version. HadGEM3 and MPI-ESM exhibit large off-equatorial maxima in their wet bias pattern that is likely related to shift in the location of their hemispheric ITCZ. The largest wet bias in HadGEM3 is in the north eastern tropical Pacific, while in MPI-ESM, it is prominent in the north Indian Ocean. CNRM-CM6 shows a distinct belt of excessive precipitation spanning across the equator from the western tropical North Pacific to the southern east Pacific which is largely similar despite a five-fold increase in resolution.

Fig. 3.2.4.2 shows the first EOF pattern of JJAS mean precipitation over the Indo-Pacific region from GPCP and the stream 1 AMIP simulations. The leading mode in GPCP precipitation explains about 25.3% of the total variance and shows opposing signs of variability between the tropical Pacific and the maritime continent and eastern Indian ocean. In comparison, the explained variance of the leading mode varies between 17.7 to 23.1% among the AMIP simulations.

Unlike the similarity in pattern of biases, the EOF patterns of precipitation show large differences across model resolution. ECMWF-IFS sees an improvement in the pattern and strength of variability with increased resolution. Interestingly, the standard resolution of CMCC-CM2 appears to be most robust in capturing the observed pattern of precipitation variability among all the models. HadGEM3 and EC-Earth3 show excessive variability over the western North Pacific. High variability over the western tropical North Pacific in CNRM-CM6 is reduced with increased resolution but worsens in CMCC-CM2 and EC-Earth3. MPI-ESM and CNRM-CM6 exhibit excessive variability over the north Indian Ocean that appear to improve slightly in CNRM-CM6 but worsens in MPI-ESM.

Key results:

Systematic improvement in mean precipitation bias and representation of the spatial mode of variability with increased resolution is not immediately evident across the Stream 1 simulations. Nevertheless, the mean absolute bias is somewhat lower in 4 out of 6 models in their higher resolution versions (Fig. 3.2.4.1). Further systematic multi-model analysis will be needed to quantify the causes of model behaviour.

Annual mean bias in Oceanic Precipitation relative to GPCP (mm/day) 1981-2010

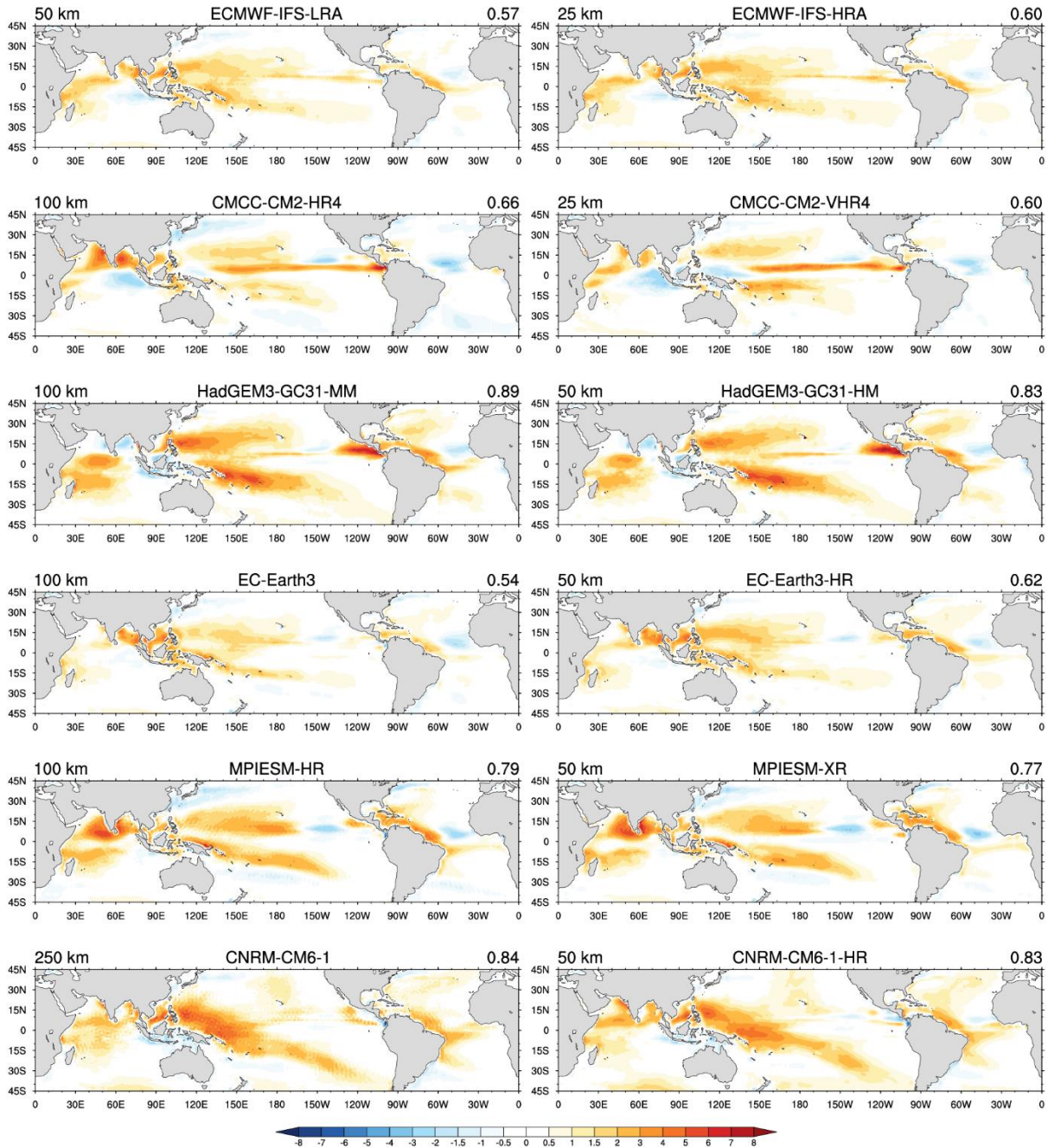


Fig. 3.2.4.1: Annual mean bias in precipitation (mm day^{-1}) relative to GPCP for 1981-2010 in the standard (left panels) and high resolution (right panels) version of Stream 1 AMIP simulations. The top left of each panel shows the nominal resolution of the model and the top right shows the mean absolute bias.

EOF1 of Precipitation (mm day^{-1}) JJAS 1981-2010

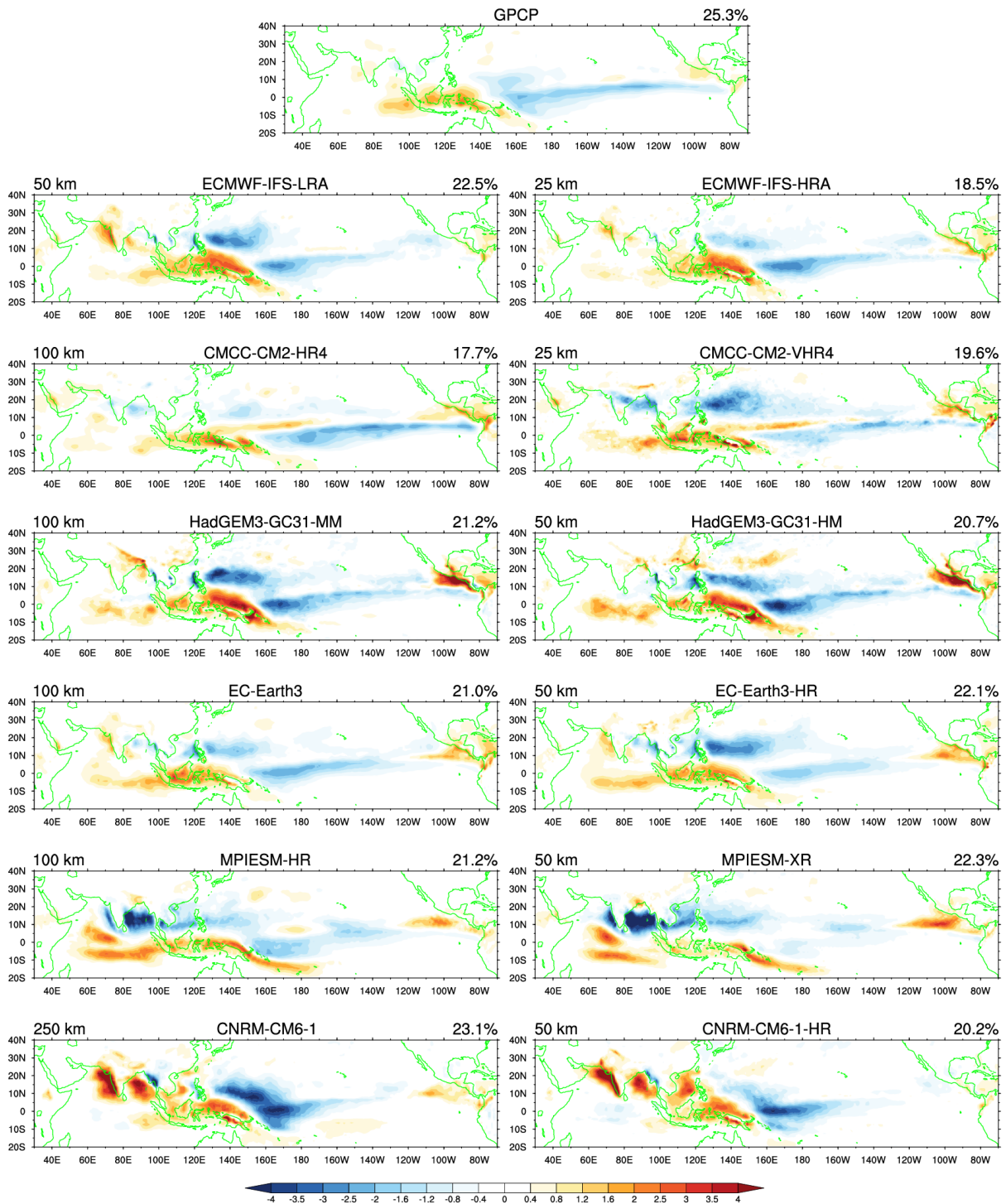


Fig. 3.2.4.2: First EOF pattern of JJAS mean precipitation over the Indo-Pacific region during 1981-2010 from GPCP and the standard (left panels) and high resolution (right panels) version of Stream 1 AMIP simulations.

3.2.5 Euro-Atlantic circulation regimes (UOXF, CNR)

Predicting the evolution of the atmospheric state over time can be understood as a question of determining likely trajectories along the atmosphere's climate attractor in phase space. Over the last two decades, evidence has begun to accumulate that suggests the geometry of this attractor exhibits interesting local structure which manifests itself in the form of quasi-persistent weather regimes (e.g. Straus et al. 2007, Woollings et al. 2010, Franzke et al. 2011, Hannachi et al. 2017). In particular, such regimes have been identified in the Euro-Atlantic region, and there is a growing recognition of their importance in modulating European weather (Ferranti et al. 2015, Matsueda et al. 2018, Frame et al. 2013) and, conjecturally, the regional response to anthropogenic forcing (Palmer 1999, Corti et al. 1999). Representing these regimes correctly is therefore an important goal for any general circulation model (GCM). Previous studies (Dawson et al. 2012) had suggested that high horizontal resolution may be an important factor in achieving this, though the result was only for a single model. We extended this analysis to the full PRIMAVERA Stream 1 dataset, as well as pre-PRIMAVERA data to obtain a multi-model picture of the sensitivity of the regimes to resolution in atmosphere-only mode.

Regimes are identified by applying a k-means clustering algorithm to the daily 500hPa geopotential height anomalies, following the methodology of Dawson et al. 2012. Both NCEP and ERA-Interim re-analysis products show evidence for the existence of four regimes in the period 1979-2015 covered by these products (dubbed NAO+, NAO-, Blocking and Atlantic Ridge), shown in figure 3.2.5.1. Therefore, the algorithm was specified to look also in model data for four distinct clusters, and these were then matched with the regimes in figure 3.2.5.1 based on pattern correlation (Dawson et al. 2012). To diagnose a model simulation's ability to represent these regimes well, we considered three aspects of the data. Firstly, how tightly clustered is the model data compared to re-analysis (i.e. how robust is the regime structure). Secondly, how similar the regime patterns of the model data are compared to those in re-analysis. Finally, what are the persistence statistics of the model regimes compared to those in re-analysis.

Figure 3.2.5.2 shows how the 'significance metric' changes in the stream 1 models when increasing resolution. This metric gives a measure of how tightly clustered the dataset is relative to what is expected from random sampling variability (see Dawson et al 2012 for details), and so measures the robustness of the model regimes. It can be seen that for three of the models, significance goes up, while for three models it goes down, suggesting that resolution is not systematically improving this metric. However, work on pre-PRIMAVERA data, where multiple ensemble members were available for a subset of three models (EC-Earth3, HadGEM, and the MRI model), showed that there is significant sampling variability in this metric across ensemble members: while some of the high-resolution simulations did perform worse for this metric than some low-resolution simulations, when averaged over multiple ensemble members the high-resolution simulations performed better. Since all the stream 1 data considered had only 1 ensemble member, we cannot rule out considerable sampling variability. When averaging significance across all available low/high-resolution models, including pre-PRIMAVERA data with multiple ensemble members, we find that significance goes up with increased resolution by about 6%, but with a large standard deviation of around 15%. It is likely that multiple ensemble members for all stream 1 models would be required to see a more robust impact.

Figure 3.2.5.3 shows a Taylor diagram summarizing the impact on the spatial patterns of the regimes found in model data. While for some models and regimes, resolution improves the similarity with re-analysis, in many cases it is degraded. On average across all models (including pre-PRIMAVERA data), the impact of increased resolution is a small degradation of the pattern. Figure 3.2.5.4 shows an explicit example of this, for the HadGEM model, where the blocking regime matches re-analysis less at higher resolution. Studies have linked the location of blocking events to the mean state of models, so it is possible that differences in the mean state between high and low resolution simulations is playing a large role here.

When it comes to the persistence of the regimes, we found a systematic improvement only with the Blocking regime, shown in figure 3.2.5.5. We estimated, for each DJF season, the persistence probability of the regime (by modelling the atmosphere's transitions between the 4 regimes during the 90 days of DJF as a first-order Markov chain), and fitted reverse log-normal probability distributions to the histograms. In general, the low-resolution models can be seen to have too weak levels of persistence, with too much weight in the low-persistence part of the distribution. For all but the CNRM and CMCC model, this was improved with increased resolution: it is possible that a bug in the CNRM model, corrupting the sea-ice in the simulations, is influencing its regime behavior.

In conclusion, increasing the horizontal resolution leads in general to improved levels of persistence for the Blocking regime, and, when averaged across enough ensemble members, to a small improvement in the robustness of the regime structure. For some models, where multiple ensemble members were available, the improved regime structure appears very robust. Due to the large sampling variability, it is unclear with the other models if resolution is improving or degrading the regimes. In terms of the spatial patterns, no meaningful change was observed with increased resolution. A paper detailing these results for pre-PRIMAVERA data is in preparation (Strommen et al. 2018).

Key findings:

Increased resolution appears to improve the geometric robustness of North Atlantic regimes, as well as the persistence statistics of the blocking regime, but there is considerable sampling variability and no other aspects of the regimes are systematically improved.

North-Atlantic weather regimes - ERA

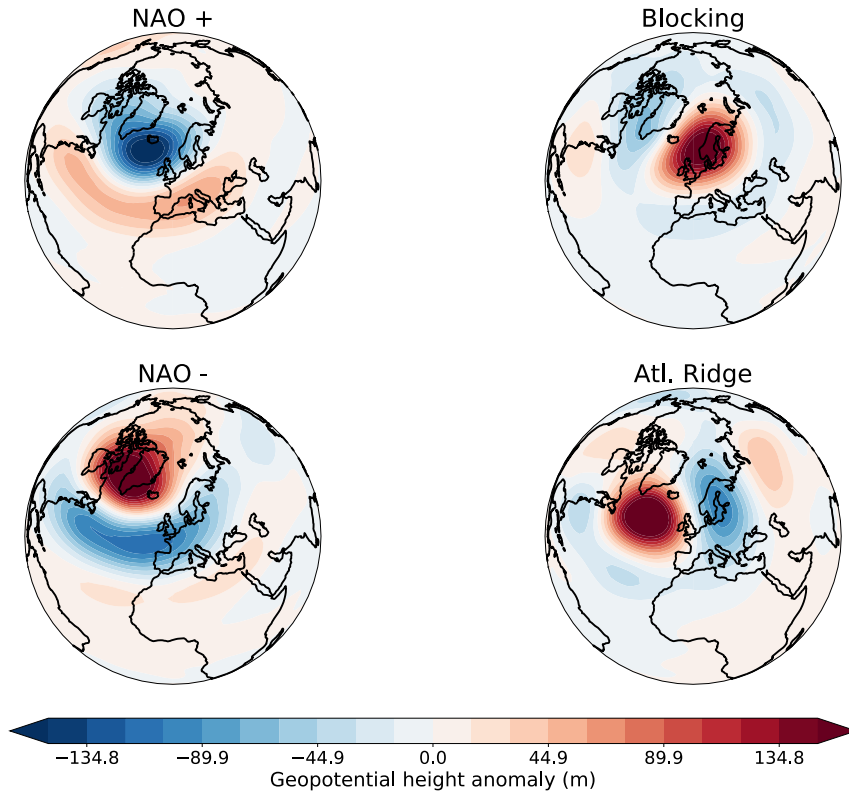


Figure 3.2.5.1: The four Euro-Atlantic regimes, as computed from the re-analysis ERA-Interim.

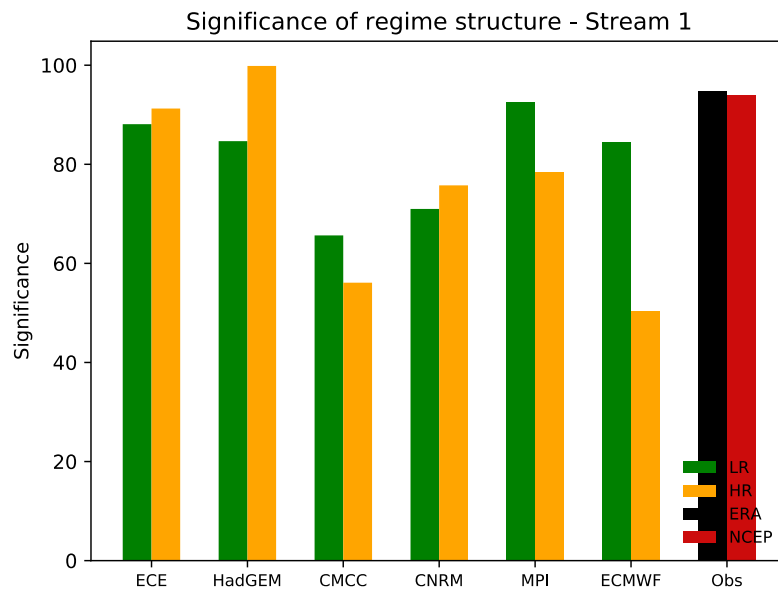


Figure 3.2.5.2: The significance of the level of clustering in the Stream 1 data.

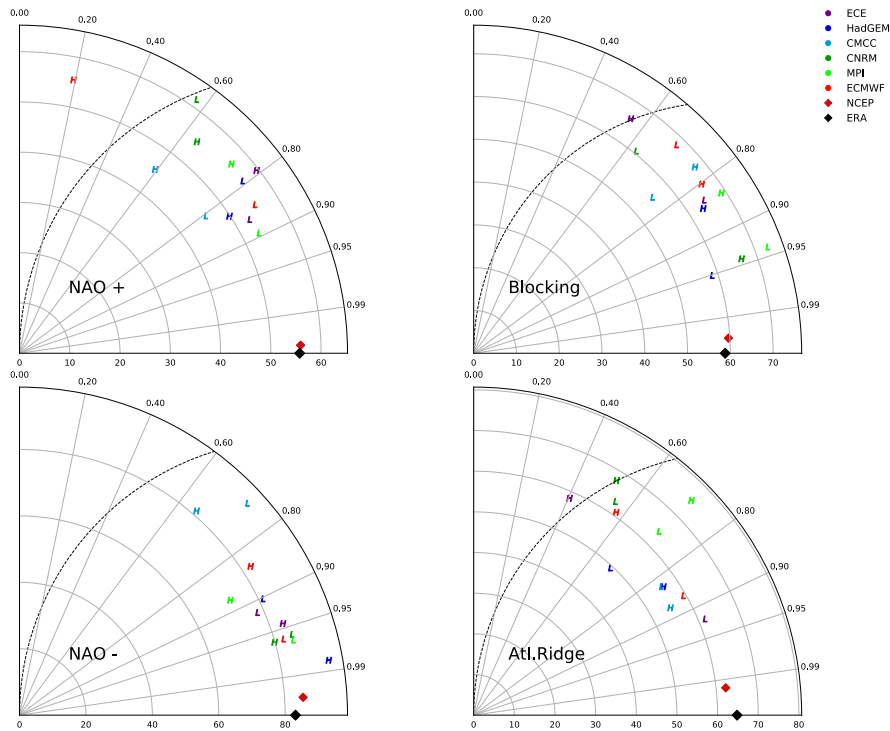


Figure 3.2.5.3: Taylor plot representation of the visual similarity between the model clusters (low resolution simulations shown with an L, high-resolution with an H) and those in re-analysis (ERA-Interim). Pattern correlation with ERA-Interim (black diamond) is denoted by the outer arc, the axes represent the standard deviation of the patterns, and the RMS error to ERA-Interim is denoted by the distance from ERA to the model point.

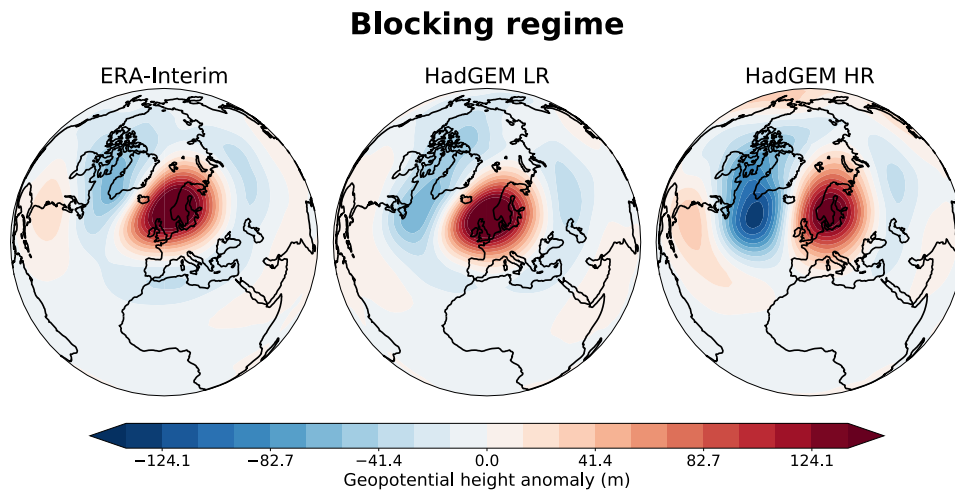


Figure 3.2.5.4: The Blocking regime in ERA-Interim (left), HadGEM low-resolution (middle) and HadGEM high-resolution (right).

PDFs of BLK persistence probabilities (1979-2014)

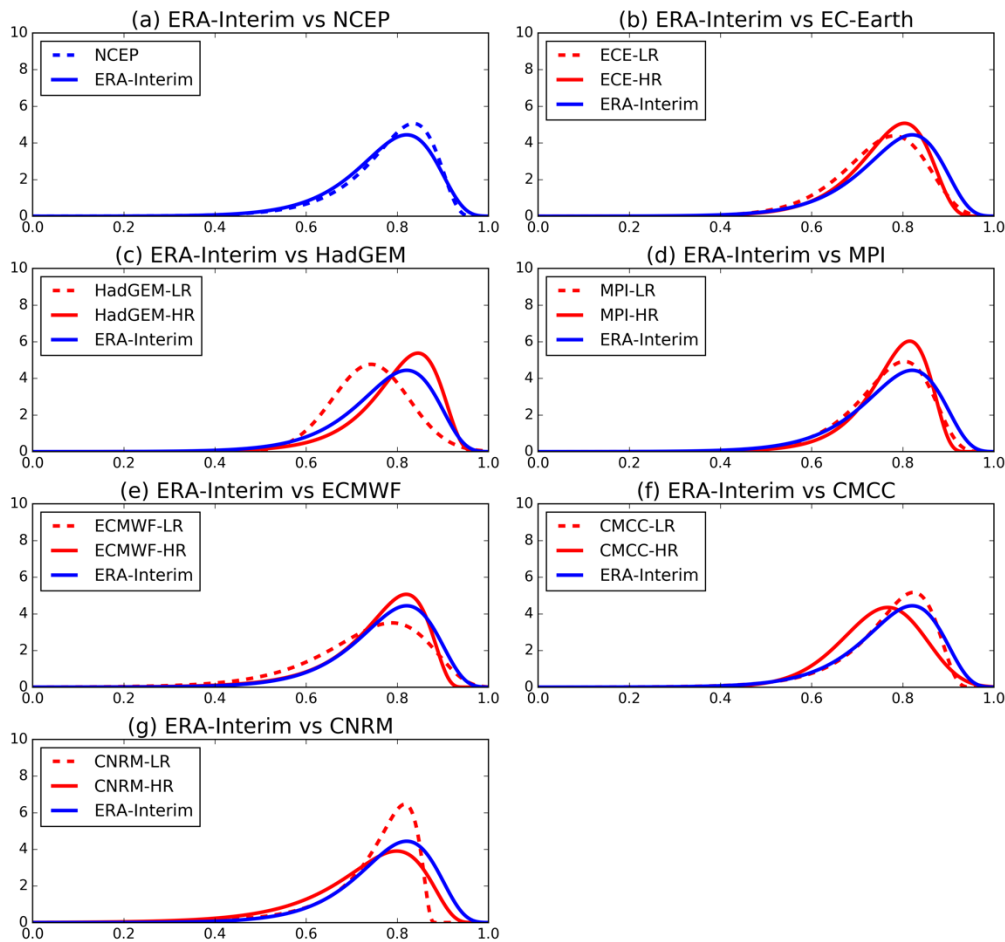


Figure 3.2.5.5: Distributions of seasonal persistence probabilities. ERA-Interim shown in blue, with low-resolution in stippled red and high-resolution in solid red.

3.2.6 Teleconnections with tropical Indo-Pacific rainfall (ECMWF)

Teleconnections from the tropics affect the atmospheric circulation in the extratropical regions on time scales ranging from sub-seasonal to inter-decadal. Although they can be detected throughout the whole yearly cycle, many teleconnection patterns affecting the northern midlatitudes reach their largest amplitude during the northern winter, when the strong vorticity gradients in the subtropical regions intensify the Rossby wave sources associated with tropical convection (eg Sardeshmukh and Hoskins 1988).

A detailed analysis of teleconnections originated from tropical Indo-Pacific rainfall anomalies during the northern winter in the ECMWF seasonal forecast System 4 was carried out by Molteni et al. (2015, MSV hereafter). In addition to the widely studied ENSO teleconnections, MSV focussed on rainfall variability in the western and central Indian Ocean as a source of teleconnections affecting the North Atlantic and Europe, with a clear impact on the North Atlantic Oscillation (NAO). Results for the DJF seasonal means were consistent with the links between Indian Ocean rainfall and the NAO detected on the sub-seasonal time scale (Cassou 2008; Lin et al. 2009).

Here, we use the same methodology as in MSV to analyse teleconnections in the AMIP-type simulations of Stream 1. Data from five models at both low and high resolution are used in the diagnostics, namely from CMCC-CM2, EC-Earth3, ECMWF-IFS, MOHC-HadGEM3 (including a mid-resolution version), MPI-ESM. The analysis procedure is applied to DJF seasonal means from 1950-51 to 2009-10, comparing model results with observational estimates based on the CERA20C re-analysis (Lalouaux et al. 2018), and consists of the following steps:

- time series of rainfall anomalies (w.r.t. a 1951-2010 climatology) are computed over two areas: the Western-Central Indian Ocean (WCIO: 40E-90E, 10N-10S) and a latitudinally widened version of the NINO4 region (NINO4w: 160E-150W, 10N-10S);
- the covariance of these time series (normalised by their standard deviation) with global anomalies of rainfall, 500-hPa geopotential height and 850-hPa temperature are computed;
- for different target regions, model teleconnections are compared to the corresponding re-analysis patterns through Taylor diagrams;
- in order to quantify the difference between model and re-analysis results, a normalised rms error is defined as the rms distance between the observed and modelled covariances, divided by the average amplitude of the two covariance patterns (by definition, this metric is bound to be between 0 and 2, with the maximum value corresponding to an exact anti-correlation of the two patterns).

As an example, the teleconnections of WCIO and NINO4w rainfall with 500-hPa height over the northern extratropics from the low- and high-resolution version of ECMWF-IFS are shown in Fig 3.2.6.1, together with the CERA20C counterparts. Although ensembles of 6 and 4 members respectively have been run for the two resolutions, results in Fig. 3.2.6.1 refer to the first ensemble member, whose data can be downloaded from the JASMIN data repository. Over the North Pacific, model and re-analysis patterns are positively correlated for both tropical sources and both model resolution. Over the North Atlantic, a positive NAO signal is associated with positive WCIO rainfall anomalies at both resolutions; however, while the teleconnection with NINO4w rainfall has a weak, negative projection on the NAO in the observations, the low-resolution model gives a nearly opposite signal, while the high-resolution version shows a much smaller error. This is quantified in the Taylor diagrams for the Euro-Atlantic region shown in Fig. 3.2.6.2, where the square marks representing the teleconnections from NINO4w are much closer to the observation reference (black square) in the high-resolution diagram (right panel) than in the low-resolution diagram (left panel). The normalised error of the NINO4w teleconnections (averaged over 500-hPa height and 850-hPa temperature) in the high-resolution model is less than half the error of the low-resolution model.

The result of the teleconnection analysis over the multi-model AMIP simulations is summarised in Fig. 3.2.6.3, which compares normalised errors for WCIO (left) and NINO4w (right) teleconnections over the Euro-Atlantic region obtained with the low- and high-resolution versions of the five models listed above. Overall, a consistent signal in favour of the high-resolution versions cannot be detected, with differences between model being as large as (or larger than) resolution impacts. For the NINO4w teleconnections, it is puzzling to note that the low-resolution version of HadGEM3 outperforms the higher resolution versions; however, this result does not apply to the early part of the winter (see the Nov-Dec results in Sect. 3.4), when the impact of ENSO variability on the North Atlantic circulation has a

radically different pattern. With regard to the ECMWF results, an analysis carried out on all ensemble members confirms that the large errors in the NINO4w teleconnection of the low-resolution model are significantly reduced by the resolution increase.

This analysis will be extended to the historical coupled simulations as soon as a comparable number of model experiments will be available for download (Molteni et al., in preparation). In the meanwhile, some preliminary results from the ECMWF coupled model are discussed in Roberts et al. (2018).

Key findings:

Teleconnections from tropical rainfall in the NINO4 region are realistically simulated by the Stream 1 AMIP-type simulations, while the connections between Indian Ocean rainfall and circulation over the North Atlantic are generally affected by larger errors. An improvement with increased atmospheric resolution cannot be consistently detected.

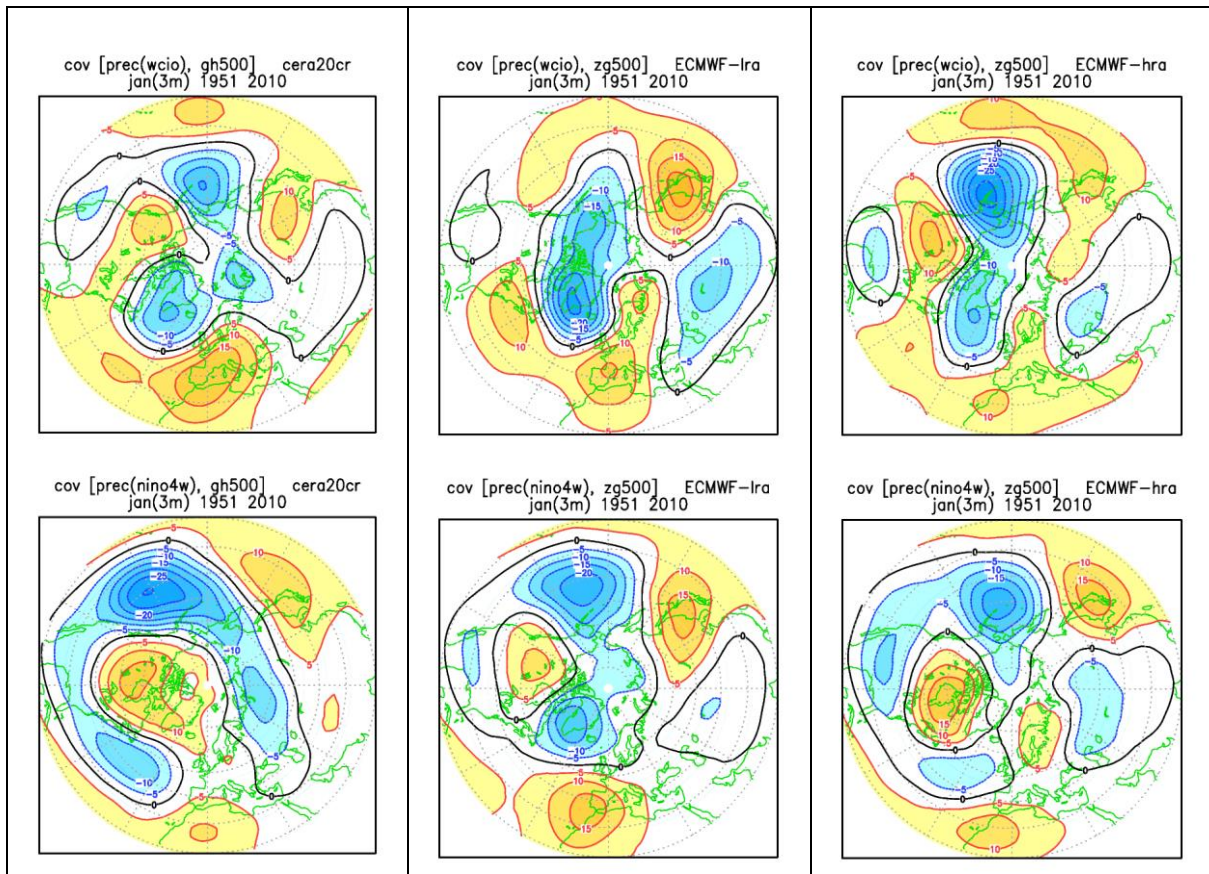


Fig. 3.2.6.1 Top row: Covariances between normalised DJF rainfall anomalies in the western/central Indian Ocean (WCIO) and 500-hPa height anomalies over the northern extratropics in 60 winters, from DJF 1950/51 to DJF 2009/10. Left panel: from CERA20C data; central panel: from the low-resolution ECMWF-IFS simulation with prescribed SST (1st ensemble member); right panel: from the high-resolution ECMWF-IFS simulation with prescribed SST (1st ensemble member). Bottom row: as in top row, but for covariances with rainfall in the NINO4w region.

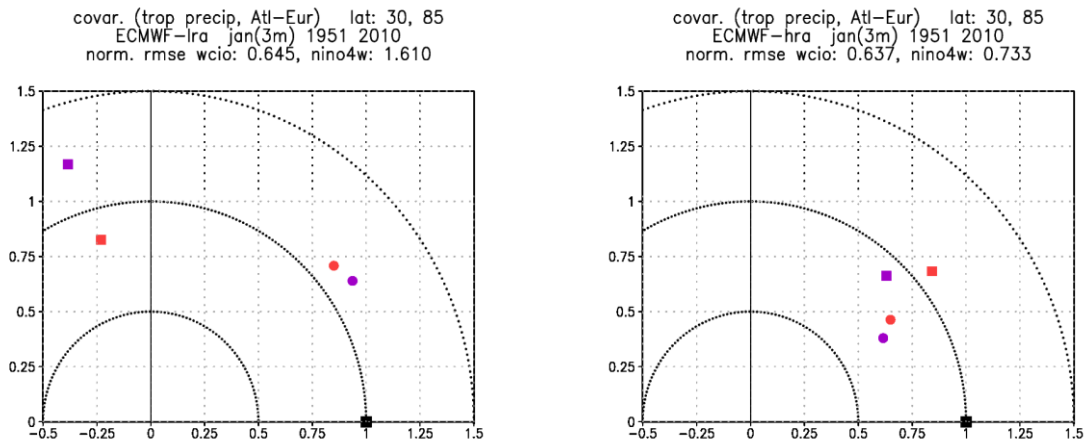


Fig. 3.2.6.2 Taylor diagram representing covariances of 500-hPa height (purple marks) and 850-temperature (red marks) in the Atlantic-European sector (30-85N, 80W-40E) with tropical rainfall in the WCIO (circles) and NINO4w (squares) region, for the low-resolution (left) and high-resolution (right) simulations of ECMWF-IFS with prescribed SST. The normalised rms error is defined as the rms distance between the observed and modelled covariances, divided by the average amplitude of the two covariance patterns.

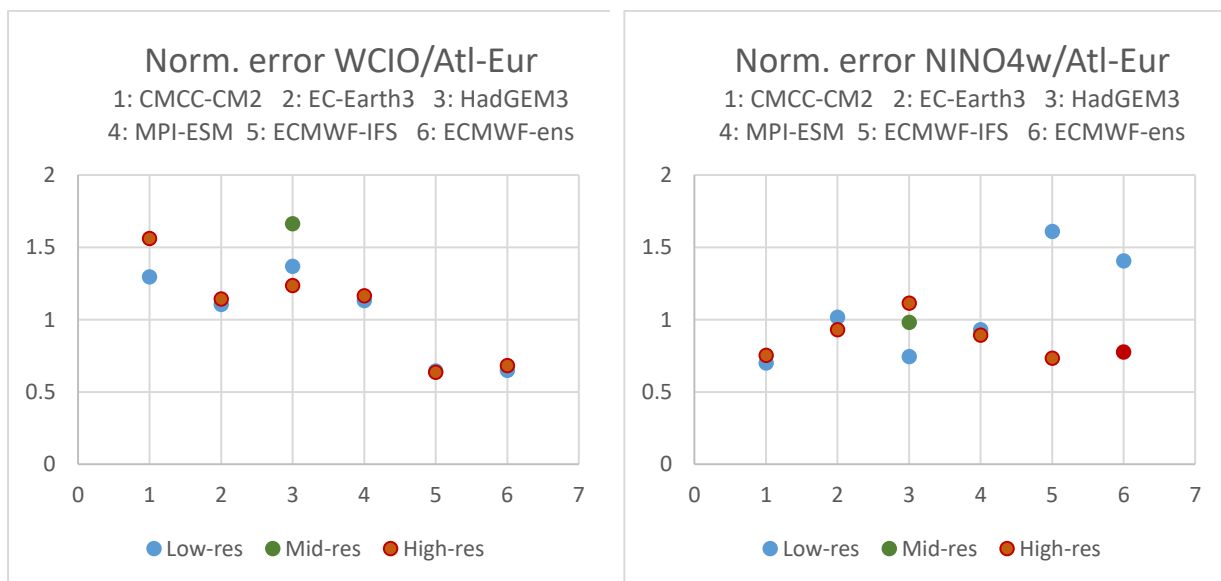


Fig. 3.2.6.3 Normalised error of covariances of 500-hPa height and 850-temperature in the Atlantic-European sector (30-85N, 80W-40E) with tropical rainfall in the WCIO (left) and NINO4w (right) region, for the low-resolution (blue circles), mid-resolution (green circle) and high-resolution (brown circles) simulations of 5 PRIMAVERA models with prescribed SST. All data are from single-member simulations, except for the last two values on each diagram, which represent errors of covariances averaged over a 6-member low-resolution and a 4-member high-resolution ensemble with ECMWF-IFS (blue and brown circles respectively).

3.2.7 Tropical cyclones (MOHC, KNMI, CMCC)

a) Analysis of tropical cyclones using tracking algorithms (MOHC)

A manuscript describing the multi-model tropical cyclone (TC) performance of the atmosphere-only simulations, following the HighResMIP experimental design, in the North Atlantic is close to submission (Roberts et al.). This analysis uses the TRACK feature tracking algorithm (Hodges et al. 2017). As expected, the higher resolution models typically have more TCs, and are able to simulate more intense TCs (see figure 3.2.7.1). For most models this increased intensity is mainly due to deeper mean sea-level pressures (MSLP) minima, but for CNRM-CM6 and CMCC-CM2 models an improvement in the near-surface wind speed is also particularly notable, taking them closer to observations. Higher resolution also typically improves the storm structure, and the TC spatial distribution, all of which are important for climate impacts.

Assessing the skill in simulated variability is more difficult using only one ensemble member, due to weather noise. Hence the HadGEM3-GC3.1 model has been assessed with 13 members in the 1979-2014 period (at the two lower resolutions), and clearly shows an increase in skill between LM and MM resolutions (nominally 250km and 100km respectively), with little further change to HM (nominally 50km) – see figure. There is potential to include more models in this analysis, where more ensemble members with the required output data is available.

A second tracking algorithm called TempestExtremes (Ullrich and Zarzycki, 2017) has also been implemented to complement these TRACK results, and the above conclusions are robust to algorithm changes. A second manuscript on comparing the algorithms has also been started. The tropical cyclone tracks have been written to formatted netcdf files with a view to publishing them on CEDA archives, and hence making them accessible for CMIP6 and IPCC communities. They are also being used for a variety of other studies within the project.

Key finding:

Higher resolution leads to the simulation of more intense tropical cyclones, while to assess skill in interannual variability skill at least 5 members or more are needed.

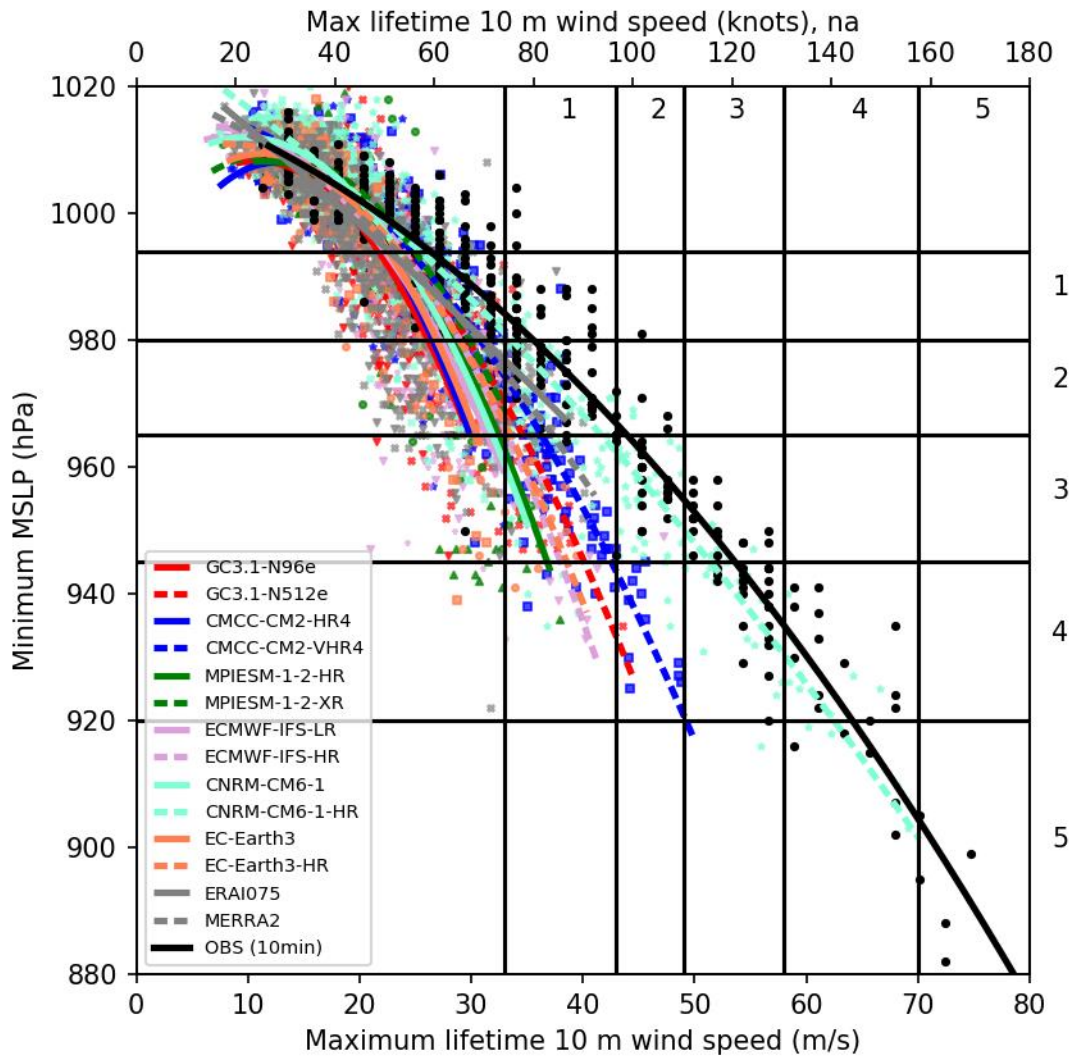


Figure 3.2.7.1: Tropical cyclone mean sea-level pressure (MSLP) vs 10m wind speed at peak intensity. Lower resolution models have solid lines, and higher resolution dashed. Tropical cyclone intensities (measured by Cat 1-5) are indicated for both the accepted wind speed measure, and also for a measure based on pressure. GC3.1 model is HadGEM3-GC31 - N96e is resolution LM (nominally 250km), N512e is HM (nominally 50km).

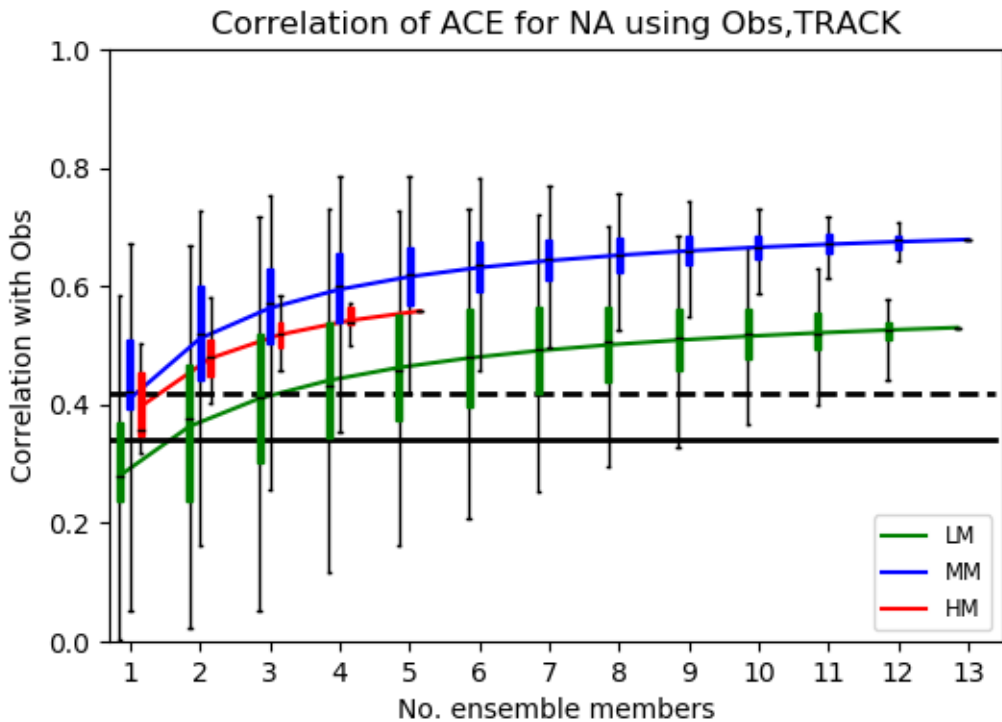


Figure 3.2.7.2: Correlation of model tropical cyclone ACE (Accumulated Cyclone Energy) for the North Atlantic (NA) over 1979-2014 against observations for ensembles of simulations (a total of 13 members at both MM (nominally 100km) resolution and LM6 (nominally 250km), and 5 members at HM (nominally 50km resolution)). For each combination of n ensemble members (x axis), a box and whiskers are plotted (the box showing the lower to upper quartile range, with a line at the median, while the whiskers show the range of the data). The mean correlations for each n ensemble member correlation are joined up by the line. The solid and dashed lines indicate the 95% and 99% confidence levels respectively (assuming each of the 36 years are independent samples).

b) Cyclones with a tropical origin that reach Europe (KNMI)

Before the start of PRIMAVERA, KNMI has analyzed, using high-resolution simulations of EC-Earth2.3, the possibility that hurricanes become a threat for Europe in a warmer climate. Those results showed a marked increase of storms with hurricane intensity that have a tropical origin. Further analyses revealed that those storms are characterized by a warm seclusion structure. Within the PRIMAVERA project we have verified this for the observed storms that have reached Europe using the MERRA re-analyses data set. The results indeed show that the strongest cyclones with a tropical cyclone that reach Europe are warm-seclusion storms (Dekker et al. 2018).

For the Stream 1 AMIP simulations (1950-2014) we have analyzed the statistics and characteristics of the cyclones with a tropical origin that reach Europe. This has been done in collaboration with the Met. Office and the Univ. of Reading. The Met. Office has computed the tracks and analyzed the characteristics of tropical cyclones. We have used those tracks to investigate the tropical cyclones that reach Europe. We analyzed the statistics of those storms, such as frequency, tracks, duration and seasonal dependence and compared them with observed storms using different re-analyses data sets. The re-analyses data sets were

analyzed by the University of Reading, who provided us with their results. Next to these statistics we have focused on the question whether indeed in the PRIMAVERA models the strongest storms reaching Europe have the warm-seclusion structure.

All models exhibit a good response in reproducing the above-mentioned processes apart from CMCC-CM2-VHR4 and MPIESM-1-2-XR. This result is mainly attributed to data limitations for the former model, but possibly to a poor performance for the latter model. CNRM-CM6-HR and HadGEM3-GC31-HM generate a higher than normal number of tropical cyclones in general whereas EC-Earth3-HR and MPIESM-1-2-XR generate a lower number. Concerning the number of tropical cyclones that arrive in Europe, CNRM-CM6-HR and HadGEM3-GC31-HM are the only models simulating a realistic value. In general, no distinct preferable genesis region for the systems that reach Europe was observed, however, the systems which additionally transform into warm-seclusion storms originate from the western tropics. The Hart-phase diagrams for all models, apart from MPIESM-1-2-XR and CMCC-CM2-VHR4, demonstrate the typical evolution of these systems that reach Europe, beginning from the tropical stage to extra-tropical, to warm seclusion and then to decay. The same models simulate more than or close to 50% of the systems that arrive in Europe to be warm-seclusion storms which also acquire the highest intensity. The comparison with re-analysis data reveals similar features for the pressure although it displays small discrepancies concerning the genesis regions and the frequency of the TCs that reach Europe. A draft is being prepared and will be submitted in the beginning of 2019. The analyses will be extended to 2050 as soon as the CMIP6 future forcing is available and the simulations have been completed and uploaded to JASMIN.

Key findings:

Most PRIMAVERA models simulate qualitatively correctly the statistics and dynamics of tropical cyclones that reach Europe. In particular, those that represent a warm seclusion structure occur predominantly and are also the strongest ones.

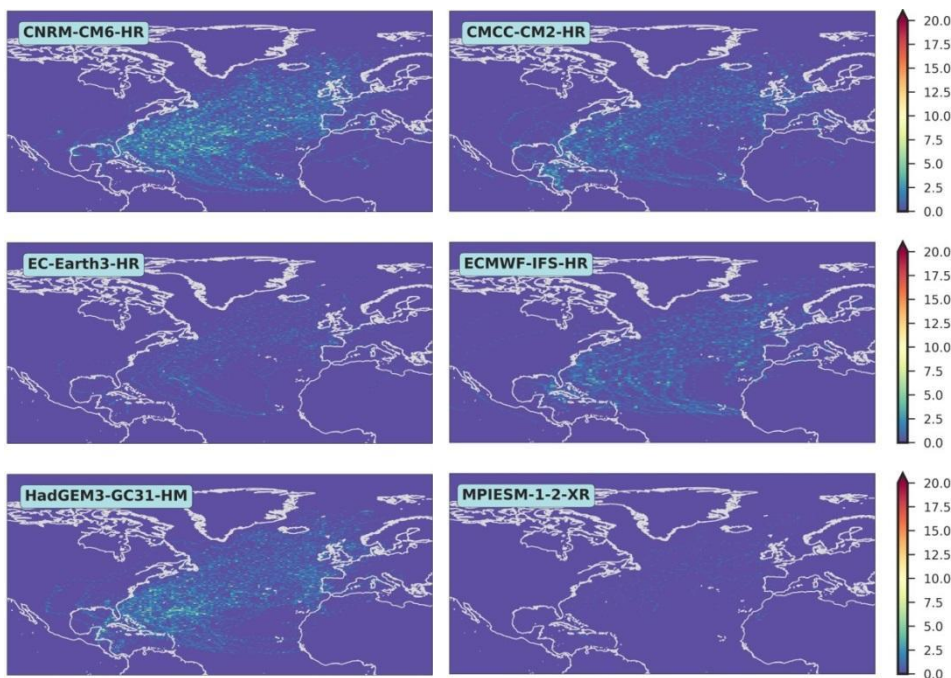


Figure 3.2.7.3. Track density of tropical cyclones in PRIMAVERA that enter Europe for 1950-2014.

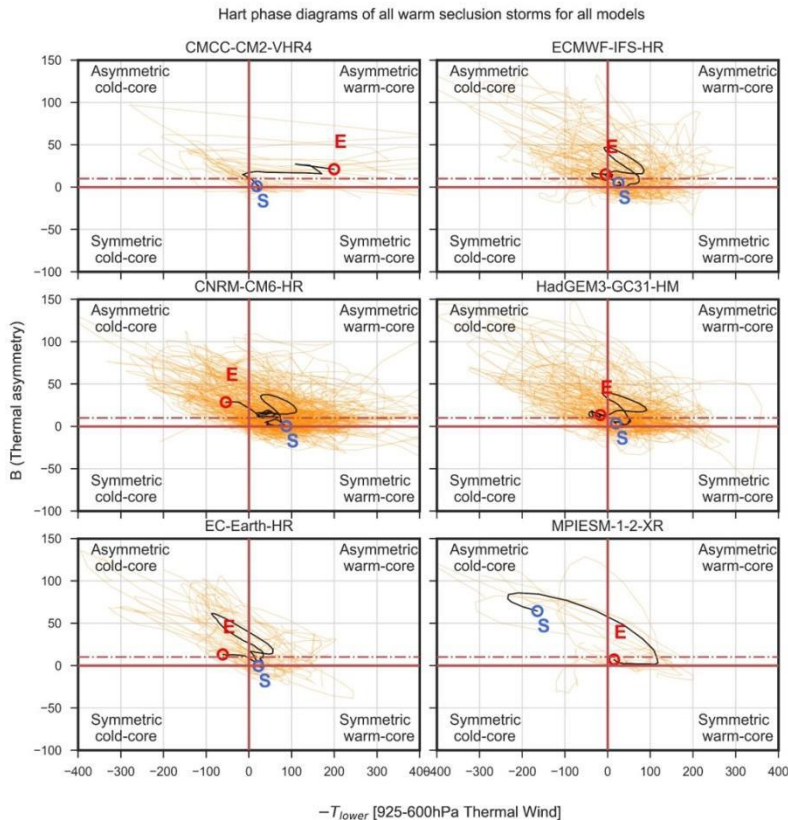


Figure 3.2.7.4 Hart phase diagram of B - T_{lower} for all warm seclusion storms that reach Europe.

c) Link between North Atlantic tropical cyclones water content and environmental conditions (CMCC).

The moisture associated with Tropical cyclones (TCs) across the North Atlantic and its relation with environmental conditions is investigated in a multi-model set of highresSST-present (AMIP-like) experiments (atmosphere-only simulations forced with observed SSTs for the 1950-2014 historical period) performed at different spatial resolutions, under the HighResMIP protocol (Table 1).

TC tracks from different PRIMAVERA general circulation models have been diagnosed following the TRACK tracking algorithm (Hodges 1995, 1996, 1997; Bengtsson et al. 2007), while the observed ones have been computed from the IBTRACS dataset (Knapp et al., 2010; Figure 3.2.7.5). For the present analysis, the more recent 1985-2014 period has been considered. The radial average values of specific humidity computed following each TC track is used as representative of the water content related to each TC. This calculation is applied to seven vertical levels (1000, 925, 850, 700, 600, 500, and 250 hPa). The fields of the JRA55 (Kobayashi et al. 2015) reanalysis are used as observational counterpart (Figure 3.2.7.6).

At this stage, the comparison between model results and observations highlights a general underestimation of specific humidity related to TCs compared to observations (Figure

3.2.7.6). However, the increase in model resolution leads to a better reproduction of specific humidity related to TCs (Figure 3.2.7.6), envisaging an improvement in the representation of TCs water content in models' high-resolution configuration.

Afterwards, the amount of water related to each TC track is vertically integrated to obtain a measure of the time evolution of moisture associated to each TC, as a function of radial distance from the TC center (Figure 3.2.7.7a). To emphasize the diverse impact of TCs along the North Atlantic basin, the computed values are clustered into six classes defined by six latitudinal bands (5-15°N, 15-25°N, 25-35°N, 35-45°N, 45-55°N, 55-65°N).

Finally, the values are integrated also along the radial distance axis in order to obtain an index of the annual amount of moisture related to the TC (Figure 3.2.7.7b). This index, then, is compared with environmental condition denoted by local climate indexes, such as North Atlantic Oscillation (NAO) and Atlantic Multidecadal Oscillation (AMO). When comparing observed TC moisture index and NAO, a negative correlation is found for all of the six latitudinal bands (Table 2), conversely a direct relation is obtained between TC moisture index and AMO except for the 35-45°N latitudinal band where no significant correlation is found. When applied to models, this analysis reveals a wide range of behaviors. While, for a large set of latitude bands no significant correlation between the TC moisture index and the selected climate variability indices is found, it is interesting to notice how one specific model reveals an emergent consistency with the observations after increasing the horizontal resolution. Specifically, CMCC-CM2-VHR4 shows the same type of relation as the observed one for both NAO and AMO, differently from its low-resolution configuration (CMCC-CM2-HR4, Table 2). Further investigation is ongoing to disentangle the role of TC persistence over the different meridional bands in determining the TC associated humidity dependence on the different NAO and AMO phases. A similarly consistent relation between model and observations is found for EC-Earth3, although no significant impact of resolution is found.

	CMCC-CM2	EC-Earth3	HadGEM3-GC31
Low Resolution	100 km	100 km	100 km
High Resolution	25 km	50 km	50 km

Table 1: nominal resolution of the set of highresSST simulations used in this analysis.

	5-15N	15-25N	25-35N	35-45N	45-55N	55-65N
JRA55						
NAO	-0.41	-0.47	-0.38	-0.26	-0.26	-0.37
AMO	0.53	0.64	0.38	0.22	0.53	0.53
CMCC-CM2-HR4 low resolution						
NAO	0.43	0.38	0.10	-0.16	0.02	-0.06
AMO	0.33	0.10	-0.04	0.05	0.24	0.06
CMCC-CM2-VHR4 high resolution						
NAO	-0.05	-0.13	-0.29	-0.33	-0.24	0.07
AMO	0.56	0.09	0.07	0.19	0.27	0.44
EC-Earth3-LR low resolution						
NAO	-0.13	-0.05	-0.07	-0.12	-0.05	-0.30
AMO	-0.09	0.45	0.47	0.24	0.07	0.07
EC-Earth3-HR high resolution						
NAO	-0.10	-0.17	-0.41	-0.18	-0.33	-0.02
AMO	0.28	0.16	0.32	-0.15	-0.18	-0.24
HadGEM3-GC31-MM low resolution						
NAO	-0.24	0.14	0.05	0.10	-0.21	-0.14
AMO	0.04	-0.17	0.11	0.19	-0.02	0.19
HadGEM3-GC31-HM high resolution						
NAO	-0.01	-0.04	0.04	-0.10	0.13	-0.43
AMO	-0.19	0.11	-0.02	0	-0.56	-0.08

Table 2: correlation values between TCs moisture index and NAO and AMO indexes. Values in blue cells exhibits a direct relation between indexes, while an inverse relation characterizes orange cells. The values reported in the coloured cells are significant at 90%, tested by means of a Monte Carlo method. The non-significant values are reported in white cells.

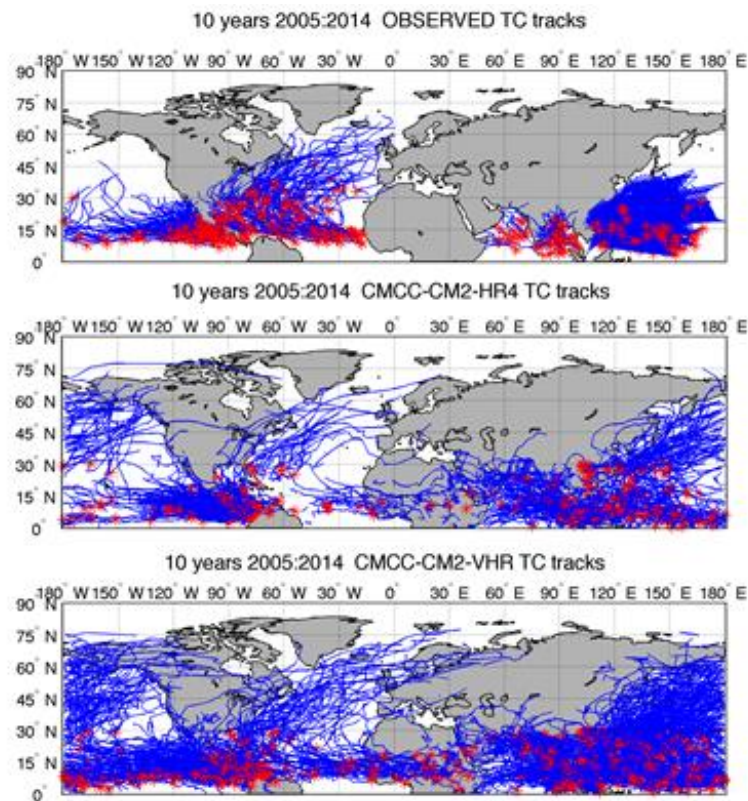


Figure 3.2.7.5: TC tracks in one of the involved models (the CMCC-CM2 one), at two different resolutions (100 km and 25 km) under a 10-year period compared to IBTRACS observations.

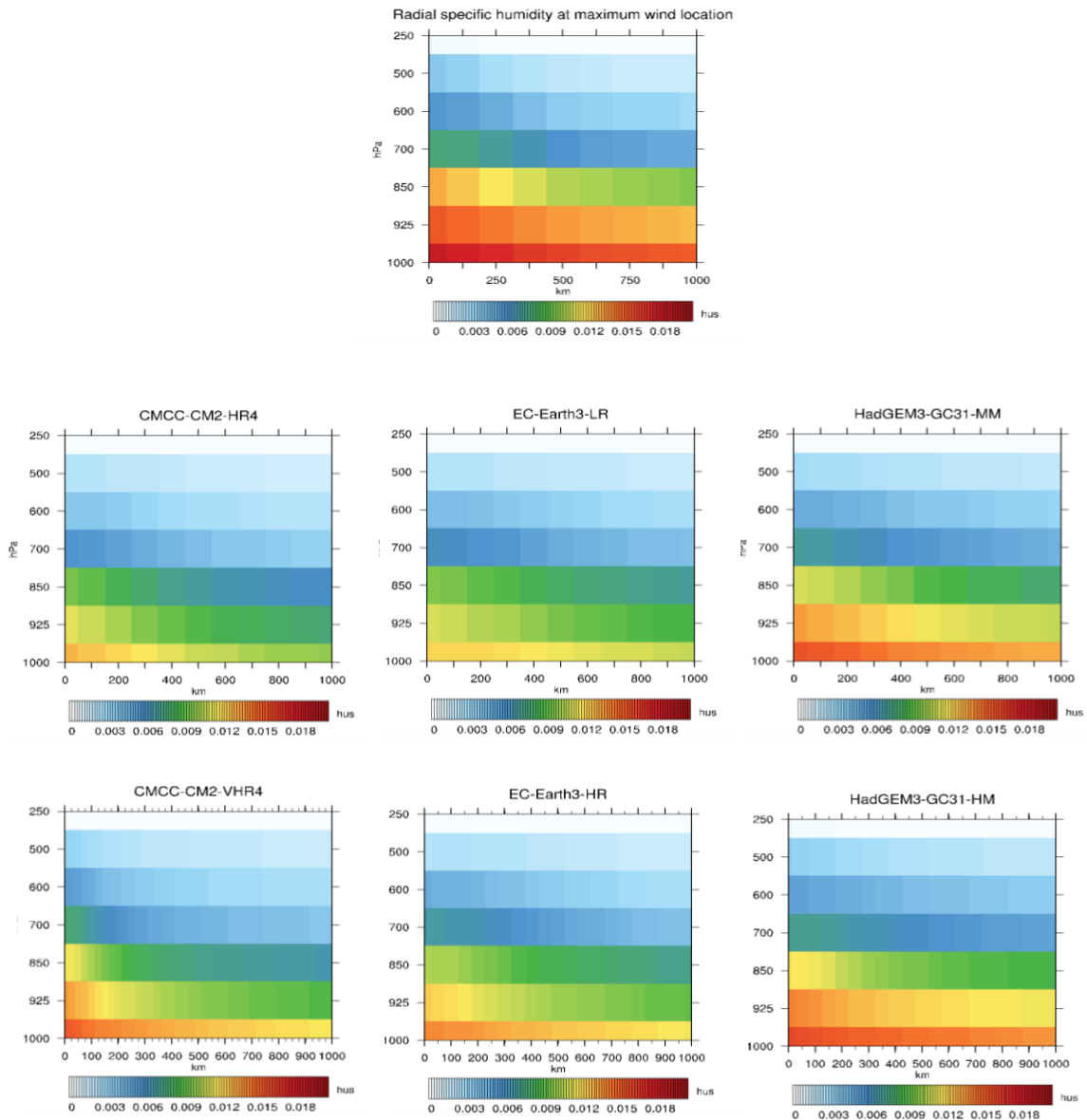


Figure 3.2.7.6: TC radial distribution of specific humidity at maximum wind position. Values are averaged over the entire set of TCs over the period 1985-2014. First row: observed values (JRA-55); Second row: low-resolution models; Third row: high-resolution models. Note that the number of bins varies as a function of resolution.

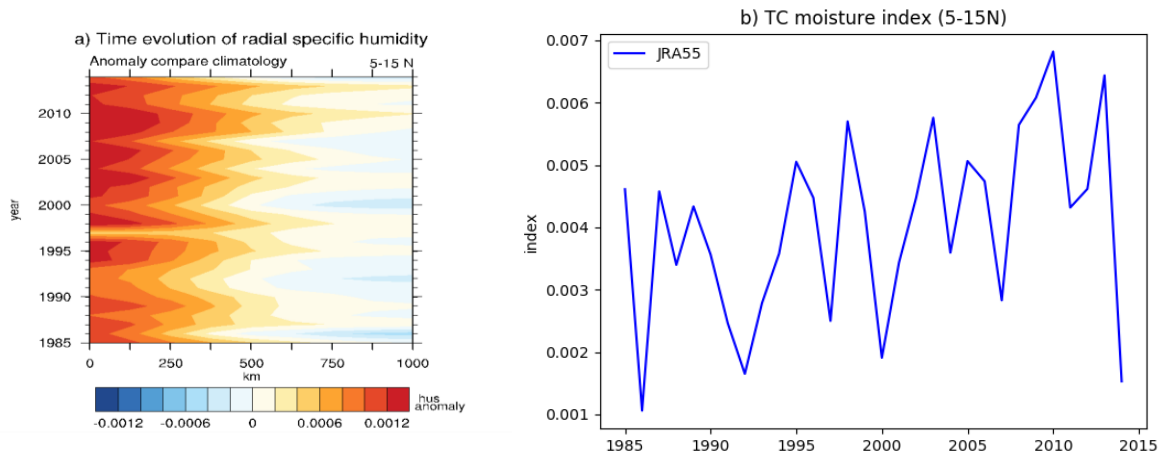


Figure 3.2.7.7: (a) Time evolution of observed anomaly integrated radial specific humidity in the 5-15N latitudinal band up to 1000km. (b) TC moisture index computed from panel a by integrating the anomaly along the radial distance.

3.2.8 Extratropical storm intensity over Europe (MOHC, UREAD; link to WP10/11)

The highest loss hazards that concern the insurance industry, as discovered in WP11 investigations, are wind storms and floods. Due to the lack of sufficient observational data, climate models can be used to augment observational datasets to estimate long return period losses. Since extra-tropical cyclones (ETCs) are the main cause of winter European wind storms, as well as being associated with flooding, we compared ETC characteristics between a re-analysis dataset, the PRIMAVERA models, and also the CMIP5 models to investigate whether the PRIMAVERA models show any improvement.

One ensemble member from each modelling centre, using the higher resolution model of the atmosphere-only experiment, has been analysed. The CMIP5 present day AMIP runs from the same modelling centres (where available) and the MERRA 2 (Gelaro et al. 2017) re-analysis dataset have also been used. TRACK (Hodges 1995) has been used to track all the ETCs in the same way. All the results presented here are for winter (DJF) ETCs over the period common to all datasets (1980/81 – 2007/2008 for the MERRA2 analyses).

The intensity of ETCs was investigated using three measures - the minimum Mean Sea Level Pressure (MSLP) of the storms, the maximum vorticity of the storms and the maximum winds at 925hPa level. The analyses indicated that the biases that were identified in comparisons between the CMIP5 models and the reanalysis based storms have been largely reduced within the storms obtained from the PRIMAVERA models when considering the minimum MSLP and the maximum vorticity of the storms. For example, while the CMIP5 based storms underestimated the frequency of extreme cyclones (with MSLP < 970hPa), this underestimation is reduced in the PRIMAVERA models' based storms, but a large overestimation is also evident for one model (CMCC). Some underestimation of the frequency of less intense storms is evident in the storms based on the PRIMAVERA models.

Key finding:

Biases in extra-tropical storm intensity are reduced in PRIMAVERA simulations compared to CMIP5, which is important for assessing present day and future climate hazard.

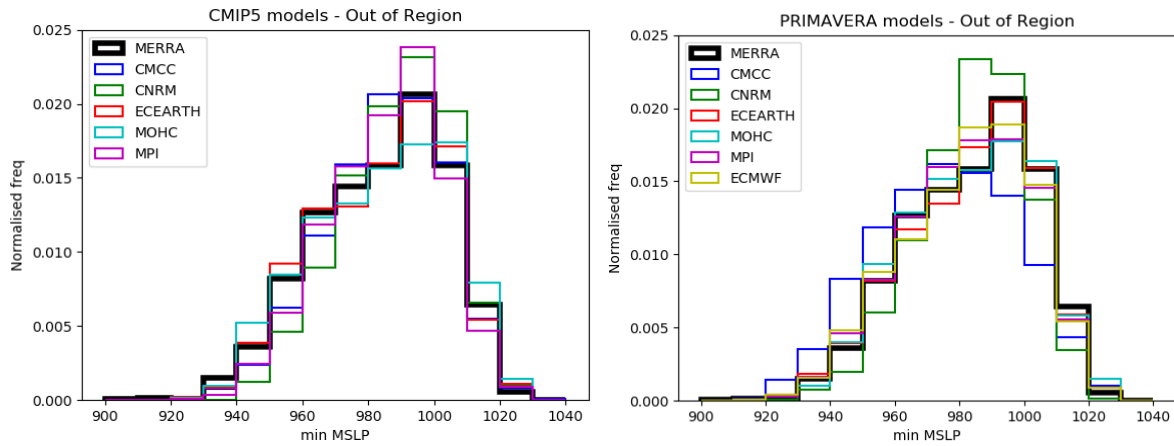


Figure 3.2.8.1: Histograms showing distribution of minimum MSLP of ETCs entering Europe for (left) CMIP5 models and (right) PRIMAVERA higher resolution models, vs MERRA2.

3.2.9 Representation of the North Atlantic eddy-driven jet (CMCC, UREAD)

Introduction

State-of-the-art climate models exhibit biases in the representation of the North Atlantic eddy-driven jet, particularly its climatological mean position and variability (e.g. Iqbal et al., 2018). Despite improvements over previous model generations (Hannachi et al., 2013), an accurate representation of the pulses and the latitudinal shifts of the eddy-driven jet remains a challenge, upon which also depends the representation of important aspects of European climate, including weather extremes and the frequency of severe prolonged anomalies such as cold spells (Woollings, 2010).

Within PRIMAVERA, we aim to assess the added value of increasing climate model resolution. Here, we evaluate the mid-latitude atmospheric circulation over the North Atlantic using atmosphere-land-only simulations forced by historical sea surface temperatures for the period 1950–2014 (‘highresSST-present’). We compare low- (LR) and high-resolution (HR) simulations. For brevity, we herein focus on winter (DJF).

Methodology

To identify the eddy-driven jet, daily mean u-wind field at 850 hPa was extracted from each highresSST-present simulations and interpolated from native model grids to a 2.5°x 2.5° regular grid. Following Woollings et al. (2010) and Woollings et al. (2018) and applying an additional orography mask (to account for the 850 hPa isobaric level being underground over most of Greenland). Jet latitude and jet speed are defined over the domain 0-60W and the respective bivariate distributions were determined for each simulation and the NCEP/NCAR

reanalysis, binned at 2.5° latitude and 1.0 m s^{-1} speed and smoothed by a PDF kernel (Silverman, 1986). The results are largely insensitive to the kernel estimation method, the practical effect of which is smoothing.

Results

The model biases displayed in Fig. 3.2.9.1 (LR left, HR right) make evident that there is a considerable inter-model variability in the representation of the North Atlantic jet. EC-EARTH3 and ECMWF-IFS models, which share the same dynamical core, exhibit very small biases in the bivariate distribution of the jet. HadGEM3-GC31 and MPIESM-1-2-HR exhibit moderate biases, mainly in the representation of the trimodal character of the jet latitude distribution, whilst CMCC-CM2 shows significant biases also in the jet speed (over 2 m s^{-1} overestimation in mean jet speed and much less variability in the latitudinal position of the jet). These results underline the need for using processed-based model metrics such as those developed in WP1.

In general, as indicated in Fig. 3.2.9.2 showing the distributions of jet latitude for both resolutions of each model, the forced stream 1 simulations (highresSST-present) capture quite well the trimodality of the eddy-driven jet, unlike many CMIP5 models. In the same figure there is evidence that increased resolution causes a slight poleward shift in jet occurrences. Furthermore, Fig. 3.2.9.3 shows that most stream 1 simulations successfully reproduce the seemingly negative linear relationship between jet latitude variability and jet speed percentile (as in Woollings et al., 2018), while the HR version of the most faithful models (ECMWF-IFS, EC-EARTH3, HadGEM3-GC31 and MPIESM-1-2-HR) appears to exhibit slightly higher latitude variance across the majority of jet speed percentiles.

It is worth mentioning that the present analysis is based on single realizations (no ensembles in stream 1). Therefore, it is fair to ask whether the above-discussed findings would hold for a different realization. Fortunately, results from a recent study (Kwon et al., 2018) using large ensembles, referring to the Large Ensemble Simulations (LENS) run with the Community Earth System Model (CESM) v.1, provide evidence that the jet statistics over a similar historical period (1951–2005) exhibit very little intra-ensemble spread. This gives us confidence that for certain diagnostics single-member analyses are a viable option.

Forthcoming research

- Eddy-driven jet tilt diagnostics.
- Extension of these analyses to coupled simulations upon delivery by PRIMAVERA partners.

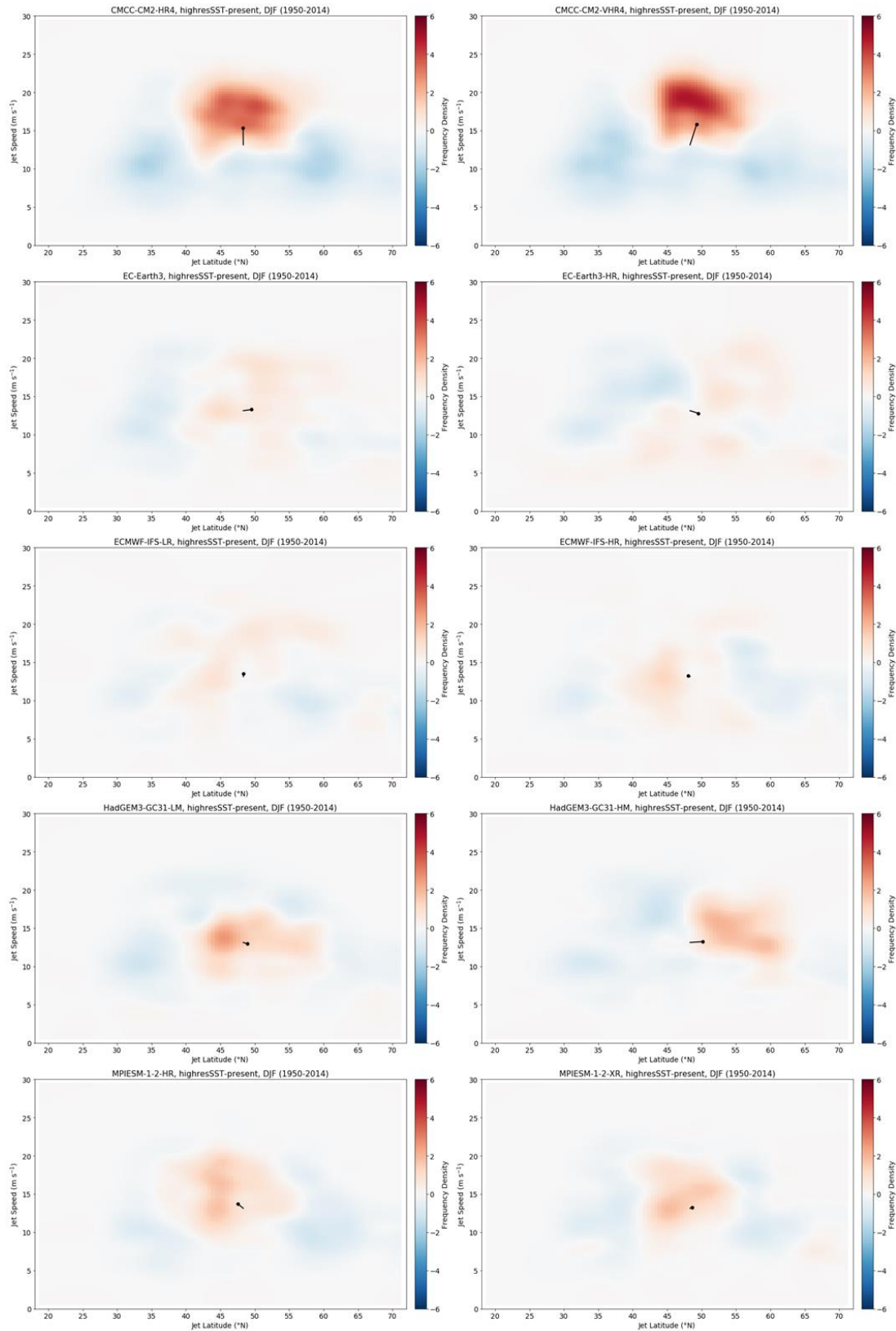


Figure 3.2.9.1. Model biases in the bivariate distribution of the North Atlantic eddy-driven jet. The jet latitude (x-axis) and jet speed (y-axis) correspond to the respective indices defined daily as described in the text. Biases are computed in respect to the NCEP/NCAR reanalysis for the same period (1950–2014). The black line segment at the center of each panel connects the mean position and strength of the jet in the reanalysis and in the model (round marker). Units: relative frequency density multiplied by 10^3 . Distributions are estimated by a PDF kernel (see text for details).

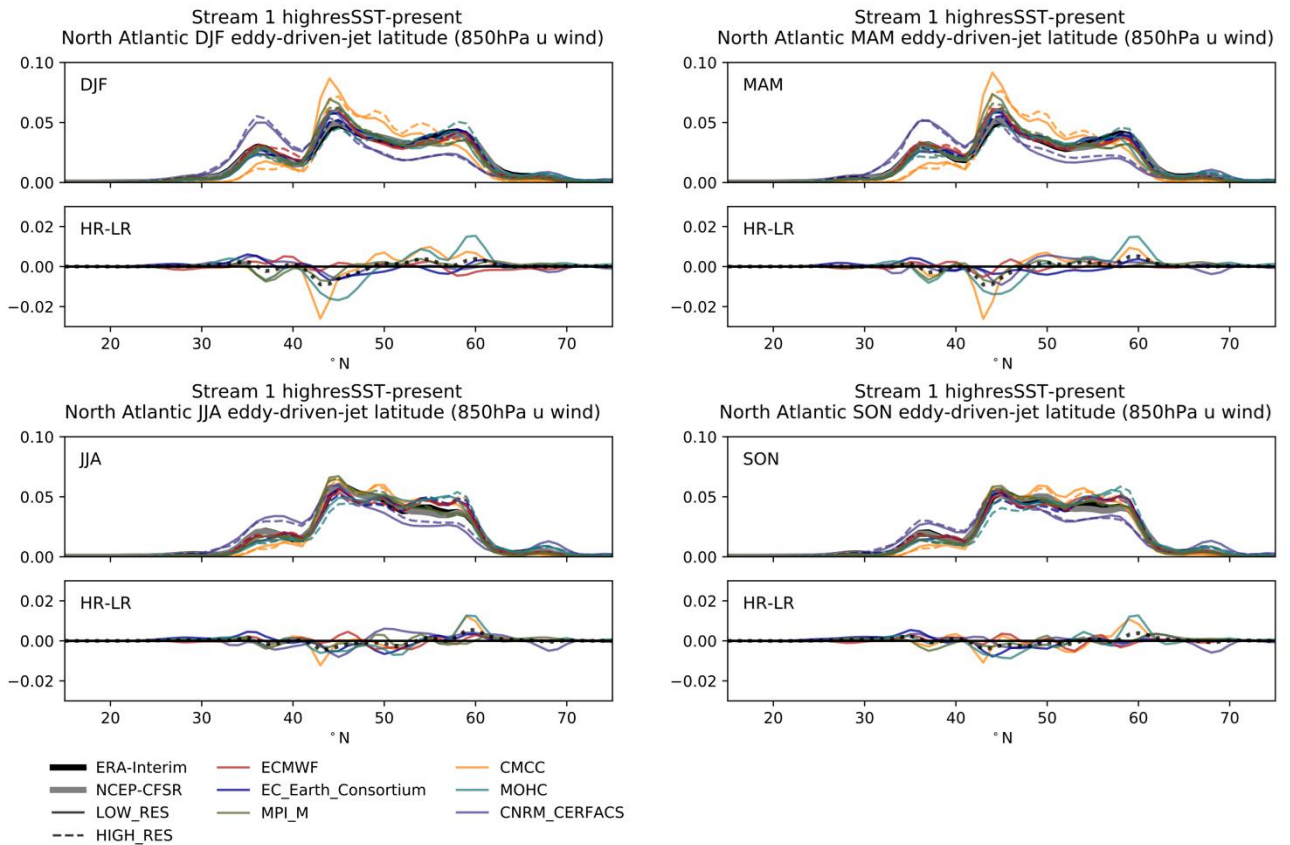


Figure 3.2.9.2. Probability density functions of eddy-driven jet latitude for highresSST-present simulations and the ERA-Interim (black) and NCEP-CFSR (grey) reanalyses, each computed following Woollings et al. (2010). The CNRM-CERFACS model contains an error affecting this analysis, and will therefore be re-analysed upon completion of replacement model runs. ECMWF refers to the IFS model. For each season, the upper panel shows the jet latitude probability density function for LR (solid lines) and HR (dashed lines) simulations. The lower panel shows the HR-LR difference and the blacked dashed line shows the multi-model mean HR-LR difference.

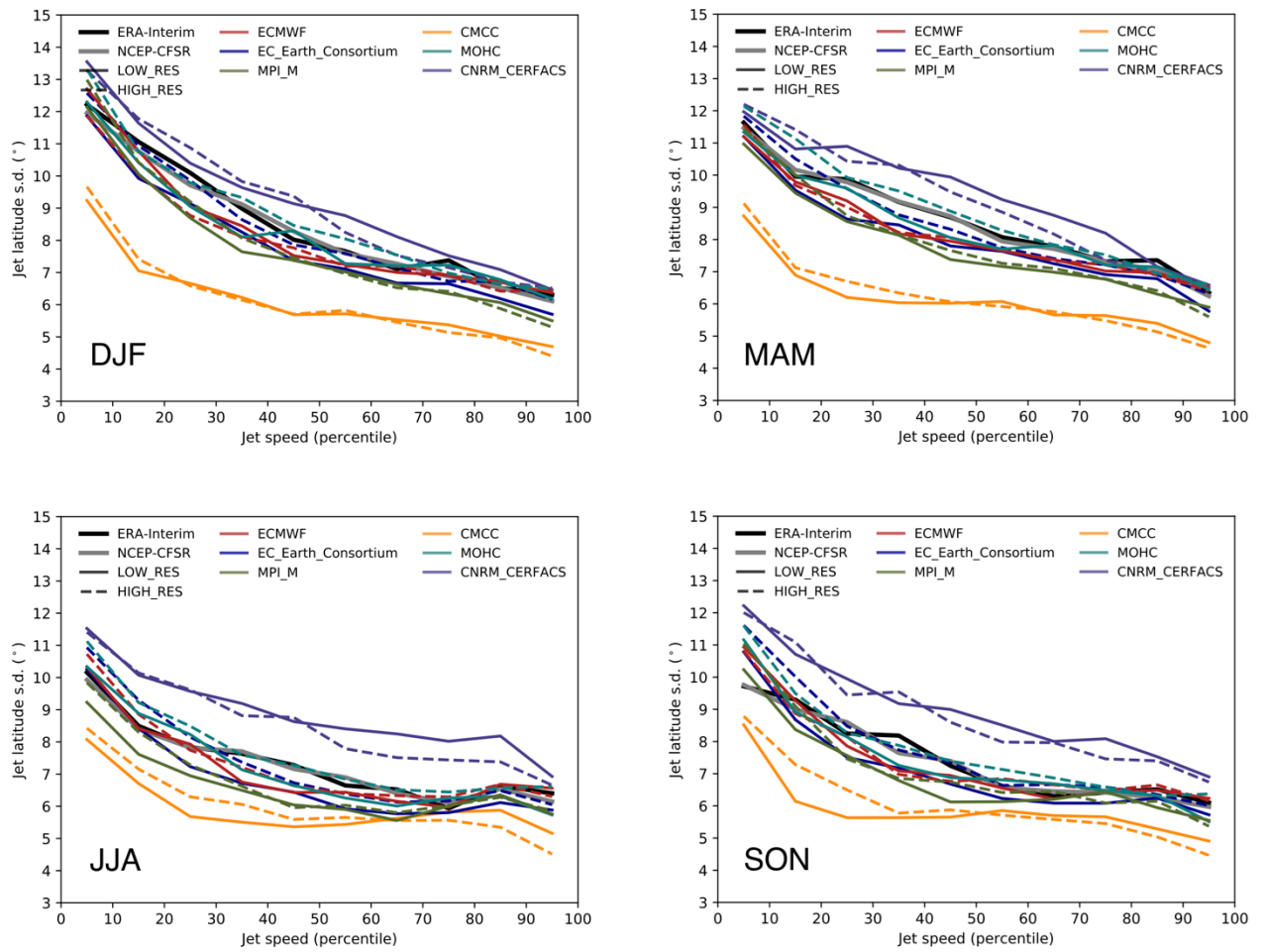


Figure 3.2.9.3. Relationship between eddy-driven jet latitude variance and speed, computed as the square-root of the sum of the squares of both u and v winds, previously low-pass filtered following Woollings et al. (2018). Speed is plotted as a percentile to allow model-to-model comparisons. The CNRM-CERFACS model will be re-analysed upon completion of re-runs.

3.3 Impact of resolution in coupled multi-model experiments

3.3.1 Extreme European precipitation (UREAD)

Introduction

We evaluated the impact of increased horizontal atmospheric resolution on extreme daily precipitation across the Stream 1 ensemble of atmosphere-land only and fully coupled simulations. Here, we show the added value of increased atmospheric resolution for winter (DJF) precipitation over Europe and the North Atlantic.

Methodology

We employed generalised extreme value (GEV) analysis and applied the parametric block maxima method globally. At each model grid point, globally, 1-day precipitation maxima were computed for each canonical season. GEV distributions were fitted to these seasonal precipitation block maxima time series, described the location (μ), scale (σ) and shape (ξ) parameters, which determine the change in return value as a function of return period. Here, we focus on two quantities: μ determines the vertical position of the GEV curve and thereby ‘typical’ return values and σ determines the slope of the GEV curve and thereby the year-to-year variability in extremes. We show results for highresSST-present simulations as delivery of coupled runs from PRIMAVERA partners is ongoing. An example of the application of GEV analysis model integrations is given in Schiemann et al. (2018).

Key results

Increasing resolution increases μ across the mid-latitudes in all models (Figure 3.3.1.1a). Increased extremes are simulated over much of the North Atlantic, particularly the storm track region in winter (and the equinoxal seasons – not shown). Simulated μ is closer to observational Global Precipitation Climatology Project data (Huffman et al. 2001) over this region (Figure 3.3.1.1b). However, simulated σ is further from observational estimates, indicating that typical return values are better-simulated in high-resolution forced simulations than inter-seasonal variability. Importantly, increased extreme precipitation is coterminous with reduced error over the north-eastern North Atlantic, Mediterranean and European orographic regions, exhibiting the added value of high-resolution integrations across much of the Euro-Atlantic domain of immediate interest to PRIMAVERA partners and stakeholders.

Forthcoming research

- Assess observational uncertainty over European land.
- Extend analysis to remaining coupled simulations upon delivery.
- Link GEV evaluation to analyses of ETC activity and associated precipitation as well as North Atlantic eddy-driven jet variability (CMCC collaboration).
- Link evaluation of extremes to post-tropical cyclone analyses (KNMI collaboration).

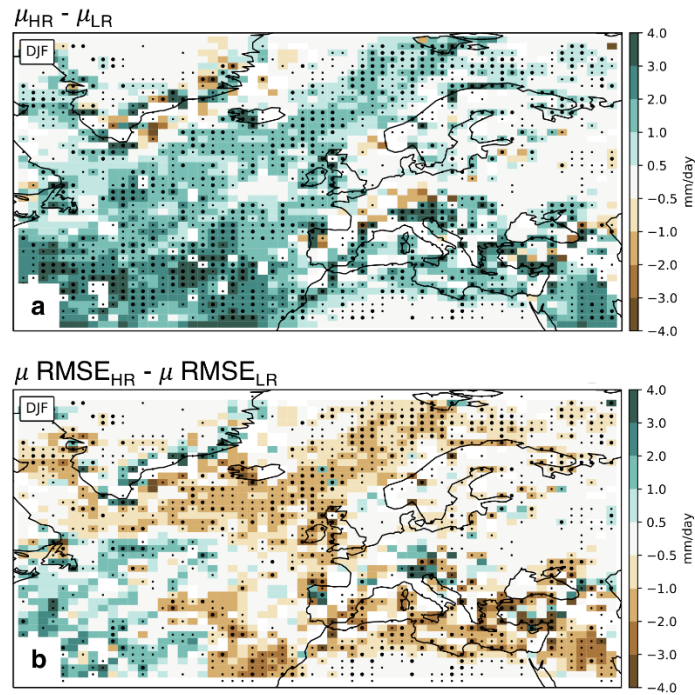


Figure 3.3.1.1. Multi-model wintertime mean difference in (a) μ (high-resolution minus low-resolution) and (b) μ root-mean-square error (RMSE). Positive (negative) values indicate increased (decreased) μ or μ RMSE at high-resolution. Large (small) stippling indicates all six (five out of six) models agree on sign of μ change with resolution increase. RMSE is computed versus GPCP daily, gridded (1°) precipitation data, available for 1996-2013 (Huffman et al., 2001).

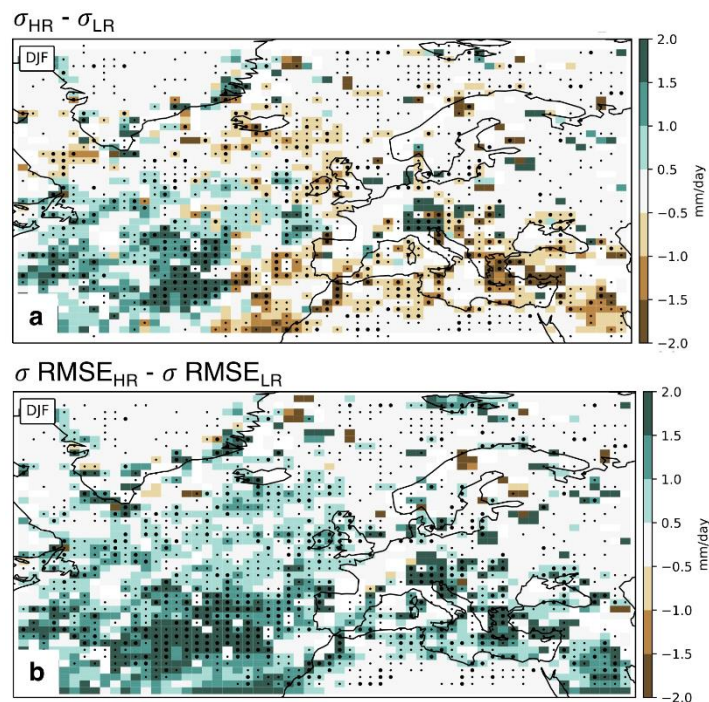


Figure 3.3.1.2. As Fig. 3.3.1.1 but for σ .

3.3.2 Snow cover and summer precipitation over northern Scandinavia (SMHI)

Snow cover

Snow cover is one of the most important components of the cryosphere and exhibits strong interannual temporal and spatial variation. Roughly 98% of seasonal snow cover lays in the North Hemisphere. Numerous studies show that snow cover plays a crucial role in regulating climate. Firstly we analyse the annual cycle of snow cover extent in different regions (North Hemisphere, Eurasia and North America) based on present-day Stream1 data. In the North Hemisphere (Figure 3.3.2.1), the seasonal cycle of snow cover shows a broad agreement across all models with observation. The impacts of model resolutions on the seasonal cycle of snow cover are quite small, while the largest discrepancies are due to inter-model spread. It is also noted that the differences between the atmosphere-only and coupled runs are large and the atmosphere-only simulations have a better agreement with observation. Similar snow variations are also found in Eurasian and North America. The snow cover trend analysis reveals that the snow trend variations are seasonal dependent. In spring, high resolution leads to a more consistent trend with observation and the improvement in the atmosphere-only runs are not as prominent as in the coupled runs. While in winter, effect of resolution is minor. Weaker improvements are seen in high resolution simulations. Spatial pattern analysis of snow depth illustrates that more detailed snow cover distributions are captured by high resolution simulations, which could partly contributed to snow cover trend variation.

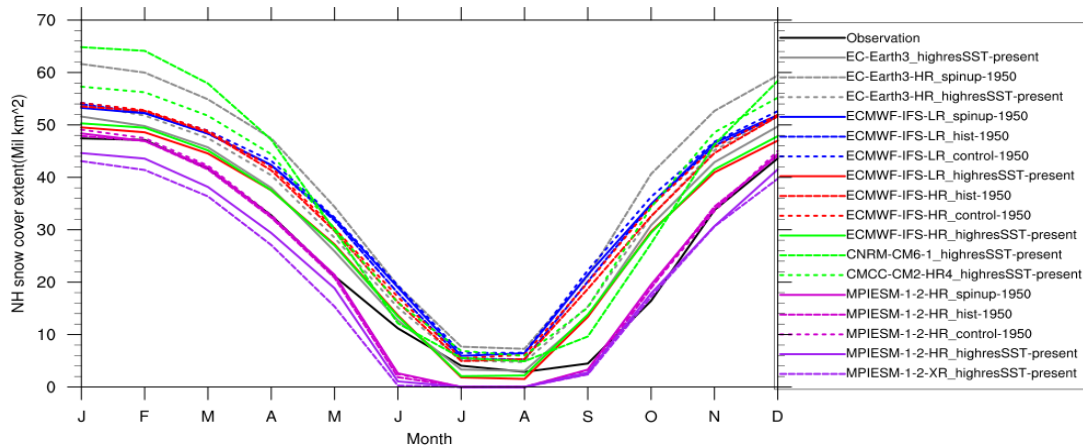


Figure 3.3.2.1: Annual cycle of snow cover extent over North Hemisphere from observation and present-day stream1 data

Linkage of summer precipitation over Northern Sweden and Finland to ENSO

We found a relatively strong relationship between summer precipitation over Northern Sweden and Northern Finland (NorSweFin) with El Niño-Southern Oscillation (ENSO), with the three wettest Augusts (1992, 1998 and 2016) in the last forty years occurring after El Niño phases during the previous winter, and three of the driest summers occurring after a winter with negative anomalies over the equatorial Pacific (weak La Niña). According to Timmermann et al. (2018), El Niño events usually start in boreal spring, grow during the

summer and autumn, reach their maximum intensity in winter and decay rapidly during late winter and spring. In most cases, they transition to La Niña events by the subsequent summer. Therefore, the wet summers over NorSweFin happened during summers with the beginning of La Niña.

Our hypothesis is that ENSO sets an ocean-atmospheric precondition for wet summers after El Niño, due to an increased likelihood of cyclones reaching NorSweFin region due to an intensified cyclogenesis over North America and the eastern coast of USA. However a further analysis is needed to find a clear mechanism for this observed NorSweFin – ENSO relationship. In order to assess how strong this observed relationship is, we use as predictors geopotential height at 500hPa from ERA-Interim in two different regions where negative anomalies during El Niño and positive anomalies during La Niña are found. Both predictors are located regions that exhibit the greatest variability in the typical PNA pattern. Predictor 1 (x_1) was defined as the average geopotential height at 500hPa within the region enclosed by the following coordinates 144.44E and 57.16N, 169.94 E and 62.6N, 179.54E and 56.43N, 158.97E and 55.16N. In turn predictor 2 (x_2) was defined as the average geopotential height at 500hPa within the region enclosed by the following coordinates 108.65W and 23.3N, 101.3W and 24.89N, 100.5W and 22.97N, 106.7W and 21.83N. The predictors were standardized (subtracting the temporal mean and dividing by their standard deviation) and we used multiple linear regression to fit observed precipitation. Our precipitation model then is defined as:

$$(1) \quad P_{\text{NorSweFin}} = -0.43x_1 + 0.24x_2$$

This simple regression model, provides predictability for precipitation over NorSweFin to explain 26% of the variance (Figure 3.3.2.2). Cross validation was performed by fitting the model for the period 1979-1998 and predicting 1999-2018, and vice versa, finding correlation of observations and model of $r=0.48$ and $r=0.44$ respectively, which shows that this ENSO-NorSweFin precipitation relationship holds in the cross-validation test.

Global Models participating in the EU H2020 PRIMAVERA project were analysed to assess how they represent the observed ENSO-NorSweFin precipitation relationship, first analysing atmosphere only HighResMIP simulations, in which the Sea Surface Temperature is prescribed. By correlating z500 (every grid point) with NorSweFin precipitation we found that none of them (low or high resolution) capture the observed relationship (not shown). In turn, when analysing coupled simulations, we found that the low resolution simulations fail to reproduce the observed composite pattern of geopotential height at 500hPa (Figure 3.3.2.3 top) but the high resolution models show many similarities to observations. For example they reproduce the negative anomalies over the North Pacific (which would mean a deepening of the Aleutian low during winter), negative anomalies across the Atlantic Ocean and over Europe and the positive anomalies over Greenland and Iceland. The difference between high and low resolution is shown in Figure 3.3.2.3 (bottom left). Similar results are found for dry summers.

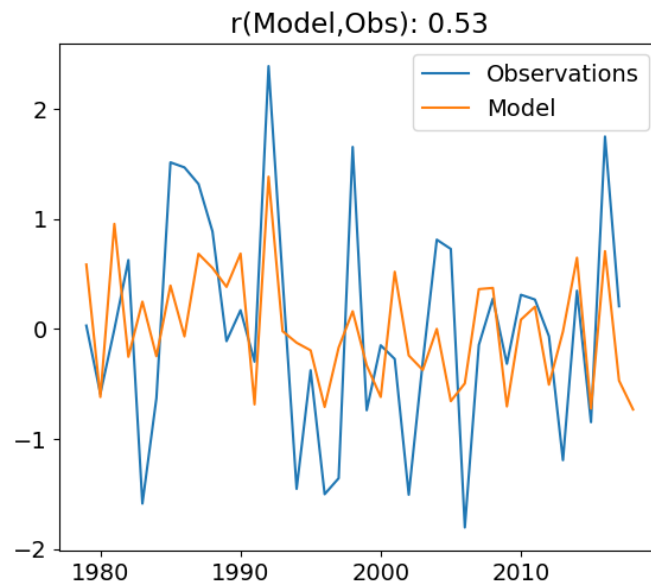


Figure 3.3.2.2: Observed August precipitation over the NorSweFin region from EOBS (blue), and the predicted precipitation using model described in equation 1. Units in y axis are standard deviations.

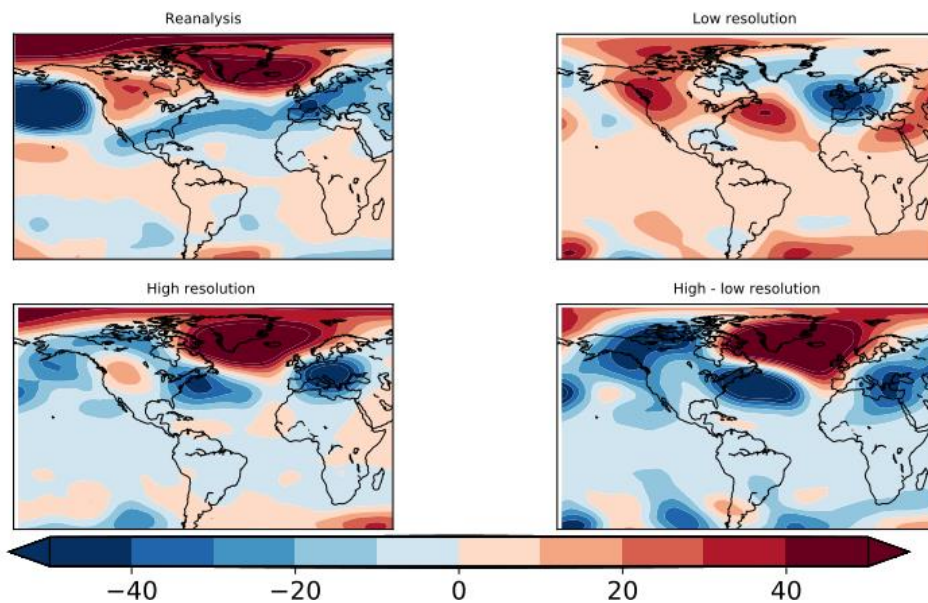


Figure 3.3.2.3 Composite of z500 anomalies during the winter preceding wet summer over NorSweFin region. The models used were ECMWF-IFS-LR and HadGEM3-GC31-LL for low resolution while ECMWF-IFS-LR and HadGEM3-GC31-MM for high resolution. For observations, we consider the three wettest augusts within 1979-2018 period, while for the simulations we consider six Augusts within 1950-2014.

3.3.3 Global hydrological cycle (NCAS)

Demory *et al.* (2014) have demonstrated that the global water cycle is sensitive to global climate model (GCM)'s horizontal resolution, up to about 60 km, where the intensity of hydrological processes reaches a plateau. While ocean precipitation decreases with higher resolution, land precipitation increases due to higher moisture convergence over land. The contribution of moisture transport to land precipitation also increases, whereas moisture recycling, a quantity that is known to be overestimated by state-of-the-art GCMs, tends to decrease. One question that came out of this study is whether such mechanisms are model dependent. To answer this question, we analysed an ensemble of twelve atmosphere-only and six coupled GCMs, with different model formulations and with resolutions spanning those of state-of-the-art coupled GCMs, i.e. from resolutions coarser than 100 km to resolutions finer than 25 km.

Results

Regarding hydrological processes, our results are the following: (1) there is an increase of global precipitation with increasing resolution in all models (up to $40 \times 10^3 \text{ km}^3 \text{ year}^{-1}$) but the partitioning between land and ocean varies among models; (2) the fraction of total precipitation that falls on land is on average 10% larger at higher resolution in grid point models, but it is smaller in spectral models; (3) grid points models simulate an increase of the fraction of land precipitation due to moisture convergence twice as large as in spectral models; (4) grid point models, which have a better resolved orography, show an increase of orographic precipitation of up to $13 \times 10^3 \text{ km}^3 \text{ year}^{-1}$ which explains most of the change in land precipitation (see Fig. 3.3.3.1); (5) we did not find asymptotic convergence of hydrological processes with resolution in the range of resolutions covered by this study.

Key findings:

Our results support recent high estimates of global precipitation (Stephens *et al.* 2012) and stress the need to reduce both the uncertainty of observed orographic precipitation and moisture advection to land to estimate the global precipitation with more accuracy.

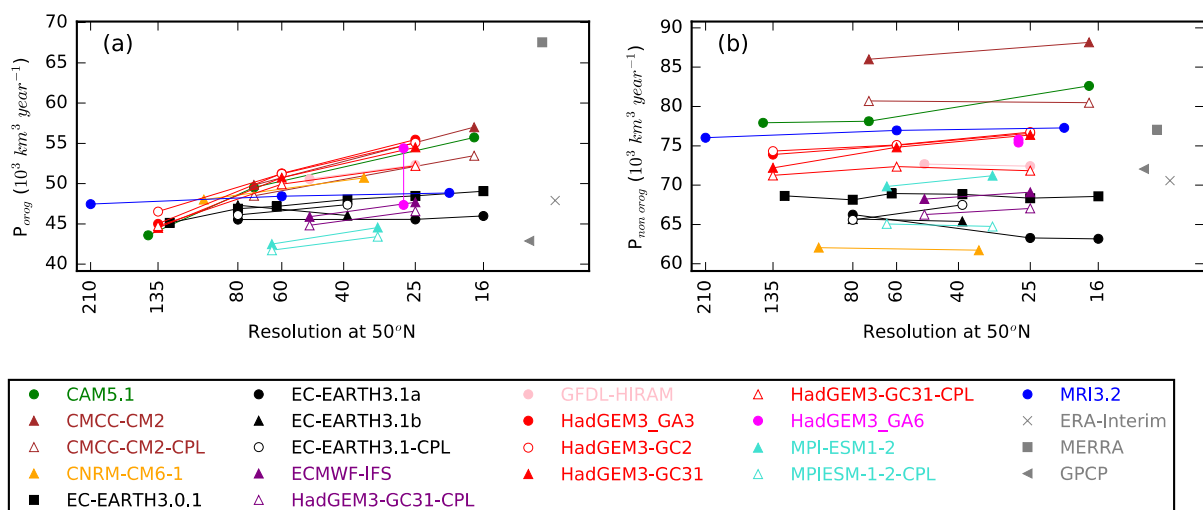


Figure 3.3.3.1: Partitioning of precipitation into (a) orographic and (b) non-orographic precipitation, using a mask based on ERA-Interim.

3.3.4 Blocking (NCAS, CMCC)

Introduction

Multiple studies have shown that an increase in atmospheric resolution generally benefits the representation of blocking in climate models, though blocking simulation is also sensitive to a number of other factors including vertical resolution, sea surface temperature, the representation of orography, physical parameterisations, and the dynamical core numerical scheme (Woollings et al., 2018). This continues to hold true as the resolution in atmosphere-only simulations is increased from $O(100\text{km})$ to $O(20\text{km})$, but several models continue to exhibit sizeable biases even at about 20km resolution (Schiemann et al., 2017), and improvements seen in blocking have been shown to be due to compensating biases in the representation of eddies in one high-resolution model (Davini et al., 2017). Here, we evaluate the representation of blocking in the PRIMAVERA Stream 1 multi-model ensemble focussing in particular on whether benefits seen at higher resolution in atmosphere-only simulations are also seen in coupled atmosphere-ocean simulations.

Methods and data

We use Stream 1 simulations from four models for which both forced and coupled simulations were available (Table 1). The HadGEM3 high-resolution coupled runs are currently re-run due to a bug in the river routing scheme of this model. The results for this model should therefore be considered to be preliminary. We also compare simulated blocking in the PRIMAVERA simulations with that in 29 CMIP5 models from 15 centres. The simulated blocking climatologies are compared with a combined ERA-40/ERA-Interim reference dataset covering 1962–2011 as used in (Schiemann et al., 2017). We use the Absolute Geopotential Height (AGP) two-dimensional blocking index following (Scherrer et al., 2006) and (Schiemann et al., 2017).

This assessment is repeated in part using a one-dimensional blocking index. This tests the robustness of our results to the choice of the index, and we also use this index to determine the relationship between mean-state and blocking biases following Scaife et al., 2010. For the one-dimensional blocking analysis, daily Z500 data from each model have been interpolated from the respective native grid to a courser regular grid ($2.5^\circ \times 2.5^\circ$). At each grid point, mean bias correction has been accomplished by subtracting the model daily climatology (smoothed by 30-day running average) to compute Z500 daily anomalies and subsequently adding the respective daily observed (reanalysis) climatology. Instantaneous blocking detection along the central blocking latitude (CBL) is performed as in Athanasiadis et al., 2014. For each calendar season, the CBL is defined by ERA-Interim. The presented zonal profiles have been smoothed with a 3-point running average.

Table 3.3.4.1. Ensemble of Stream 1 simulations used in this evaluation.

Experiment (coupling)	Centre/Model	Resolution atmosphere	Resolution ocean	Notional resolution
highresSST-present (forced)	MOHC HadGEM3-GC31	N96	(0.25° daily HadISST2)	L
		N216		M
		N512		H
	ECMWF IFS	Tco199		L
		Tco399		H
	EC-Earth-Consortium EC-Earth3	TL255		M
		TL511		H
	MPI-M MPI-ESM1-2	T127		L
		T255		M
	hist-1950 (coupled)	MOHC HadGEM3-GC31		N96
N216			¼°	MM
N512			¼°	HM
N512			1/12°	HH
ECMWF IFS		Tco199	1°	LL
		Tco399	¼°	HM
EC-Earth-Consortium EC-Earth3		TL255	1°	ML
		TL511	¼°	HM
MPI-M MPI-ESM1-2		T127	TP04	LM
		T255	TP04	MM

Selected results

The frequency of blocked days over European domains for winter and summer is shown in Figure 3.3.4.1. During winter, the PRIMAVERA Stream 1 simulations underestimate blocking frequency, which is a long-standing bias in climate models, yet some models attain about 80% of the observed blocking frequency. There appears to be a small improvement with resolution for the four coupled models, but not in the forced models. Three of the four models simulate higher blocking frequencies than seen in the CMIP5 multi-model mean, yet this is not seen when considering the CMIP5 mean from the same modelling centres only. During summer, the models underestimate European blocking by about 50%, more so than in winter and also more than seen in the CMIP5 models. There is no systematic resolution sensitivity in this metric.

We proceed by evaluating the geographical pattern of blocking occurrence (Figure 3.3.4.2). This figure shows scatter plots of the root-mean-square error and the spatial correlation with respect to the reanalysis climatology so that the better the agreement between a model simulation and the reanalysis, the further will the corresponding entry be located in the lower right of the scatter plot. During winter, an improvement in the simulated pattern can be seen in three out of the four forced simulations, and in the coupled simulations the improvement is larger and can be seen for all four models. It can also be seen that the high-resolution PRIMAVERA Stream 1 models show an improvement with respect to the CMIP5 multi-model mean, even if only models from the same modelling centres are considered. Similar conclusions can be drawn for summer. Across the four models considered here, a model's ability to capture the pattern of blocking occurrence in winter is no indication of how well it will perform in summer, as seen, for example, by the comparatively close agreement with reanalysis of the MOHC HadGEM3-GC31 model in winter and the comparatively large disagreement with reanalysis of the same model in summer.

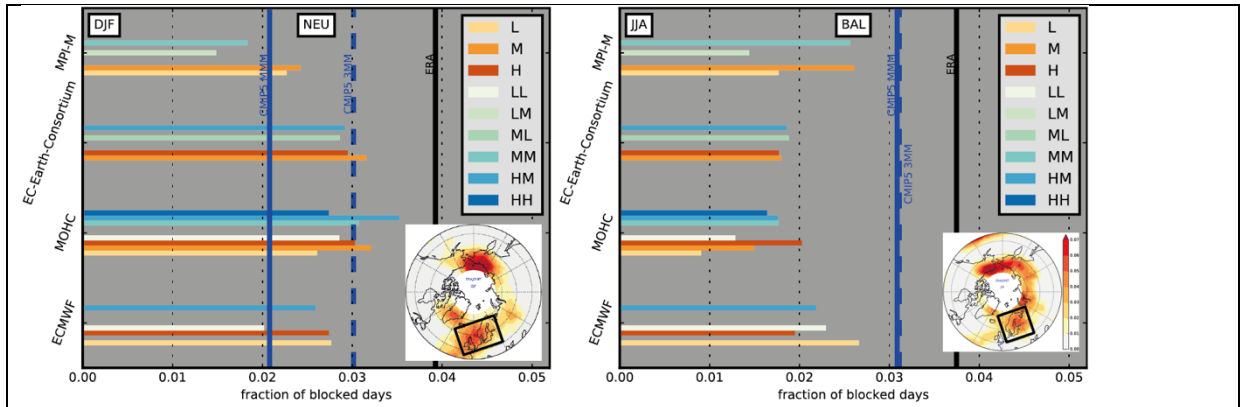


Figure 3.3.4.1. Domain-mean blocking frequency for (left) DJF and a Northern European domain (reanalysis climatology and domain in inset) and (right) JJA and a Baltic domain. Forced and coupled models are shown in terms of their notional resolutions (Table 1). CMIP5 MMM denotes the CMIP5 multimodel mean and CMIP5 3MM denotes the mean over the models from three centres only (EC-Earth Consortium, MOHC, MPI-M). ERA denotes the reanalysis mean.

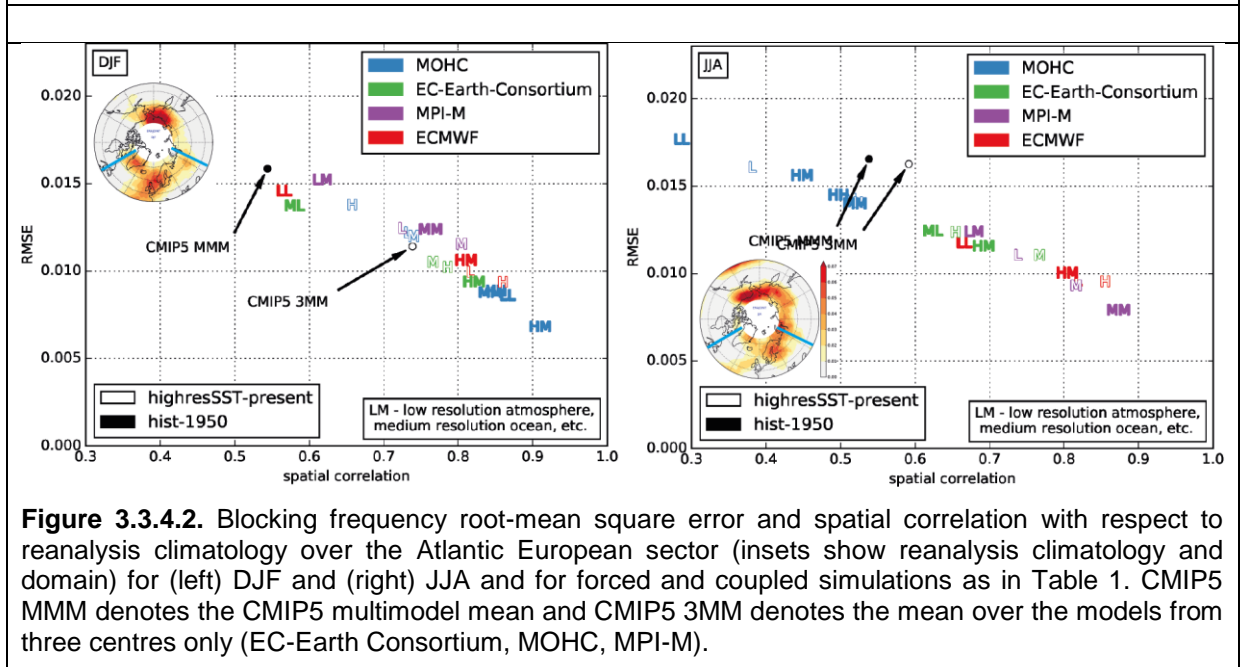
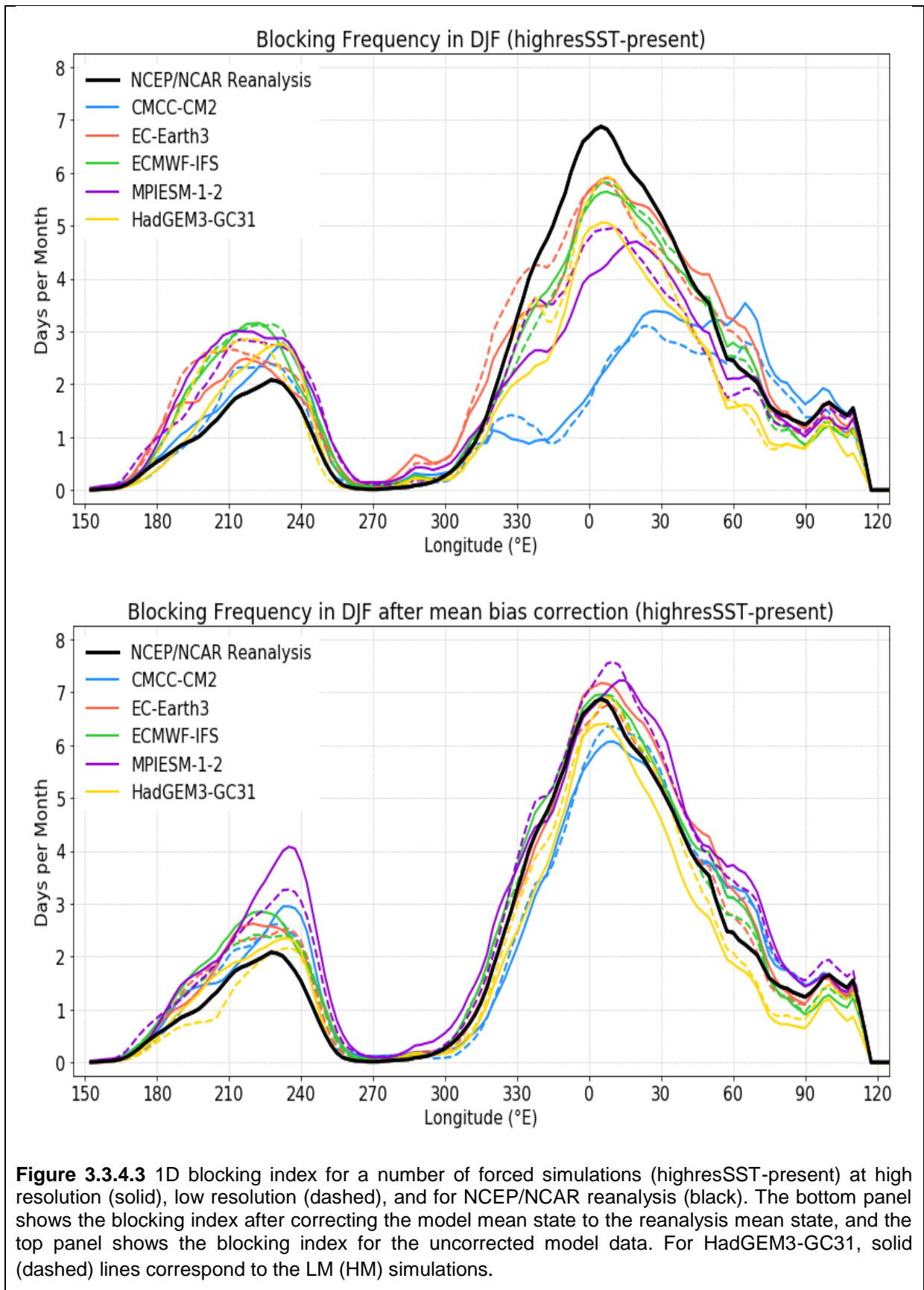
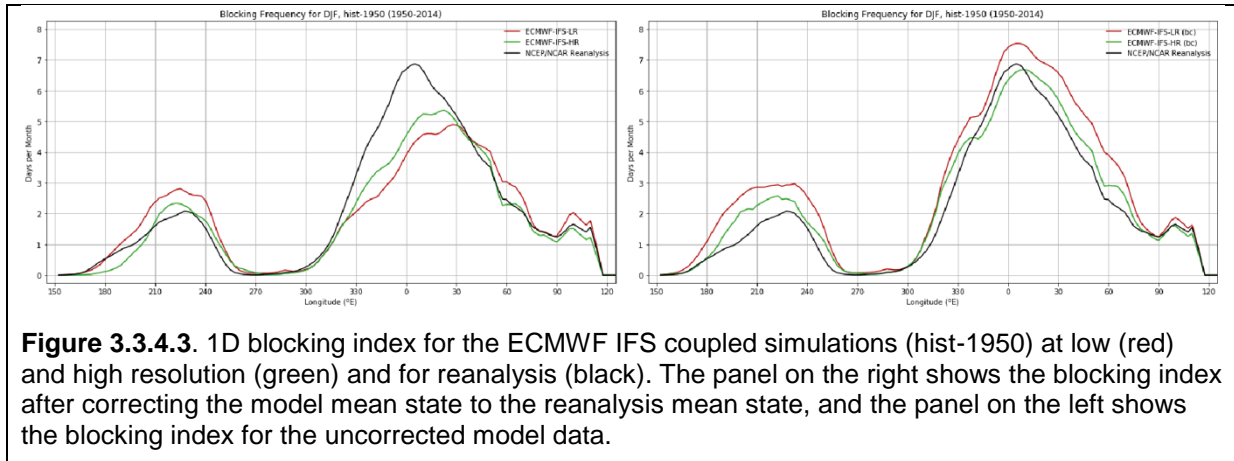


Figure 3.3.4.2. Blocking frequency root-mean square error and spatial correlation with respect to reanalysis climatology over the Atlantic European sector (insets show reanalysis climatology and domain) for (left) DJF and (right) JJA and for forced and coupled simulations as in Table 1. CMIP5 MMM denotes the CMIP5 multimodel mean and CMIP5 3MM denotes the mean over the models from three centres only (EC-Earth Consortium, MOHC, MPI-M).

The effect of correcting the model mean state to the reanalysis mean is shown in **Error! Reference source not found.** for winter and for a number of forced simulations and in Figure 3.3.4.3 for one coupled simulation. In agreement with previous studies (Berckmans et al., 2013; Schiemann et al., 2017), we find that the representation of blocking is closely associated with the mean state for all five forced models tested here. At the same time, and also in agreement with these previous studies, we find some improvement at higher resolution even after correcting for the mean-state biases. So far we have found this for a single coupled model (Figure 3.3.4.3), and will test the robustness of this result across the model ensemble and the two indices used in future work.





Summary and outlook

Using a two-dimensional blocking index, we have evaluated the representation of blocking in an ensemble of four PRIMAVERA Stream 1 models for which coupled (hist-1950) data were available, and for reference also in the CMIP5 historical simulations. We find that:

- Models continue to underestimate the number of blocked days in Europe considerably, both in winter and summer. There may be a small improvement (higher blocking frequency with resolution in winter (Figure 3.3.4.1– DJF, and Figure 3.3.4.3), but not in summer. PRIMAVERA Stream 1 simulations do not show improvement in this metric over CMIP5 historical simulations.
- At the same time, the geographical pattern of Euro-Atlantic blocking occurrence improves distinctly with resolution in the PRIMAVERA Stream 1 simulations, and more strongly so in the coupled (hist-1950) simulations than in the uncoupled (highresSST-present) simulations (Figure 3.3.4.2). The statistical significance of these results has not been tested here, but comparing with previous results from other simulations (Schiemann et al., 2017) indicates significance. The high-resolution PRIMAVERA Stream 1 models improve upon the CMIP5 models in this respect.
- All four models, both coupled and uncoupled, underestimate the relative number of long-lived blocking events, and overestimate the relative number of short-lived blocks (not shown here). The sensitivity to resolution of blocking persistence is currently under investigation.
- As seen in previous studies, our preliminary analysis suggests that mean-state biases are closely associated with blocking biases also in the PRIMAVERA Stream 1 simulations (**Error! Reference source not found.** and Figure 3.3.4.3). Work relating blocking biases to North Atlantic jet biases is in progress.

3.3.5 Ocean-atmosphere interactions over the Gulf Stream (KNMI)

Before the availability of the Stream 1 simulations we have investigated the impact of resolution on several aspects of the ocean-atmosphere interaction. In deliverable D2.1 we already reported that increasing atmosphere resolution enhances and thereby improves the intense precipitation over the Gulf Stream region (Scher et al. 2016). In addition we have analyzed the impact of the Gulf stream front storm development. Since D2.1 this work has now been published (de Vries et al. 2018).

In coupled ocean-atmosphere framework we have analyzed the impact of ocean and atmosphere resolution for the ocean-atmosphere interaction over the Gulf stream. This has been done using ensemble seasonal forecast simulations of EC-Earth at different ocean and atmosphere resolutions. The results show that increasing atmosphere resolution affects strongly the mean climate and moderately the variability of the North Atlantic-European winter. In contrast increasing ocean resolution affects strongly the variability but has hardly an impact on mean climate. Key in the impact of the ocean on atmospheric variability is the ability to generate ocean meso-scale variability.

These results represent the first comprehensive, statistically-significant evidence supporting the notion that increased ocean resolution, towards eddy-resolving, yields a stronger impact of the surface oceanic circulation on the atmospheric circulation. The manuscript will be submitted in autumn 2018.

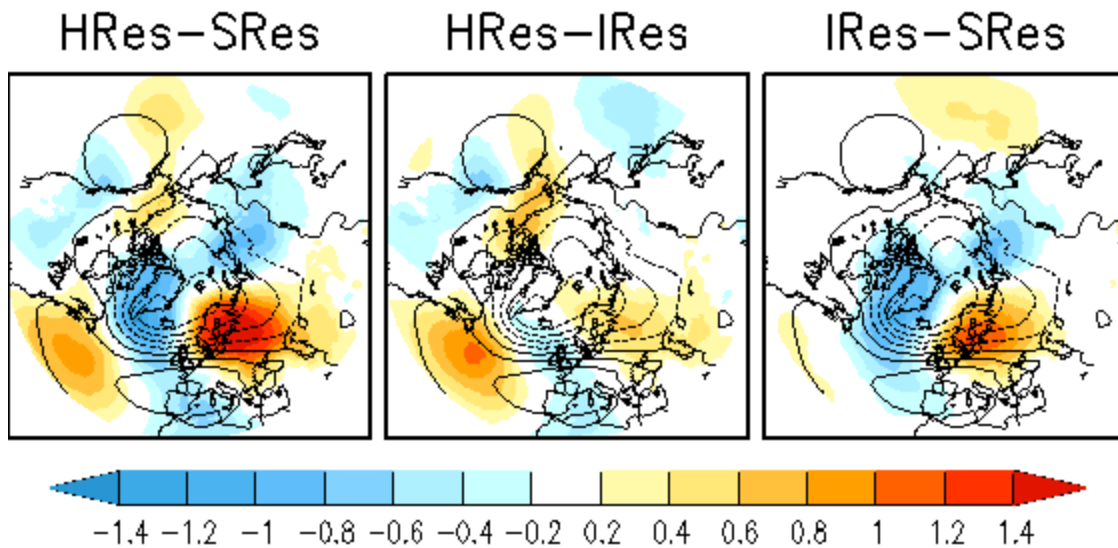


Figure 3.3.5.1. EC-Earth 10 member seasonal forecast (Dec-Jan) for the period 1993-2009. Contours: First EOF of MSLP of the SRes (T255, Orca1.0). Shading: differences in EOF of MSLP between HRes (T511, Orca0.25), IRres(T255, Orca0.25) and SRes. The figures show that both increasing ocean and atmosphere resolution affect the first EOF pattern.

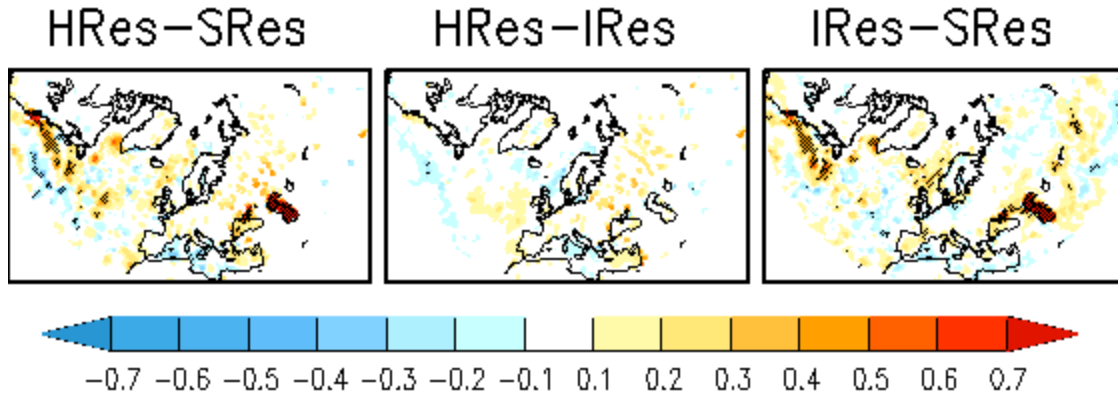


Figure 3.3.5.2. As Fig.3.3.5.1 but now for the correlation between the seasonal mean SST and turbulent (latent plus sensible) heat flux. Stippling denotes 95% significance indicating that increasing the ocean resolution increases the ocean-atmosphere coupling over the Gulf stream.

The results obtained with EC-Earth, demonstrating the importance of meso-scale ocean dynamics for inter-annual atmospheric winter variability, are now being tested using the Stream 1 coupled simulations. So far, the HADGEM3, MPI and ECMWF are being analyzed. This will be extended to the other models when they become available on JASMIN. The first analyses so far confirm our hypothesis. Indeed, enhanced ocean resolution to eddy-permitting resolution appears to be the main cause of the enhanced ocean-atmosphere interaction along the Gulf stream for those three models.

Key findings:

Increasing ocean resolution to eddy-permitting strongly enhances the impact of the ocean on the interannual atmospheric winter variability

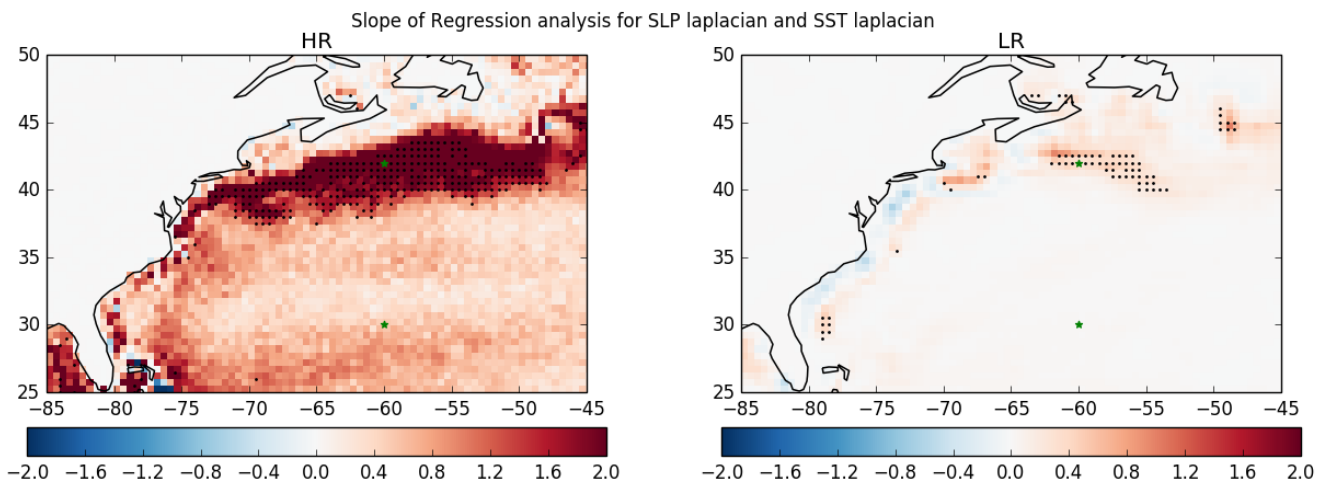


Figure 3.3.5.3. Regression between the laplacians of sea level pressure (SLP) and of sea surface temperature (SST) for winter (Dec.-Jan.) seasonal means of the high and standard resolution version of the ECMWF coupled model. Stippling denotes 95% significance. Significant ocean-atmosphere coupling exists over the Gulfstream region in the high resolution that is almost absent in the standard version.

3.3.6 Arctic sea-ice and Atlantic ocean heat transport (UCLouvain)

Methodology

The impact of model resolution on Arctic sea-ice and poleward Atlantic ocean heat transport (OHT) has been analyzed in four different coupled General Circulation Models (GCMs) participating to Stream 1 experiments (historical and control runs). For each model, we have investigated two different configurations. In HadGEM3-GC3.1, ECMWF-IFS and AWI-CM-1-1, the resolution is increased in both the atmosphere and ocean, while in MPI-ESM1-2, the resolution varies only in the atmosphere and stays constant in the ocean (Table 3.3.6.1).

Model configuration	Atmosphere resolution	Ocean resolution
HadGEM3-GC3.1-LL	N96 (250km)	1°
HadGEM3-GC3.1-MM	N216 (100km)	0.25°
ECMWF-IFS-LR	Tco199 (50km)	1°
ECMWF-IFS-HR	Tco399 (25km)	0.25°
AWI-CM-1-1-LR	T63 (250km)	24-110km (unstructured mesh)
AWI-CM-1-1-HR	T127 (100km)	10-60km (unstructured mesh)
MPI-ESM1-2-HR	T127 (100km)	0.4°
MPI-ESM1-2-XR	T255 (50km)	0.4°

Table 3.3.6.1: Atmosphere and ocean resolutions of the 8 model configurations used in this analysis. The nominal resolution of the atmosphere component is provided in brackets.

Key results

In HadGEM3-GC3.1, ECMWF-IFS and AWI-CM-1-1, increased model resolution leads to reduced Arctic sea-ice area (Fig. 3.3.6.1) and volume, as well as enhanced poleward Atlantic OHT (Fig. 3.3.6.2). In MPI-ESM1-2, a finer resolution results in slightly higher Arctic sea-ice area, lower sea-ice volume and lower Atlantic OHT. The different behavior of the latter model is probably explained by the change in atmosphere resolution only, compared to a change in both atmosphere and ocean resolutions in the three other models. This is in agreement with previous studies that suggest a stronger role of ocean resolution compared to atmosphere resolution in the representation of Atlantic OHT (Hewitt et al., 2016; Roberts et al., 2018).

We have also looked at the impact of the resolution on the correlation between Arctic sea-ice and Atlantic OHT, but we have not found any systematic difference across the different configurations, despite the strong link between Arctic sea-ice and Atlantic OHT.

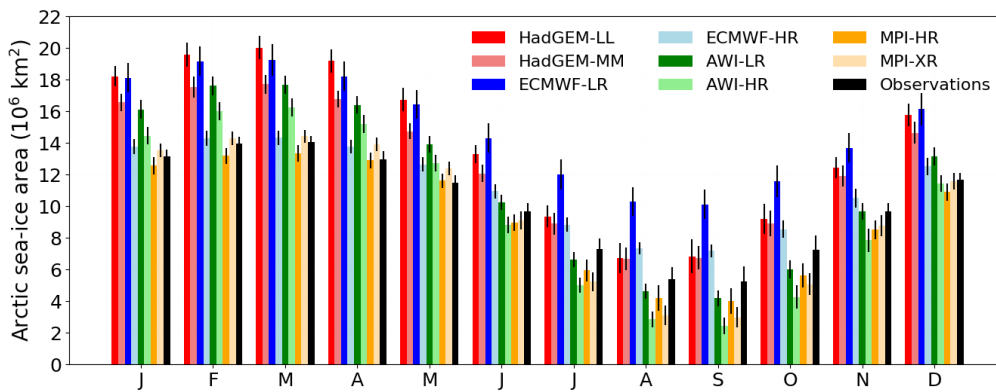


Figure 3.3.6.1: Monthly mean Arctic sea-ice area averaged over 1979-2014. Results from HighResMIP Stream 1 hist-1950 model outputs and OSI SAF satellite observations. The black line on top of each bar indicates the temporal standard deviation.

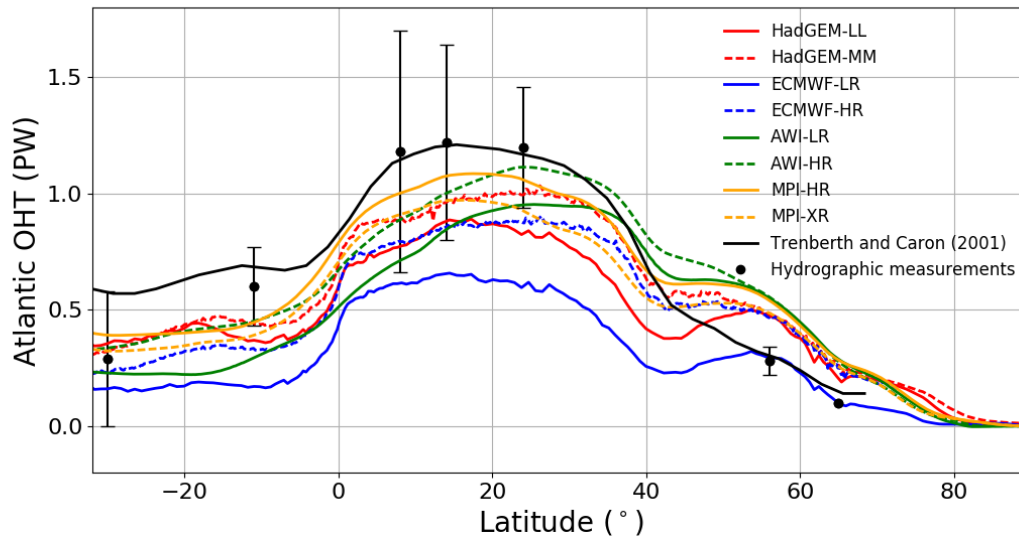


Figure 3.3.6.2: Latitudinal transect of Atlantic ocean heat transport (OHT) integrated over all longitudes and vertical layers and averaged over 1950-2014. Results from HighResMIP Stream 1 hist-1950 model outputs, compared to OHT estimates based on NCEP/NCAR reanalysis from Trenberth and Caron (2001) as well as hydrographic measurements (with error uncertainty).

3.3.7 Deep water formation in the North Atlantic (SMHI)

During the past decades, the idea of a weakening and even collapsing Atlantic Meridional Overturning Circulation (AMOC) as a response to global warming, and its possible impact on the climate of Europe, has been a recurrent and heated debate within the climate community. The main argument for a possible decline of the AMOC is the reduction of deep wintertime convective mixing in the northern North Atlantic. Here, we analyzed the impact of resolution on the representation of the North Atlantic deep convection in coupled climate models. Coupled Stream 1 historical and control simulations in different resolution from two PRIMAVERA models (ECMWF-IFS-LR, ECMWF-IFS-HR, HadGEM3-GC31-LL, HadGEM3-

GC31-MM) have been analyzed to study the impact of high resolution on the deep oceanic convection. The results from these two models are compared to the results from high and low resolution simulations from five coupled pre-PRIMAVERA models.

The low resolution version of the ECMWF-IFS model is not producing any deep convection in the Labrador Sea and the Greenland Sea, while the low resolution version of the HadGEM-GC31 model is reasonably well reproducing observed mixing depth from ARGO-floats in the Labrador Sea, but overestimating convection in the Greenland Sea (Figure 3.3.7.1). With increased resolution (ECMWF-IFS-HR, HadGEM3-GC31-MM), convection in the Labrador Sea is strongly increased and too strong compared to observations. In contrast, convection in the Greenland Sea is reduced in HadGEM-GC31-MM. These results agree well with the analysis of the five coupled pre-PRIMAVERA models, which show robustly across models an increase of the deep convection in the Labrador Sea and a decrease in the Greenland Sea with increased resolution (more details in deliverable D2.1). The results from the pre-PRIMAVERA simulations also indicated that increasing ocean resolution is the main reason for increased convection while increased atmosphere resolution instead leads to slightly reduced deep convection.

The convection in the Labrador Sea is largely governed by the ocean heat release to the atmosphere in the convection area. Northwesterly atmospheric flows, often connected to a positive state of the North Atlantic Oscillation, increase the ocean heat release and thus the density of the ocean surface. The high-resolution models show stronger surface heat fluxes than the standard resolution models in the convection areas, which agrees with the stronger convection in the Labrador Sea. Also in the GIN-Seas, high resolution leads to an increased ocean heat release to the atmosphere. However, here, the relation between surface heat fluxes and convection is strongly model dependent.

Key findings:

The high resolution models tend to overestimate the surface heat fluxes in the convection regions compared to observational based estimates and they particularly severely overestimate the Labrador Sea deep convection. This does not necessarily mean that high resolution is generally degrading the representation of deep water formation but could be due to the fact that the models in standard resolution are well tuned while the high resolution versions are not.

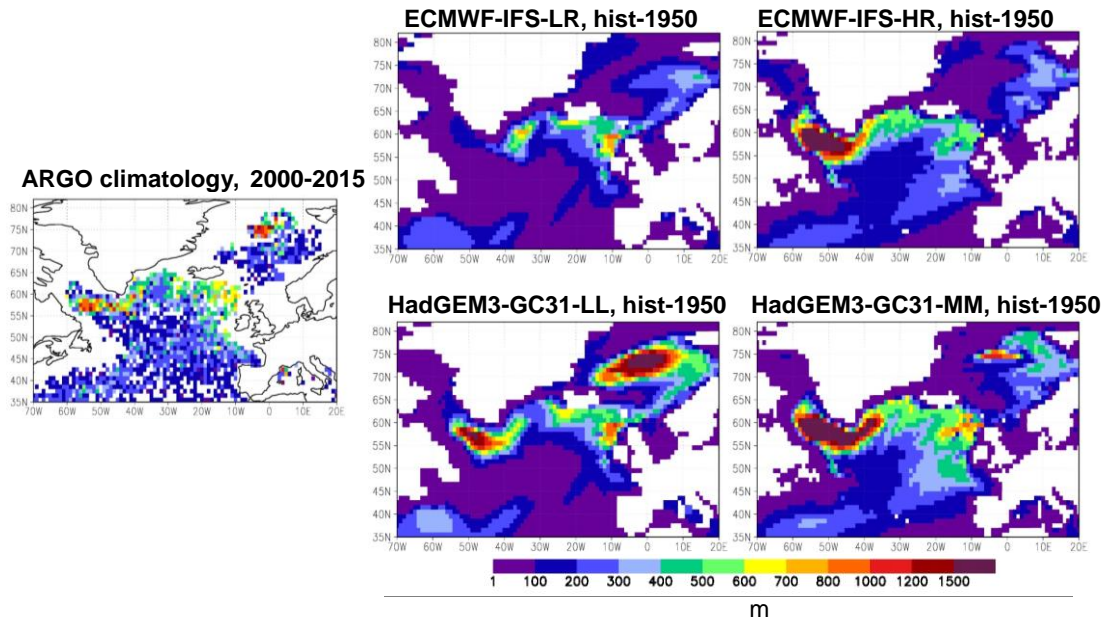


Figure 3.3.7.1: Mixed layer depth in March in observations from ARGO floats and in historical simulations in different resolution with the ECMWF-IFS-LR and the HadGEM3-GC31 coupled models.

3.3.8 Arctic freshwater content and transport in pre-Stream1 simulations (SMHI)

We compare the representation of the Arctic liquid and solid freshwater volumes, and their transports to/from the Arctic, using simulations with different ocean and atmosphere model resolutions from models participating in the EU H2020 PRIMAVERA project, particularly we used three different coupled global climate models (GCMs) from the so-called pre-PRIMAVERA data set: EC-Earth3.1, HadGEM3-GC2 and CMCC-CM2. Regarding ocean resolution, we find that higher resolution shows lower liquid freshwater volume over the Central Arctic Ocean and higher volume over the Kara and Laptev Seas compared with lower resolution (Figure 3.3.8.1).

The solid freshwater (ice) volume does not show a systematic behaviour across models. In terms of atmospheric resolution, we find systematically less liquid and solid fresh water volume in high resolution simulations compared with lower resolution simulations. We also analyze differences of Arctic liquid and solid freshwater volumes caused by pre-Industrial and historical atmospheric forcings. Pre-industrial simulations show less freshwater volume and increased ice volume and export from the Arctic compared with present day simulations. Furthermore, we find that the impact of the freshwater transport from the Arctic on the oceanic convection in the North Atlantic depends on the atmospheric resolution, showing higher impact with increased atmospheric resolution.

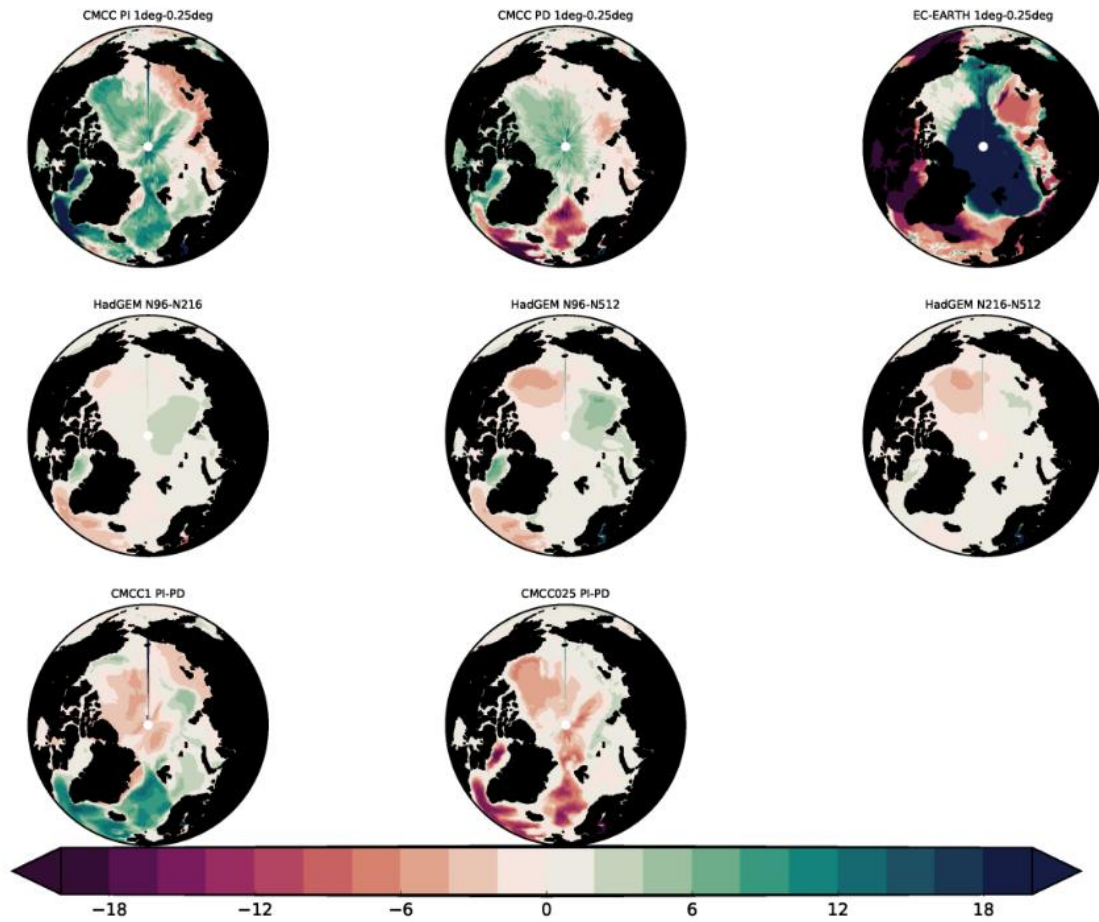


Figure 3.3.8.1: First row: Difference of liquid FWC between coupled simulations using ORCA1 minus simulations using ORCA025 for CMCC-CM2 PI (left), CMCC-CM2 PD (middle), EC-Earth (right). Second row: Difference of liquid FWC between HadGEM simulations using different atmospheric resolutions: N96 minus N216 (left), N96 minus N512 (middle) and N216 minus N512 (right). Third row: Difference of liquid FWC between CMCC simulations using different forcings (present day or pre-industrial) using the same ORCA1 (left) and ORCA025 (middle) grid resolutions. The average periods are based on the total number of years of every simulation. Unit is m.

3.4 Case studies based on different configurations of a single model

3.4.1 Impacts of ocean and atmosphere resolution in Stream 1 ECMWF-IFS (ECMWF)

This section provides an executive summary of recent work to evaluate the resolution sensitivity of the European Centre for Medium-Range Weather Forecasts Integrated Forecast System (ECMWF-IFS; Roberts et al., 2018). We present results from the following model configurations that have different combinations of ocean and atmosphere resolution: (i) ECMWF-IFS-LR (100km ocean, 50km atmosphere), (ii) ECMWF-IFS-MR (25 km ocean, 50km atmosphere), and (iii) ECMWF-IFS-HR (25 km ocean, 25 km atmosphere).

Climatological biases in radiation and surface properties in ECMWF-IFS are relatively insensitive to an increase in atmospheric resolution from ~50 km to ~25 km (figure 3.4.1.1a-b). However, increasing the horizontal resolution of the atmosphere while maintaining the same vertical resolution enhances the magnitude of a cold bias in the lower stratosphere (figure 3.4.1.1c-d). This bias is thought to be a consequence of spurious mixing across the tropopause associated with small scale variability that is intensified at horizontal higher resolutions with the cubic octahedral grid and improved by increased vertical resolution in the atmosphere (not shown). A more thorough assessment of the impact of atmospheric resolution on variability and extremes is ongoing. Other processes affected by the change in atmospheric resolution include the conservation characteristics of the semi-Lagrangian advection scheme and the net planetary energy balance.

In coupled configurations, surface biases exhibit a strong sensitivity to an increase in ocean model resolution from ~100 km to ~25 km (figure 3.4.1.2). The impacts of increased ocean resolution are particularly evident in the North Atlantic and Arctic, where they are associated with an improved Atlantic meridional overturning circulation, increased meridional ocean heat transports, and more realistic sea-ice cover. The negative effects of increased ocean resolution include an amplification of a Southern Ocean warm bias, weakening of the Antarctic circumpolar current, and a dramatic decline of Antarctic sea-ice. These effects are likely a consequence of the “eddy-permitting” rather than “eddy resolving” nature of the ECMWF-IFS-MR/-HR ocean configuration in the Southern Ocean and the disabling of the eddy parameterizations that are used in ECMWF-IFS-LR.

In the tropical Pacific, increased ocean resolution is associated with improvements to the magnitude and asymmetry of ENSO variability and better representation of non-linear SST-radiation feedbacks during warm events. There is tentative evidence that both ocean coupling and increased atmospheric resolution can improve teleconnections between tropical Pacific rainfall and geopotential height anomalies in the North Atlantic.

Key results: Climatological surface biases in ECMWF-IFS are relatively insensitive to an increase in atmospheric resolution from ~50 km to ~25 km

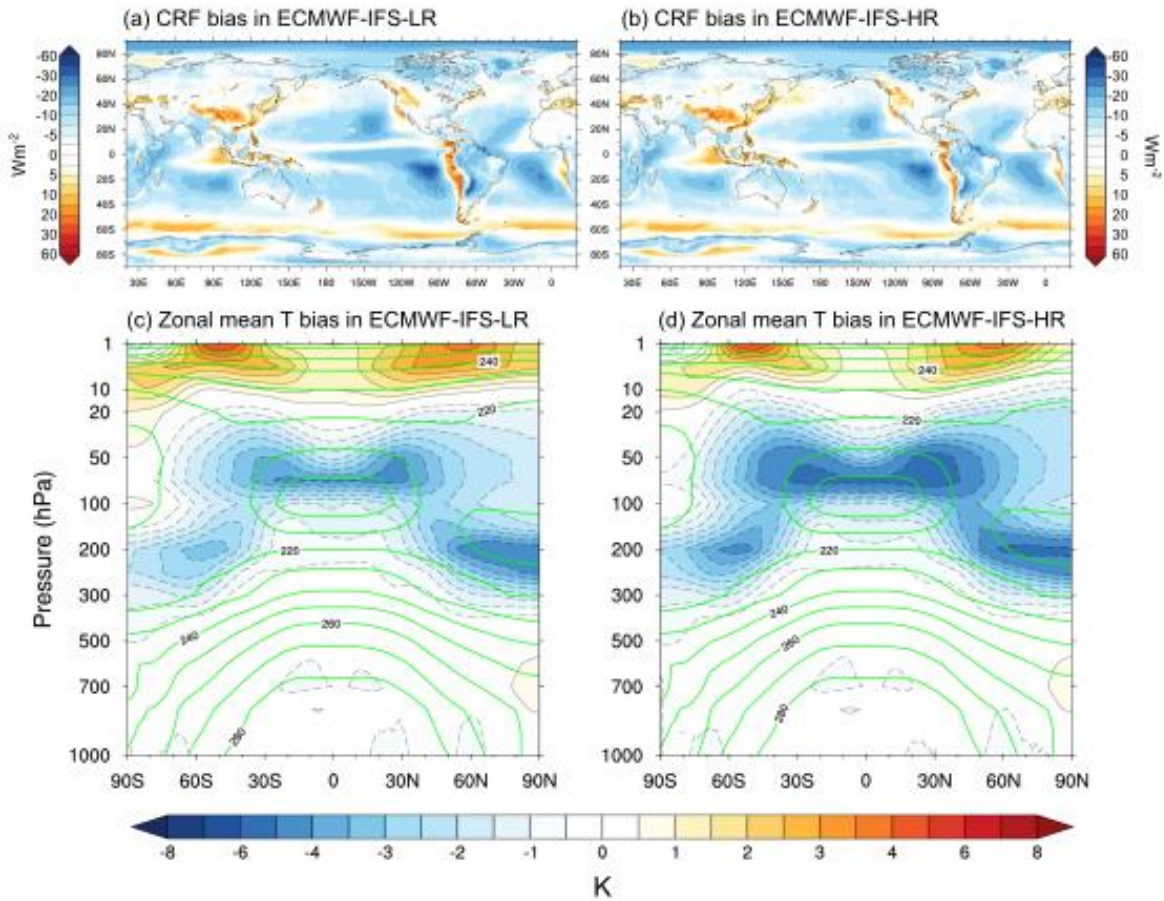


Figure 3.4.1.1 (a-b) Annual mean bias in total cloud radiative forcing (CRF) in atmosphere-only experiments with ECMWF-IFS relative to CERES-EBAF Surface Fluxes Edition 4.0 (Kato et al., 2013) for the period 2001-2014. (c-d) Annual mean bias in zonal mean temperature relative to the ERA-interim reanalysis (Dee et al. 2011) for the period 1981-2010.

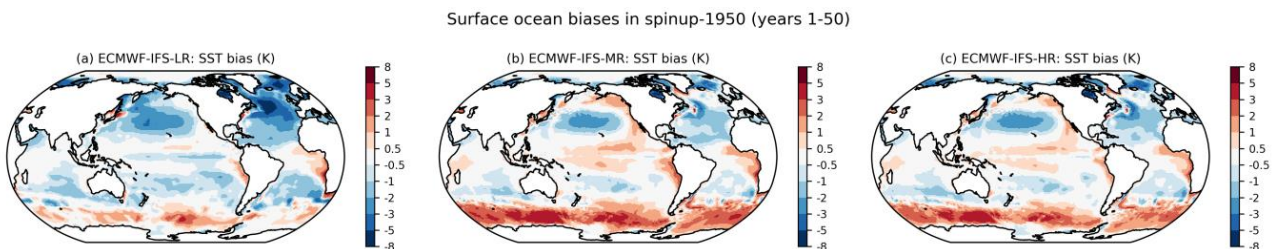


Figure 3.4.1.2 Annual mean sea surface temperature biases in coupled experiments with ECMWF-IFS for years 1-50 of *spinup-1950* relative to an observational climatology representative of the period 1950-1954 (Good et al. 2013).

3.4.2 The impact of ocean model resolution in ECMWF-IFS: a seamless approach (ECMWF)

Recent studies have emphasized the importance of ocean-atmosphere coupling for numerical weather prediction (Brassington et al. 2015; Mogensen et al. 2017) and argued that increases in ocean model resolution will lead to improved predictions across weather and climate timescales (Hewitt et al. 2017). However, previous studies have typically evaluated the impacts of resolution in uninitialized simulations in which the ocean biases are well established. The relevance of such studies for initialized predictions that cover operational timescales ranging from days to months is much less well understood. Here, we augment results from multidecadal PRIMAVERA climate integrations with data from sub-seasonal and seasonal forecast experiments to systematically evaluate the sensitivity of ECMWF-IFS to an increase of ocean model resolution from ~100 km to ~25 km, which corresponds to a transition from the 'eddy-parameterized' to 'eddy-permitting' regime. The model configurations used in this study are listed in table 3.4.2.1. ECMWF-IFS-LR and ECMWF-IFS-MR are PRIMAVERA/HighResMIP configurations (Roberts et al., 2018) and SEAS-HR corresponds to the latest version of the ECMWF seasonal forecast system (Johnson et al. 2018).

This study is focussed on the North Atlantic during the winter season (DJF), a region that is known to be particularly sensitive to changes in ocean model resolution in multi-decadal climate integrations with ECMWF-IFS (Roberts et al. 2018; section 3.4.1). Despite this large sensitivity on decadal timescales, North Atlantic SST biases in ENS-LR and ENS-HR are extremely similar at sub-seasonal timescales and to a large extent are inherited from the ocean analysis that provides forecast initial conditions (figure 3.4.2.1 a-d). It is only on seasonal timescales that the impact of ocean resolution begins to have a substantial impact on mean SST biases (figure 3.4.2.1 e-f).

Similarly, the spatial derivatives of SST are reproduced reasonably well on sub-seasonal timescales (figure 3.4.2.1 i-o, figure 3.4.2.2a-b). At longer lead-times, the path of the Gulf Stream breaks down in eddy-parameterized ocean model configurations, which has corresponding impacts on convergence in the atmospheric boundary layer and the position and intensity of the precipitation maximum south of Gulf Stream. In contrast, the mean spatial gradients in the eddy-permitting ocean model configurations are maintained much better on multi-decadal time-scales.

The impact of ocean model resolution on the nature of air-sea exchange over the Gulf Stream is substantial and insensitive to lead-time (figure 3.4.2.2h-n). This is a consequence of the subdued mesoscale activity in the eddy-parameterized ocean model configurations that cannot be ameliorated by initialization with observed conditions. In contrast, other aspects of variability such as atmospheric blocking are sensitive to the magnitude of the mean SST bias and thus show larger impacts at longer lead times (figure 3.4.2.3).

Key results: The impact of ocean model resolution in initialized predictions is time-scale dependent and sensitive to the relative importance of mean-bias and variability effects. These impacts will be further quantified in a forthcoming manuscript (Roberts et al., *in preparation*).

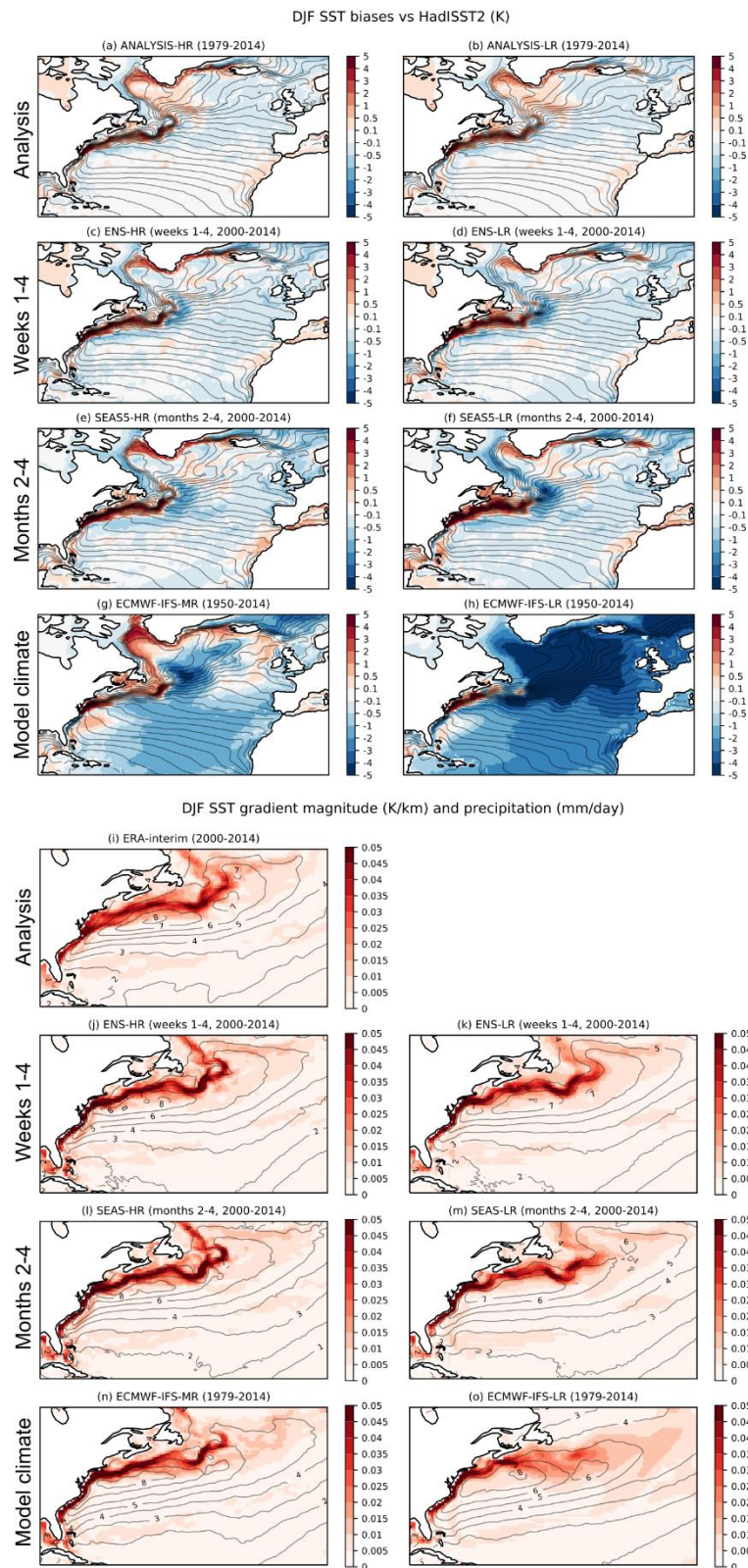


Figure 3.4.2.1 (a-h) DJF sea surface temperature (SST) climatologies at different lead times (1K contour interval) and SST biases (colours) relative to observations (HadISST2; Rayner et al. 2016). (i-o) DJF climatologies of SST gradient magnitude (colours) and precipitation (1 mm/day contour interval) at different lead times.

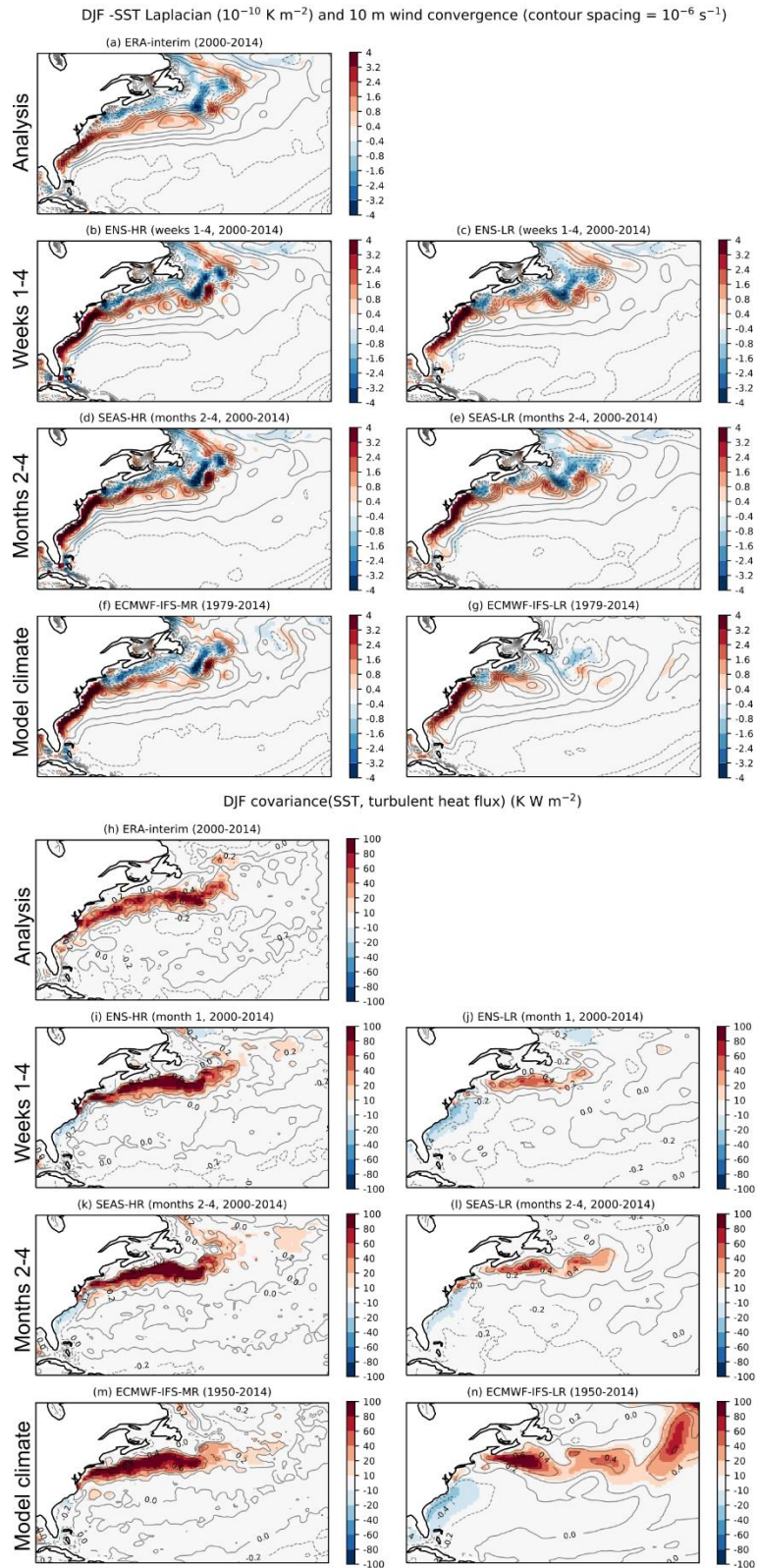


Figure 3.4.2.2 (a-g) DJF climatologies of $-\nabla^2(\text{SST})$ (colours) and 10 m wind convergence (contour intervals of 10^{-6} s^{-1}). Derivatives are calculated on a regular 0.5×0.5 degree grid and the resulting grid-point noise is suppressed with 4 applications of a weighted averaged 9-point smoother. (h-n) Covariance (colours) and correlations (contour intervals of 0.2; negative values dashed) between monthly anomalies of SST and turbulent heat fluxes.

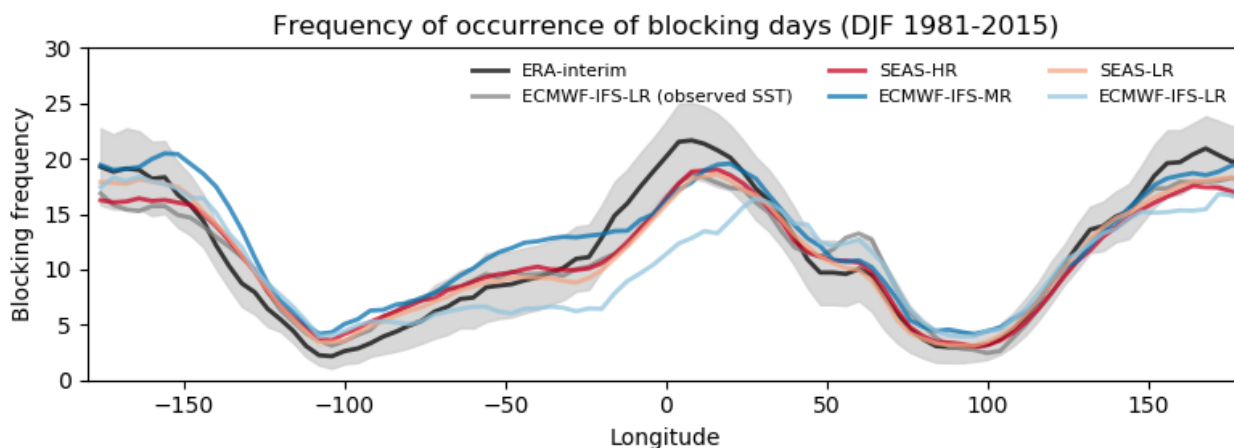


Figure 3.4.2.3 (a-g) Frequency of blocked days in the ERA-interim analysis (Dee et al. 2011), seasonal forecast configurations with different ocean model resolutions (SEAS-HR, SEAS-LR), coupled configurations of ECMWF-IFS with different ocean model resolutions (ECMWF-IFS-LR, ECMWF-IFS-MR) and an atmosphere only version of ECMWF-IFS-LR forced with observed SSTs.

Table 3.4.2.1 Configurations of ECMWF-IFS used to evaluate the sensitivity to increased ocean model resolution at different timescales.

Configuration	Ocean	Atm.	Period
ENS-LRO	100 km	30 km	12 start dates per year 1989-2016, 5 members x 31 days.
ENS-HRO	25 km	30 km	12 start dates per year 1989-2016, 5 members x 31 days.
SEAS-LRO	100 km	30 km	2 start dates per year 1981-2016, 5 members x 7 months.
SEAS-HRO	25 km	30 km	2 start dates per year 1981-2016, 5 members x 7 months.
ECMWF-IFS-LR	100 km	50 km	1950-2014 (50 year spinup from climatology)
ECMWF-IFS-MR	25 km	50 km	1950-2014 (50 year spinup from climatology)

3.4.3 Early winter response to ENSO in HadGEM3 (MOHC)

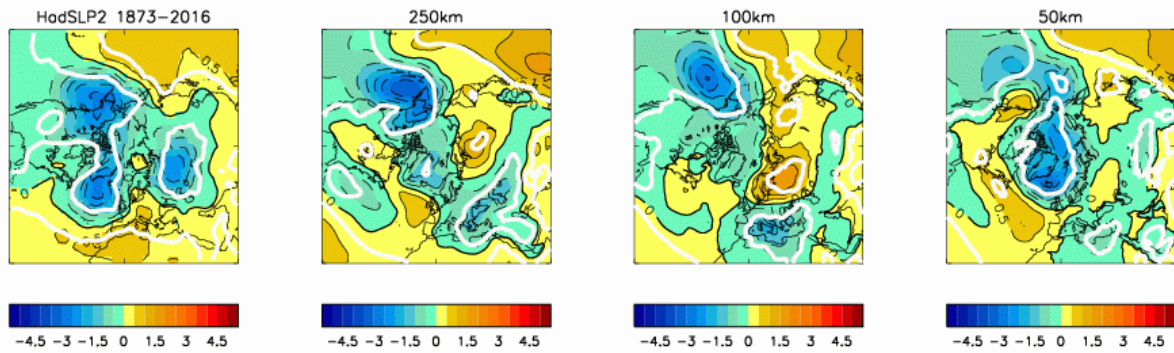
The European/North Atlantic late winter (January-February) response to El Niño (La Niña) resembles the negative (positive) phase of the NAO and can be simulated by climate models providing the stratosphere, which is involved in the teleconnection pathway, is well resolved. However, this response does not simply grow throughout the winter period, rather observations show a different and more wave-like pattern in early winter (November-December). The mechanism for this early winter pattern was not well understood and the teleconnection pathway has been explored in a recent publication, Ayarzagüena et al. 2018. It appears to be linked to ENSO related precipitation anomalies over the Gulf of Mexico/Caribbean Sea. While initialised predictions are able to capture this signal, it does not appear in free running CMIP5 coupled simulations. In the Met Office AMIP PRIMAVERA

ensembles (3 members at 250, 100 and 50km resolution) we find that the La Niña teleconnection is generally well reproduced, although the anomalous filling of the Aleutian low and the positioning of the ridge to the west of the UK is least well simulated at N216. This may be due to sampling issues. However, during El Niño there is no significant response to the west of the UK at either 250 or 100km resolution. At 50km there is low pressure to the north west, but the pattern does not extend far enough south.

Key findings:

Early winter European response to ENSO is not robustly simulated in a small ensemble of one model at any resolution.

November–December response to El Niño



November–December response to La Niña

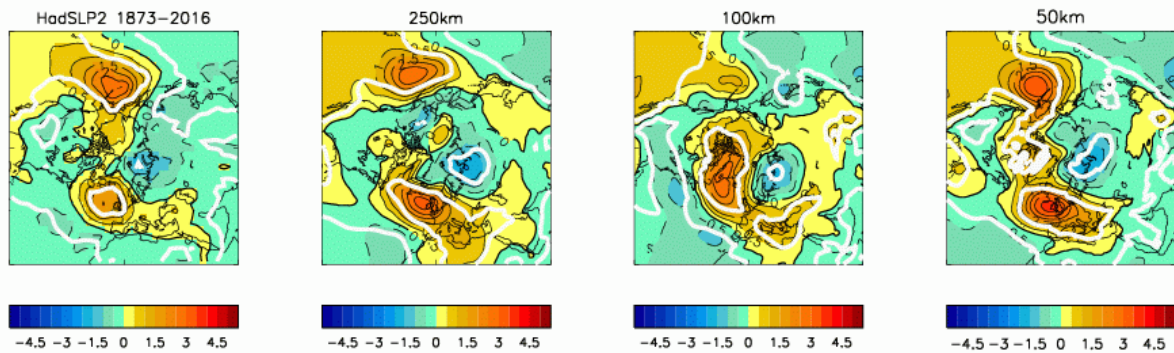


Figure 3.4.3.1 Composite sea-level pressure response to El Niño (top row) and La Niña (bottom row) in HadSLP2 data (left) and AMIP Stream1 simulations with HadGEM3 at low, medium and high resolution.

3.4.4 Dependence of Atlantic Ocean heat transport on model resolution in HadGEM3 (NERC)

Model resolution dependent changes in Atlantic Ocean heat transport (AOHT) and surface heat fluxes have been examined (Grist et al. 2018). The different roles of changes in atmospheric and ocean resolution are isolated using three different climate models (*CMCC2-CM2*; *HadGEM3 GC2.0*; *EC EARTH 3.1*) and comparing Pre-Stream1 runs in which a) only the ocean resolution changes; b) only the atmosphere resolution changes and c) both change. Enhancing ocean resolution from eddy parameterized (about 1°) to eddy permitting (about $1/4^\circ$), both while holding the atmospheric resolution constant and while simultaneously increasing atmospheric resolution, increases the AOHT throughout the basin significantly, bringing the AOHT into better agreement with observations in the tropics and sub-tropics, but into worse agreement in the subpolar regions (where the modelled AOHTs are larger than the observed). The increases in AOHT are balanced to first order by increased Latent Heat loss in the subpolar regions. These results are described more fully in Deliverable 2.1.

In this report, we note the effect of increased atmospheric resolution alone in more detail for HadGEM3 GC2.0. For this model, increasing the atmospheric resolution alone (from 250km to 50km nominal resolution) while ocean resolution remained at a constant $1/4^\circ$, had little impact on the AOHT. Although there was little change in the ocean heat transport divergence and thus the net surface heat flux, there were significant regionally compensating changes in the components of the net heat flux. Specifically, there was an increase in incoming shortwave radiation at the ocean surface over much of the north and equatorial Atlantic which was largely compensated by an increased oceanic heat loss from the latent heat flux (Fig. 3.4.4.1 a and b) Grist et al. 2018). The increase in shortwave was associated with a reduction of cloud cover while an increase in latent heat flux resulted from higher sea surface temperatures and stronger surface wind. The compensating nature of the changes in these processes is most evident in the Equatorial Atlantic (Fig. 3.4.4.1 c and d).

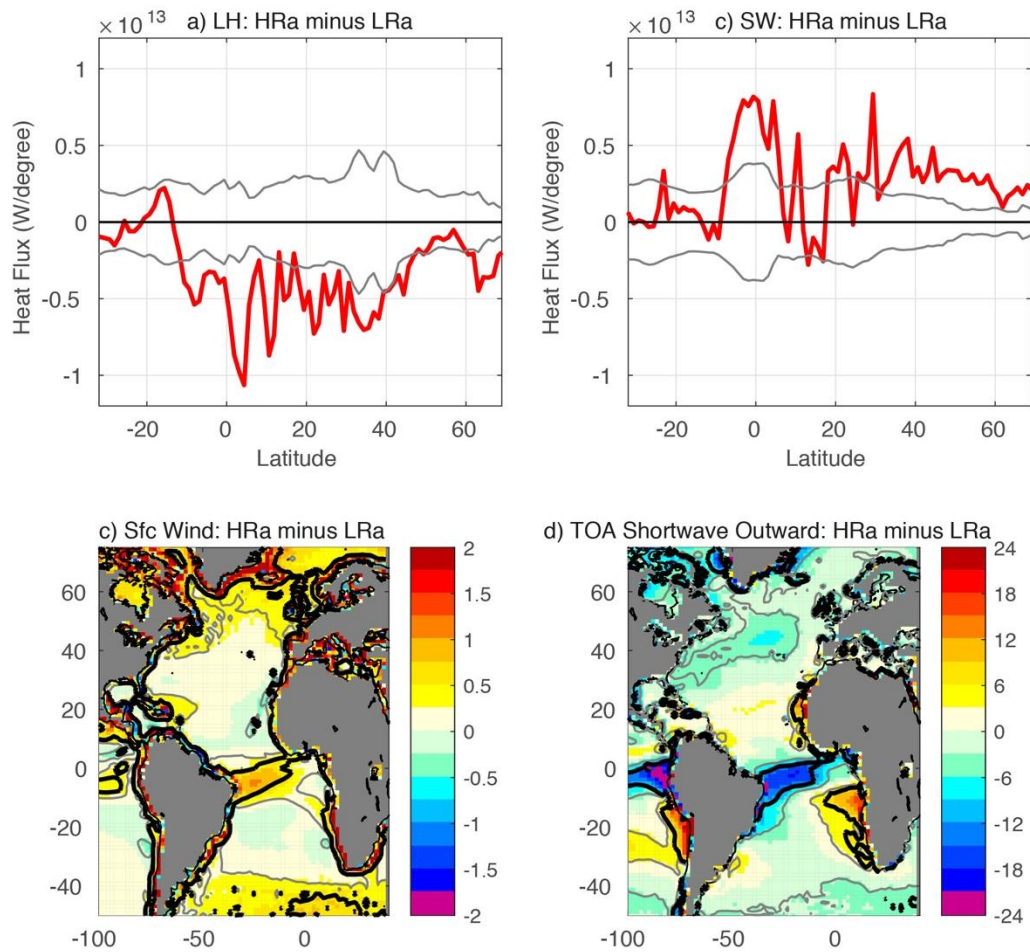


Figure 3.4.4.1. Annual mean high minus low atmosphere resolution versions of HadGEM3 GC2.0 of the zonally integrated heat flux components for the Atlantic basin (Units W per degree latitude): a) latent heat flux, b) shortwave. Grey lines indicate \pm the LRa interannual standard deviation. c) and d) annual mean of the high minus low atmosphere resolution versions of HadGEM3 GC2.0, for a) ocean surface air temperature ($^{\circ}\text{C}$); b) ocean surface wind speed (m s^{-1}); c) top of the atmosphere (TOA) outgoing shortwave radiation over the ocean (Wm^{-2}). Where positive (negative) outgoing TOA is taken to be representative of an increase (decrease) in cloud cover. Grey and black contours are one and two standard deviations from the low-resolution atmosphere respectively.

3.4.5 Contribution of internal climate variability to the ocean heat uptake and its sensitivity to model resolution in EC-Earth3P (BSC)

It has been shown that in a forced climate there is a linear relationship between the radiative forcing F and the global mean surface temperature change T , $F = \rho T$ (Gregory and Forster, 2008). The net top-of-the-atmosphere (TOA) radiation N , equal to the difference between F and the radiative feedback λT , can be written as

$$(1) \quad N = F - \lambda T = (\rho - \lambda) T = \kappa T = dH/Dt$$

where H is the ocean heat content (OHC). During hiatus periods ($dT/dt \leq 0$), Equation 1 implies $dN/dt = dF/dt$, i.e. there is an accelerated ocean heat uptake. It is unclear from observations whether accelerated heat content uptake or increase in TOA radiation occurs in the case of a hiatus. Recent studies revisited the energy budget discussing that the previous relationships are different under a context of internally generated variability than in a forced climate (Xie et al., 2016, Drijfhout, 2018). These studies analysed CMIP5 simulations in the most commonly used resolutions of about 1 deg in both the ocean and the atmosphere. The impact of increased model resolution on the energy budget has not been addressed.

Here, we analyse and compare the energy budget in high and standard resolution (HR and SR, respectively) sets of present-day control HighResMIP experiments performed with the EC-Earth climate model (version EC-Earth3P). We look in particular at the potential contributions of the Atlantic Meridional Overturning Circulation (AMOC), which largely controls the ocean energy transport from the Equator to Arctic, to the global and local heat uptake. We have produced 3 members in order to remove the model drift, which is characterized by the ensemble mean.

The change in resolution leads to different model biases in the polar region, associated with different biases in sea-ice volume and polar temperature and rather distinct variability in the AMOC, which shows substantially higher variability at subpolar latitudes in the SR version. This could be related to the fact that the main region of deep convection occurs in the Labrador in the HR simulations, and in the Nordic Seas in the SR ones. SR is also warmer in the northern high latitudes and has comparatively less sea-ice.

The regression patterns in Fig 3.4.5.1 inform about the concomitant changes between the AMOC strength and the upper ocean temperatures, and thus about the global impact that the AMOC can play on the heat uptake by the ocean. Important differences can be observed between the two resolutions. While in the LR simulations, the impact of AMOC on SSTs is almost exclusively restricted to a warming in the North Atlantic subpolar gyre and over the Arctic, the HR experiments (which are eddy-permitting) seem to additionally represent other key processes and interactions. The associated regression exhibits, for example, a region of substantial cooling in the Atlantic downstream of the Agulhas Current, as well as massive warmings over the Southern Ocean. These preliminary results thus suggest that the model resolution will play an important role in the representation of the AMOC, and by extension of its contribution to the global heat budget.

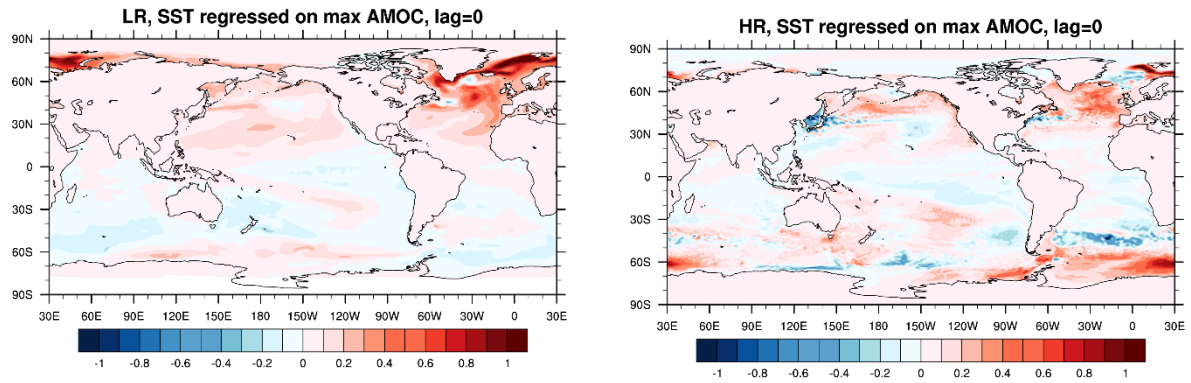


Figure 3.4.5.1: Regressions of SST on the maximum AMOC strength (at any latitude and depth) for standard resolution (left) and high resolution (right). Data have been smoothed using a 13-year running means.

3.5 Peer-reviewed articles arising from the project

Published articles:

- Bloemendaal, N., S. Muis, S. R. J. Haarsma, M. Verlaan, M. Irazoqui, Apecechea, H., de Moel, H., P. J. Ward, J. C. J. H. Aerts. (2018) Global modeling of tropical cyclone storm surges using high-resolution forecasts. *Climate Dynamics*, doi:10.1007/s00382-018-4430-x
- Dekker M.M., Haarsma R.J., Vries H., Baatsen, M., van Delden A.J (2018). Characteristics and development of European cyclones with tropical origin in reanalysis data *Clim. Dyn.* 50: 445-455. doi: 10.1007/s00382-017-3619-8
- Haarsma, R. J., M.J. Roberts, P. L. Vidale, C. A. Senior, A. Bellucci, Q. Bao, von Hardenberg, J. (2016). High resolution model intercomparison project (HighResMIP v1. 0) for CMIP6. *Geoscientific Model Development*, 9(1), 4185-4208.
- Roberts, C. D., R. Senan, F. Molteni, S. Boussetta, M. Mayer, S. P. E. Keeley (2018). Climate model configurations of the ECMWF Integrated Forecast System (ECMWF-IFS cycle 43r1) for HighResMIP. *Geoscientific Model Development*, doi: 10.5194/gmd-11-3681-2018.
- Scher S., Haarsma R. J., De Vries H., Drijfhout S. S., van Delden A. J. (2017). Resolution dependence of extreme precipitation and deep convection over the Gulf Stream. *J. Adv. Model. Earth Syst.*, 9(2), 1186-1194. doi:10.1002/2016MS000903.
- Vries H., Scher S., Haarsma R., Drijfhout S., van Delden A.J. (2018). How Gulf-Stream SST-fronts influence Atlantic winter storms *Clim. Dyn.* doi: 10.1007/s00382-018-4486-7

Submitted articles:

- De Vries, H, S. Scher, R. Haarsma, S. Drijfhout (2018). How Gulf-Stream SST-fronts influence Atlantic winter storms: Results from a downscaling experiment with HARMONIE to the role of modified latent heat fluxes and low-level baroclinicity. *Climate Dynamics* (accepted).
- Docquier, D., J. P. Grist, M. J. Roberts, C. D. Roberts, T. Semmler, L. Ponsoni, F. Massonnet, D. Sidorenko, D. Sein, D. Iovino, T. Fichet. (2018). Impact of model resolution on Arctic sea ice and North Atlantic Ocean heat transport. (submitted to *Climate Dynamics*)
- Grist, J. P., Josey, S.A., New, A. L., Roberts, M., Koenig, T., and Iovino, D. (2018) Increasing Atlantic Ocean heat transport in the latest generation coupled ocean-atmosphere models: The role of air-sea interaction. Submitted to *Journal of Geophysical Research – Oceans*.
- Van der Linden, E, R. J. Haarsma, G. van der Schrier. Impact of climate model resolution on soil moisture projections in central-western Europe (2018). Submitted to *HESS*.
- Vanniere B., M.-E. Demory, P. L. Vidale, R. Schiemann, M. J. Roberts, C. D. Roberts, M. Matsueda, L. Terray, T. Koenig and R. Senan. (2018) Multi-model evaluation of the sensitivity of the global energy budget and hydrological cycle to resolution. *Climate Dynamics*, under review.

Articles to be submitted or in preparation:

- Haarsma R.J., García-Serrano J., Prodhomme C., Bellprat O., Davini P., Drijfhout S. (2018). Sensitivity of winter North Atlantic European climate to resolved atmosphere and ocean dynamics. To be submitted.
- Klaver R., Haarsma R.J., Vidale P.L., Hazeleger W. (2018). Effective resolution in high resolution global models for climate studies. To be submitted.
- Molteni F., Roberts C., Senan R. et al.: Teleconnections from the tropical Indian Ocean in historical HighResMIP simulations with European climate models. In preparation.
- Roberts, C. D. et al. (in preparation). The impact of increased ocean model resolution in coupled forecasting system: a seamless approach.
- Roberts, M.J, Camp, J., Vidale, P.L., Hodges, K., Vanniere, B., Mecking, J., Haarsma, R., Bellucci, A., Scoccimarro, E., Caron, L.-P., Chauvin, F., Putrasahan, D., Roberts, C. Impact of model resolution on tropical cyclone simulation using the HighResMIP-PRIMAVERA multi-model ensemble. In preparation.
- Strommen K., Mavilia I., Corti S., Davini P., Matsueda M., von Hadenberg J., Vidale P-L., Mizuta R. (2018). The Sensitivity of Euro-Atlantic Regimes to Model Horizontal Resolution. To be submitted to GRL

3.6 Other references

- Athanasiadis, P. J., Bellucci, A., Hermanson, L., Scaife, A. A., Maclachlan, C., Arribas, A., et al. (2014). The representation of atmospheric blocking and the associated low-frequency variability in two seasonal prediction systems. *Journal of Climate*, 27(24), 9082–9100. <https://doi.org/10.1175/JCLI-D-14-00291.1>
- Ayarzagüena, B., Ineson, S., Dunstone, N. J., Baldwin, M. P., & Scaife, A. A. (2018). Intraseasonal Effects of El Niño–Southern Oscillation on North Atlantic Climate. *Journal of Climate*, doi: 10.1175/JCLI-D-18-0097.1
- Berckmans, J., Woollings, T., Demory, M.-E., Vidale, P.-L., & Roberts, M. (2013). Atmospheric blocking in a high resolution climate model: influences of mean state, orography and eddy forcing. *Atmospheric Science Letters*, 14(1), 34–40. <https://doi.org/10.1002/asl2.412>
- Bhend J., Whetton P. (2013). Consistency of simulated and observed regional changes in temperature, sea level pressure and precipitation. *Climatic Change*, doi:10.1007/s10584-012-0691-2
- Brassington, G. B., Martin, M. J., Tolman, H. L., Akella, S., Balmeseda, M., Chambers, C. R. S., Chassignet, E., Cummings, J.A., Drillet, Y., Jansen, P.A.E.M, & Laloyaux, P. (2015). Progress and challenges in short-to medium-range coupled prediction. *Journal of Operational Oceanography*, 8(sup2), s239-s258.
- Cassou, C., 2008: Intraseasonal interaction between the Madden-Julian Oscillation and the North Atlantic Oscillation. *Nature* **255**, 523-527.
- Corti S., Molteni F., Palmer T. (1999). Signature of climate change in frequencies of natural atmospheric circulation regimes. *Nature*, doi: 10.1038/19745.
- Davini, P., Corti, S., D’Andrea, F., Rivière, G., & von Hardenberg, J. (2017). Improved Winter European Atmospheric Blocking Frequencies in High-Resolution

- Global Climate Simulations. *Journal of Advances in Modeling Earth Systems*, 9(7), 2615–2634. <https://doi.org/10.1002/2017MS001082>
- Dee, D. P., Uppala, S. M., Simmons, A. J., Berrisford, P., Poli, P., Kobayashi, S., Andrae, U., Balmaseda, M.A., Balsamo, G., Bauer, D.P., Bechtold, P., et al. (2011). The ERA-Interim reanalysis: Configuration and performance of the data assimilation system. *Quarterly Journal of the Royal Meteorological Society*, 137(656), 553-597.
 - Dawson A., Palmer T., Corti S. (2012). Simulating regime structures in weather and climate prediction models. *Geophysical Research Letters*, doi:10.1029/2012GL053284
 - Ferranti L., Corti S., Janousek M. (2015). Flow-dependent verification of the ECMWF ensemble over the Euro-Atlantic sector. *Quarterly Journal of the Royal Meteorological Society*, doi:10.1002/qj.2411
 - Franzke C., Woolings T., Martius O. (2011). Persistent circulation regimes and preferred regime transitions in the North Atlantic. *Journal of the Atmospheric Sciences*, doi:10.1175/JAS-D-11-046.1
 - Gelaro, R., and Coauthors (2017). The modern-era retrospective analysis for research and applications, version 2 (MERRA-2). *Journal of Climate*, 30(14), <https://doi.org/10.1175/JCLI-D-16-0758.1>
 - Good, S. A., Martin, M. J., & Rayner, N. A. (2013). EN4: Quality controlled ocean temperature and salinity profiles and monthly objective analyses with uncertainty estimates. *Journal of Geophysical Research: Oceans*, 118(12), 6704-6716.
 - Hallberg, R. (2013). Using a resolution function to regulate parameterizations of oceanic mesoscale eddy effects. *Ocean Modelling*, 72, 92-103.
 - Hannachi A. et al. (2013). Behaviour of the winter North Atlantic eddy-driven jet stream in the CMIP3 integrations. *Clim. Dyn.* 41: 995–1007.
 - Hewitt, H. T., Roberts, M. J., Hyder, P., Graham, T., Rae, J., Belcher, S. E., Bourdallé-Badie, R., Copsey, D., Coward, A., Guiavarch, C. et al. (2016). The impact of resolving the Rossby radius at mid-latitudes in the ocean: Results from a high-resolution version of the Met Office GC2 coupled model. *Geoscientific Model Development*, 9(10), 3655-3670.
 - Hewitt, H. T., Bell, M. J., Chassignet, E. P., Czaja, A., Ferreira, D., Griffies, S. M., Hyder, P., McClean, J.L., New, A.L. and Roberts, M. J. (2017). Will high-resolution global ocean models benefit coupled predictions on short-range to climate timescales?. *Ocean Modelling*.
 - Hodges, K.I., 1995: Feature Tracking on the Unit Sphere. *Mon. Wea. Rev.*, 123, 3458–3465, [https://doi.org/10.1175/1520-0493\(1995\)123<3458:FTOTUS>2.0.CO;2](https://doi.org/10.1175/1520-0493(1995)123<3458:FTOTUS>2.0.CO;2)
 - Hodges, K., Cobb, A., & Vidale, P. L. (2017). How well are tropical cyclones represented in reanalysis datasets? *Journal of Climate*, 30(14), 5243–5264. <https://doi.org/10.1175/JCLI-D-16-0557.1>
 - Huffman, G. J. et al., 2001: Global Precipitation at One-Degree Daily Resolution from Multisatellite Observations. *J. Hydrometeorol.* 2, 36-50.
 - Kato, S., Loeb, N. G., Rose, F. G., Doelling, D. R., Rutan, D. A., Caldwell, T. E., Yu, L. & Weller, R. A. (2013). Surface irradiances consistent with CERES-derived top-of-atmosphere shortwave and longwave irradiances. *Journal of Climate*, 26(9), 2719-2740.
 - Iqbal W. et al. (2018). Analysis of the variability of the North Atlantic eddy-driven jet stream in CMIP5. *Clim. Dyn.* 51: 235.

- Johnson, S. J., Stockdale, T. N., Ferranti, L., Balmaseda, M. A., Molteni, F., Magnusson, L., Tietsche, S., Decremmer, D., Weisheimer, A., Balsamo, G., Keeley, S., Mogensen, K., Zuo, H., and Monge-Sanz, B (in review). SEAS5: The new ECMWF seasonal forecast system, *Geosci. Model Dev. Discuss.*, <https://doi.org/10.5194/gmd-2018-228>.
- Kennedy, J., Titchner, H., Rayner, N., Roberts, M., 2017: input4MIPs.MOHC.SSTsAndSeaIce.HighResMIP.MOHC-HadISST-2-2-0-0-0. Version 20170505. Earth System Grid Federation. doi.org/10.22033/ESGF/input4MIPs.1221
- Kwon, YO. et al. (2018). North Atlantic winter eddy-driven jet and atmospheric blocking variability in the Community Earth System Model version 1 Large Ensemble simulations. *Clim. Dyn.* 51: 3275.
- Laloyaux, P., de Boisseson E., Balmaseda M., Bidlot J.-R., Broennimann S., Buizza R., et al. (2018). CERA-20C: A coupled reanalysis of the twentieth century. *Journal of Advances in Modeling Earth Systems*, 10, 1172–1195. <https://doi.org/10.1029/2018MS001273>.
- Lin, H., G. Brunet, and J. Derome, 2009: An observed connection between the North Atlantic Oscillation and the Madden–Julian Oscillation. *J. Climate*, **22**, 364–380.
- Matsueda M., Palmer T. (2018). Estimates of the flow-dependent predictability of wintertime Euro-Atlantic weather regimes in medium-range forecasts. *Quarterly Journal of the Royal Meteorological Society*, doi:10.1002/qj.3265.
- Mogensen, K. S., Magnusson, L., & Bidlot, J. R. (2017). Tropical cyclone sensitivity to ocean coupling in the ECMWF coupled model. *Journal of Geophysical Research: Oceans*, 122(5), 4392-4412.
- Molteni F., T. Stockdale, and F. Vitart, 2015: Understanding and modelling extra-tropical teleconnections with the Indo-Pacific region during the northern winter. *Climate Dyn.*, **45**, 3119-3140. doi: 10.1007/s00382-015-2528-y.
- Palmer T. (2009). A nonlinear dynamical perspective on climate prediction. *Journal of Climate*, 12, 575–591, doi: 0.1175/1520-0442(1999)012<0575:ANDPOC>2.0.CO;2
- Rohde R., Muller R. A., et al. (2013) A New Estimate of the Average Earth Surface Land Temperature Spanning 1753 to 2011. *Geoinformatics and Geostatistics: An Overview*, doi:10.4172/gigs.1000101
- Scaife, A. a., Woollings, T., Knight, J., Martin, G., & Hinton, T. (2010). Atmospheric Blocking and Mean Biases in Climate Models. *Journal of Climate*, 23(23), 6143–6152. <https://doi.org/10.1175/2010JCLI3728.1>
- Scher S., Haarsma R. J, de Vries H., Drijfhout S., van Delden A. J. (2017). Resolution dependence of extreme precipitation and deep convection over the Gulf Stream. *Journal of Advances in Modeling Earth Systems*, doi:10.1002/2016MS000903.
- Scherrer, S. C., Croci-Maspoli, M., Schwierz, C., & Appenzeller, C. (2006). Two-dimensional indices of atmospheric blocking and their statistical relationship with winter climate patterns in the Euro-Atlantic region. *International Journal of Climatology*, 26(2), 233–249. <https://doi.org/10.1002/joc.1250>
- Schiemann, R., Demory, M.-E., Shaffrey, L. C., Strachan, J., Vidale, P. L., Mizieliński, M. S., et al. (2017). The Resolution Sensitivity of Northern Hemisphere Blocking in Four 25-km Atmospheric Global Circulation Models. *Journal of Climate*, 30(1), 337–358. <https://doi.org/10.1175/JCLI-D-16-0100.1>

- Schiemann, R. et al., 2018: Mean and extreme precipitation over European river basins better simulated in a 25km AGCM. *Hydrol. Earth Syst. Sci.* **22**, 3933-3950.
- Silverman BW (1986). *Density Estimation for Statistics and Data Analysis*, Vol. 26, Monographs on Statistics and Applied Probability, Chapman and Hall, London, 1986.
- Straus D. M., Corti S., Molteni F. (2007). Circulation regimes: chaotic variability versus SST-forced predictability. *Journal of Climate*, doi: 10.1775/JCLI4070.1
- Timmermann, A., An, S. I., Kug, J. S., Jin, F. F., Cai, W., Capotondi, A., Stein, K. et al. (2018). El Niño–Southern Oscillation complexity. *Nature*, 559(7715), 535.
- Ullrich, P. A., & Zarzycki, C. M. (2017). TempestExtremes: A framework for scale-insensitive pointwise feature tracking on unstructured grids. *Geoscientific Model Development*, 10(3), 1069–1090. <https://doi.org/10.5194/gmd-10-1069-2017>
- Van Haren R., Haarsma R. J., van Oldenborgh G. J., Hazeleger W. (2015) Resolution dependence of European precipitation in a state-of-the-art atmospheric general circulation model. *Journal of Climate*, doi:10.1175/JCLI-D-14-00279.1
- van Oldenborgh G. J., Drijfhout S. S., van Ulden A., Haarsma R. J., Sterl A., Severijns C., Hazeleger W., Dijkstra H. A. (2009). Western Europe is warming much faster than expected. *Climate of the Past*, doi:10.5194/cp-5-1-2009
- Vries H., Scher S., Haarsma R., Drijfhout S., van Delden A.J. (2018). How Gulf-Stream SST-fronts influence Atlantic winter storms *Clim. Dyn.* doi: 10.1007/s00382-018-4486-7
- Watson P., Berner J., Corti S., Davini P., von Hardenberg J., Sanchez C., Weisheimer A., Palmer T. (2017). The impact of stochastic physics on tropical rainfall variability in global climate models on daily to weekly timescales. *Journal of Geophysical Research*, doi:10.1002/2016JD026386.
- Woollings, T., 2010. Dynamical influences on European climate: an uncertain future. *Philosophical Transactions of the Royal Society A: Mathematical, Physical and Engineering Sciences* 368, 3733.
- Woollings T., Hannachi A., Hoskins B. (2010). Variability of the North-Atlantic eddy-driven jet stream. *Quarterly Journal of the Royal Meteorological Society*, doi:10.1002/qj.625
- Woollings, T., Barriopedro, D., Methven, J., Son, S.-W., Martius, O., Harvey, B., et al. (2018). Blocking and its Response to Climate Change. *Current Climate Change Reports*, 287–300. <https://doi.org/10.1007/s40641-018-0108-z>
- Woollings T. et al. (2018). Daily to Decadal Modulation of Jet Variability. *J. Clim.* 31, 1297–1314, <https://doi.org/10.1175/JCLI-D-17-0286.1>.

4. Lessons Learnt

4.1 Impact of atmospheric resolution in AMIP-type and coupled simulations

Results on the sensitivity to atmospheric resolution in WP6 Stream 1 simulation are broadly in line with earlier findings on this topic, either from published literature or from earlier deliverables of the PRIMAVERA project (e.g. D2.1). It should be noted that the majority of models included in the “lower-resolution” category (see Table 3.1.1) have an effective atmospheric resolution of about 100km or less, and have been extensively tested and tuned in earlier collaborative research project. Raising the bar from such a baseline is not easy, and the fact that a consistent positive impact of increased resolution is detected for some phenomena but not for others should neither come as a surprise, nor be seen in a negative light.

In general, long-term biases in atmospheric variables and statistics are only weakly affected by an increase in atmospheric resolution, which contrasts with the larger response to increases in ocean resolution (see next section). With regard to the spatial pattern of large scale-modes of variability (EOFs, teleconnection patterns, circulation regimes), individual models often show significant differences between the lower- and the higher-resolution versions, but improvements with resolutions are not consistent across models (Sect. 3.2.4, 3.2.5, 3.2.6, 3.4.3). As in earlier model intercomparisons, it is found that the advantages of increasing atmospheric resolution beyond ~50km become progressively smaller as far as large-scale variability patterns are concerned.

Among the different circulation regimes affecting the European and North Atlantic region, blocking is the one showing the clearer benefits of increased resolution. This is not so apparent in statistics of average properties (mean regime pattern, frequency averaged over large domain or across latitudes), but rather in the frequency of long-lived episodes (Sect. 3.2.5) or in the spatial correlation of 2-dimensional patterns of blocking frequency between models and observations (Sect. 3.3.4).

One question raised by a number of contributors is whether results obtained from a single 65-year simulation for each model are robust enough to provide a statistically significant assessment of low-frequency variability properties. Some contributors had access to results from ensemble simulations (which were not a Stream 1 deliverable), and it was noted that ensembles of at least 3 members (Sect. 3.4.3) and possibly up to 10 members (Sect. 3.2.2) would be needed for a robust assessment of trends, teleconnections and regime properties. This requirement is supported by current practice in seasonal and sub-seasonal forecasting, where similar studies are performed on re-forecast sets where the number of simulated years (observed years times ensemble members) is at least 200, and often significantly larger (eg Johnson et al. 2018).

Aspects that showed a consistent benefit of atmospheric resolution increase are those related to extreme events and intense storms, as well as some aspects of the hydrological cycle. Over Europe and the northern extratropics, a positive impact was noted in trends of summer temperature extremes (3.2.2), statistics of extreme precipitation over Europe (Sect. 3.2.3, 3.3.1), and in biases of storm intensity (Sect. 3.2.8). For tropical cyclones, the

relationship between pressure minima and maximum lifetime and the representation of specific humidity within the cyclones (Sect. 3.2.7) is improved. Positively affected aspects of the hydrological cycle include trends in boreal spring snow cover (Sect. 3.3.2), and the overall proportion of land/orographic precipitation (Sect. 3.3.3), the latter being more evident in grid-point than in spectral models.

4.2 Ocean resolution in the coupled systems

The delays in the availability of data from WP6 have limited the number of multi-model studies of the coupled climate system that have been undertaken in WP2. However, several studies have investigated the impact ocean resolution using the available data, which in some cases has been augmented with non-PRIMAVERA data. The key messages from these studies are summarized below.

The transition from 100 km to 50-10 km ocean resolutions has a substantial impact on the mean climate (Sect. 3.3.6, 3.3.7, 3.4.1) and variability of the coupled system (sections 3.3.5,3.4.2). There is some evidence that the impact on the mean state of changes in ocean resolution are larger than the corresponding changes atmospheric resolution (Sect 3.2.4, 3.4.1). This is likely due the transition of ocean models from the eddy-parameterized (~100 km) to eddy-permitting/-resolving (< 50 km) regime, which results in a step-change in the ability of the resolved ocean dynamics to simulate sharp gradients and non-linear processes such as mesoscale eddies.

In particular, increased ocean resolution in the PRIMAVERA models is associated with improvements to the poleward transport of heat in the North Atlantic (Sect. 3.3.6, 3.4.4), which leads to improvements to related regional climate biases (e.g. Arctic sea-ice volume, North Atlantic SST biases). However, there is some evidence that the increased ocean heat transport in the eddy-permitting resolution NEMO ocean model is a consequence of unrealistically deep mixed layer depths in the Labrador Sea (section X). These results will be examined in more detail as additional coupled model data becomes available.

The move to eddy-permitting ocean resolutions is also associated with a step-change in the representation of ocean-atmosphere coupling in areas of high eddy activity such as the Gulf Stream (Sect. 3.3.5). Work is ongoing to evaluate the associated atmospheric impacts and their timescale dependence (Sect 3.4.2). This work is important to quantify the relevance of results obtained within PRIMAVERA for coupled forecasts on sub-seasonal to seasonal timescales.

Finally, we note that several models within the PRIMAVERA ensemble share a similar ocean model configuration (NEMO) and therefore results should be considered within the context of the existing literature. For instance, the NEMO model typically shows an increase in the strength of the Atlantic Meridional Overturning Circulation (AMOC) and associated heat transports at higher ocean resolutions. However, previous studies with other coupled modelling systems have found the opposite result (e.g. Winton et al. 2014). In this case, the opposing results could be a consequence of the combined impact of changes in the resolved dynamics and the impacts of disabling resolution-sensitive parametrizations, which are uncertain and model-dependent. Other processes, such as the impacts of resolved SST fronts and air-sea interactions associated with mesoscale eddies, are likely to be more

robust across models. These effects should be considered in future work considering the impact of ocean resolution in the PRIMAVERA ensemble.

References

- Johnson, S. J., Stockdale, T. N., Ferranti, L., Balmaseda, M. A., Molteni, F., Magnusson, L., Tietsche, S., Decremmer, D., Weisheimer, A., Balsamo, G., Keeley, S., Mogensen, K., Zuo, H., and Monge-Sanz, B (in review). SEAS5: The new ECMWF seasonal forecast system, *Geosci. Model Dev. Discussion.*, <https://doi.org/10.5194/gmd-2018-228>.
- Winton, M., Anderson, W. G., Delworth, T. L., Griffies, S. M., Hurlin, W. J., & Rosati, A. (2014). Has coarse ocean resolution biased simulations of transient climate sensitivity? *Geophysical Research Letters*, 41(23), 8522-8529.

5. Links Built

- The results presented in this report confirm and go beyond the previous results outlined in Deliverable D2.1, by making use of the PRIMAVERA Stream 1 model simulations.
- Strong links with WP1 have been developed to build the diagnostics used in this report.
- The work on extra-tropical storms (tracking and analysis) links with WP10/11 work on climate risk and user information. Storm strengths over Europe have been assessed, comparing back to CMIP5 models (which is what is currently used by the community) and demonstrating some improvements in simulated storm intensities with the higher resolution PRIMAVERA simulations, which is key for climate impacts and hazard.
- The work on extreme precipitation events and Euro-Atlantic regime structure establishes links with WP4, where stochastic physics schemes are also expected to have an effect which may be comparable to resolution: this will be examined further in in WP4.
- Findings from the analyses of Stream 1 simulations will inform choices for the specification of WP6 Stream 2 experiments.